Density Dependent Groundwater Flow

Salt Water Intrusion and Heat Transport

KHTP/GWM II Hydrological Transport Processes/Groundwater Modelling II
L3041/L4019

March 2001 Gualbert H.P. Oude Essink

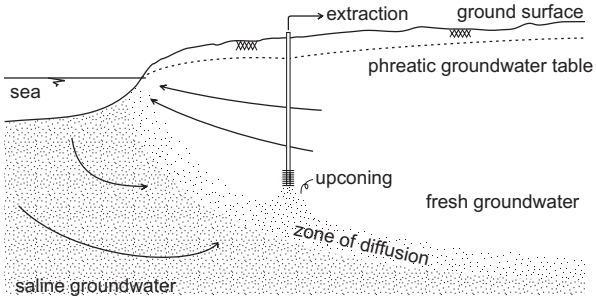

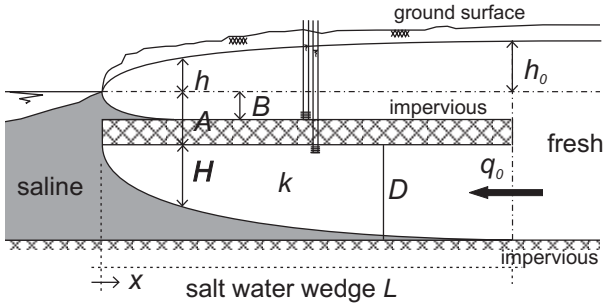

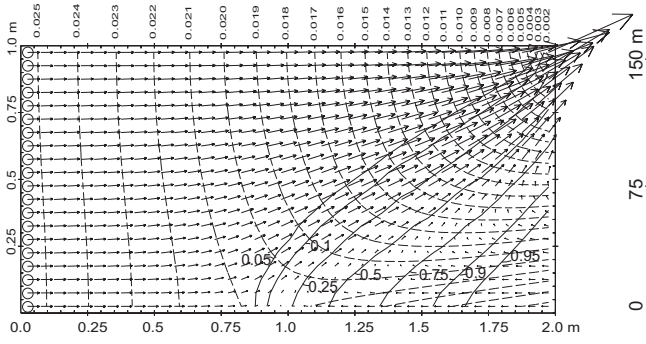

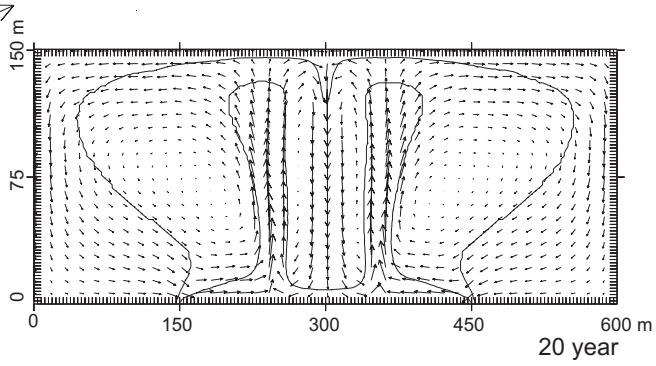

Utrecht University
Interfaculty Centre of Hydrology Utrecht
Institute of Earth Sciences
Department of Geophysics f. 12.50

General introduction

These lectures notes, which comes under the ICHU[1], are applied for two courses: Hydrological Transport Processes and Groundwater Modelling II[2]. Eventually, the aim of these lecture notes is to gain more insight in the behaviour of density dependent groundwater flow in porous media. These lecture notes are divided into two parts:

I. Salt Water Intrusion
: in this part, the processes concerning salt water intrusion in coastal aquifers, where non-uniform density distributions occur, are described. Variations in groundwater density, resulting from variations in salinity, can have a great effect on groundwater flow. It may be important to take the impact of salt water intrusion into account in the management of groundwater resources in coastal regions,

II. Heat Transport
: in this part, features of heat transport in porous media are considered. The analogy between solute and heat transport is demonstrated in two dimensions and Rayleigh's number is analysed to characterise the onset of convection.

Primarily knowledge should comprise basic knowledge on hydrogeologic processes such as the Darcy equation, the equation of continuity and the equation of solute transport. For all students, it is strongly recommended to have followed Groundwaterhydrology (HYDB). For Groundwater Modelling II (L4019), the courses Hydrological Transport Processes (L3041) and Groundwater Modelling I (L4018) are compulsory.

Gualbert Oude Essink
March 2001

[1]The Interfacultair Centrum voor Hydrologie Utrecht (ICHU) is a centre which provides a study-path Hydrologie to students from the Faculty of Earth Sciences and Department of Physical Geography.

[2]During these courses will be specified what part of these lecture notes is for Hydrological Transport Processes and what for Groundwater Modellering II.

æ

Contents

List of Figures

List of Tables

Part I

Salt water intrusion in coastal aquifers

Chapter 1

Introduction

Many coastal zones, especially low-lying deltaic areas, accommodate high density populations. For example, about 50 % of the world population lives within 60 km of the shoreline. For ages, mankind is attracted to these areas because of the availability of an abundance of food (e.g., fisheries and agriculture) and the presence of economic activities (e.g., trade, harbours, ports and infrastructure). Due to increasing concentration of human settlements, agricultural development and economic activities, the shortage of fresh groundwater for domestic, agricultural, and industrial purposes becomes more striking in these coastal zones.

Only some 2.5 % of all water on the Earth is fresh (see table 1.1). From this amount 30 % is potentially available ($\approx 10.5 \times 10^6$ km^3), mainly as groundwater. Nevertheless, fresh water is rather scarce. Compared to surface water, the advantages of groundwater are the high quality, hardly seasonal effects (constant temperature), the low storage costs (no spatial limitations) and the huge available quantities. At present, one third of fresh water use, e.g. for domestic purposes, is groundwater. This fraction is growing, as the demand of fresh groundwater increases due to:

- the rise of world population and economic growth,
- the loss of surface water due to contamination,
- the availability of huge quantities,
- the high quality (unpolluted), relative to surface water.

Table 1.1: Mondial distribution of: water on the Earth and fresh water (after Shiklomanov, 1990).

Mondial distribution of water on the Earth		
Form	**Volume, 10^6 km^3**	**%**
Oceans and seas	1351.0	97.5
Fresh water	35.0	2.5
Total quantity of water	1386.0	100.0
Mondial distribution of fresh water		
Form	**Volume, 10^6 km^3**	**%**
Ice	24.4	69.7
Surface water	0.1	0.3
Groundwater	10.5	30.0
Total quantity of fresh water	35.0	100.0

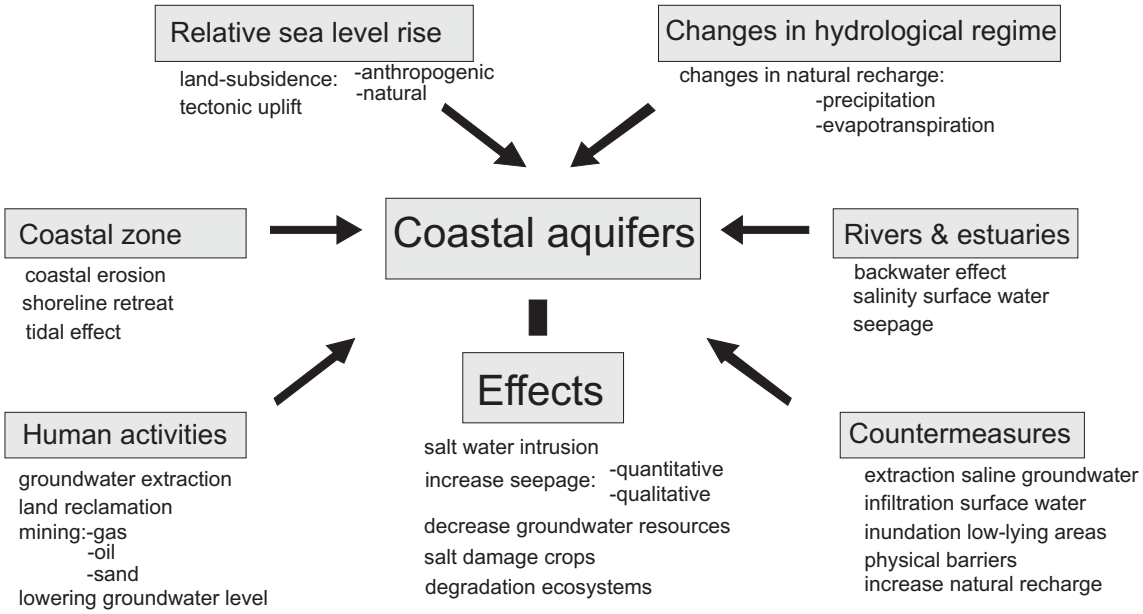

Figure 1.1: Features affecting the coastal aquifers.

Disadvantages of groundwater are high extraction costs, the high mineral content, the potential of land subsidence, and finally, the threat of salt water intrusion[1]. Salt water intrusion in the subsoil may not only be a threat for the public and industrial water supply but also for agriculture and horticulture. Although technical methods for desalinisation of saline or brackish water are available and applied, it is (still) an expensive method. As such, the conservation and protection of fresh groundwater should be promoted.

Already at this moment, many coastal aquifers[2] in the world, especially shallow ones, experience an intensive salt water intrusion caused by both natural as well as man-induced processes (Oude Essink, 2000a).

Human interferences, such as mining of natural resources (water, sand, oil and gas) and land reclamation (causing subsidence) threaten coastal lowlands. Consequently, salinities of surface water systems increase and land degradation occurs because soils become more saline. As a result, poor crop yields are produced due to salt damage and indigenous crops might be substituted by more salt-tolerant crops. If even the salt-tolerant crops cannot withstand the high salinities, the population might eventually migrate from the barren land and resettle in more fertile arable territories, which could cause social commotions.

In addition, coastal aquifers within the zone of influence of mean sea level (M.S.L.), are threatened by an accelerated rise in global mean sea level. This rise in global mean sea level, 50 cm for the coming century as the present best estimate, could even more jeopardise vulnerable coastal aquifers than they are threatened today. Subsequently, the salinisation of coastal aquifers will accelerate. This could mean a reduction of fresh groundwater resources. In addition, the present capacity of the discharge systems in several coastal lowlands may

[1]Salt water intrusion is a permanent inflow of saline groundwater in an aquifer which contains fresh groundwater

[2]An aquifer is a permeable geologic formation, where groundwater is permitted to move through.

be insufficient to cope with the excess of seepage water, especially in those coastal areas which are below M.S.L. This seepage will probably have a higher salinity than at present.

The present distribution of fresh, brackish and saline water in the subsoil has developed in geologic history and has been and still is affected by several natural processes but also by human intervention. Brackish and saline groundwater can be found in coastal areas, but also further inland. Features which affect coastal aquifers are summarised in fig. 1.1. Obviously, from a hydrogeological point of view, the most interesting coastal areas are the hydrogeologic systems with sedimentary deposits ('a porous medium[3]'), rather than hydrogeologic systems consisting of hard rocks.

1.1 Natural processes

Sedimentation of rock material in coastal areas takes place in a marine environment and consequently water in these formations is saline. Salt-containing formations may occur also more inland. Tectonic movements and climatic changes in the geologic history have resulted in changes in sea level. Formations built-up in coastal areas according to these levels also contain saline water. Sometimes already existing fresh water containing formations turned into saline via exchange, due to a density difference between fresh and saline water. In other cases extensive salt layers could develop, e.g. a shallow sea could evaporate in a warm climate, finally leading to crystallisation. Also two other natural processes have affected the distribution of saline and fresh groundwater:

- natural recharge,
- transport processes.

Natural recharge of the groundwater system (infiltrating rain) is the main source of fresh water in formations. This water travels from the recharge area through permeable formations (aquifers) to the sea or ocean. On its way it may encounter saline aquifers, replacing or mixing with the saline groundwater. The actual distribution of fresh and saline groundwater depends amongst others on hydrogeological parameters and the density differences between the liquids. Climatic changes with different rainfall regimes have also influenced salinisation. Seas, oceans, lakes and rivers act mostly as (outflow) boundaries for groundwater systems, so long-term differences in their levels will interfere in the groundwater system.

The main transport mechanism is advection: flow of water due to gravity. If density differences occur and the water is stagnant then the least dense water will float on top of the more dense water and a horizontal layering will occur. Flowing fresh and/or saline water will create sloping (density) interfaces. Apart from this, molecular diffusion, a movement of ions occurs. This process is driven by differences in concentrations, independent of flow and developing proportional to the square root of time. As can be seen in Intermezzo I (page 7), diffusion can be a slow process. Diffusion will smoothen concentration gradients, e.g. in the case of an interface between fresh and saline water, a transition zone of brackish water

[3]A porous medium is a persistent solid matrix (e.g. soil, sand, sandstone, fissured rocks or karstic limestone) and a void space which is occupied by one or more fluid phases (e.g. water and air). Flow in a porous medium takes place through a complex network of interconnected pores or openings.

will develop. Flowing water will create dispersion, a mixing process due to the different magnitude and orientation of the velocity vector of groundwater in the pores. On a larger scale irregularities in an aquifer have a similar effect (macrodispersion). The displacement of dissolved matter by dispersion is proportional to the velocity of the groundwater. Both dispersion and diffusion have a smoothing influence on differences in concentration. Dispersion and diffusion are difficult to distinguish. The joint effect of diffusion in groundwater is taken into account by means of a hydrodynamic dispersion coefficient.

1.2 Human intervention

Human intervention has affected the distribution of fresh and saline water in the subsoil. Reclamation of coastal areas, impoldering, extraction of groundwater, artificial recharge of groundwater, lowering of groundwater tables, irrigation and drainage, construction of canals, mining etc. have all led to changes in the hydrogeological regime. The response of the groundwater system is to reach a new state of equilibrium, with amongst others a different distribution of fresh and saline groundwater. This may last decennia or even centuries, as groundwater flow is, in general, a very slow process. Although this may sound rather reassuring, it also means that once an unwanted effect is observed, it will also take a long time before countermeasures become effective.

Worldwide, excessive overpumping of especially coastal aquifers is the most important anthropogenic cause of salt water intrusion. In coastal aquifers, saline groundwater is nearby and upconing of saline groundwater can easily occur. Exploiting and mining of groundwater regularly take place to mitigate droughts or supply irrigation projects, especially in (semi)-arid areas. Fossil and non-renewable groundwater basins are utilised for domestic, industrial and agricultural water supply. Furthermore, reducing recharge areas to develop touristic centres causes a decrease of outflow of fresh groundwater, inducing an inland shift of the salt water wedge.

Lowering of piezometric heads caused by excessive overpumping can also induce a severe land subsidence. For instance, table 1.2 shows the land subsidence in some coastal megacities. In some areas, land reclamation (e.g. in the Netherlands from about the seventeenth century on) caused a lowering of piezometric heads, and subsequently, sea water has rapidly been intruded the coastal aquifer even since. In fact, sea level rise is basically the same as equally lowering the land surface and thus the piezometric heads. Nowadays, lowering of the piezometric heads due to overpumping already occurs in many aquifers around the world. It is obvious that, for those systems, the impact of a (relatively small) sea level rise (e.g. 50 cm per century) on the aquifer will be of marginal importance compared to the effect of an increase in extraction rate.

1.3 Outline

In this part of the lecture notes, the interest is focussed on groundwater flow in porous media where a non-uniform density distribution occurs. In the following chapters of part I of these lecture notes, some characteristic parameters of the hydrogeologic system are described. In addition, the mathematical description of groundwater flow in a porous medium

Table 1.2: Land-subsidence in some coastal megacities (Yeung, 1999).

Megacity	**Maximum subsidence,** m	**Date commenced**
Shanghai	2.80	1921
Tokyo	5.00	1930's
Osaka	2.80	1935
Bangkok	1.60	1950's
Tianjin	2.60	1959
Jakarta	0.90	1978
Manila	0.40	1960
Los Angeles	9.00	1930's

related to salinisation will be treated. How to deal with piezometric heads in a fresh/saline environment is shown in the next chapter. Then the concept of an interface between fresh and saline groundwater is introduced and illustrated with examples. The theory behind the upconing of saline groundwater is defined. Countermeasures to control salinisation and a system to monitor salt water intrusion are described. Problems with numerical modelling of variable-density groundwater flow are discussed. A brief summary of properties and possibilities of some widely-used computer codes is given. One computer code, MOCDENS3D, is described in more detail, and an example, the evolution of a freshwater lens, is worked out numerically. Finally, a list of references and some interesting web-sites and textbooks conclude these lecture notes.

Intermezzo I: diffusion in a saline environment

The time aspect of smoothing a contrast in chloride concentration between three layers with different chloride concentration is analysed. Molecular diffusion causes constituents to be spread due to differences in concentrations. Here, the so-called diffusion equation is applicable:

$$\frac{\partial C}{\partial t} = D_m \frac{\partial^2 C}{\partial x^2} \tag{1.1}$$

where D_m=the molecular diffusion coefficient ($L^2\,T^{-1}$). Consider the following composition: between 0 m and 100 m: initial concentration C_0 is 16000 $mg\ Cl^-/l$ and D_m= 0.69 $\times$ 10^{-4} m^2/d; between 100 m and 160 m: C_0 is 6000 $mg\ Cl^-/l$ and D_m= 0.44 $\times$ 10^{-4} m^2/d; and between 160 m and 200 m: C_0 is 12000 $mg\ Cl^-/l$ and D_m= 0.69 $\times$ 10^{-4} m^2/d. The equation is numerically modelled (see the lecture notes of Groundwater Modelling I, Oude Essink, 2000c) with an explicit discretisation:

$$C_i^{t+\Delta t} = C_i^t + D_m \frac{\Delta t}{\Delta x^2}\left(C_{i+1}^t - 2C_i^t + C_{i-1}^t\right) \tag{1.2}$$

At t >0, the concentration at x=0 becomes equal to 0 $mg\ Cl^-/l$. At x=200 m, no flux of solute is assumed. Based on the stability criterion $D_m \frac{\Delta t}{\Delta x^2} < 0.5$ (see the lecture notes of Groundwater Modelling I, Oude Essink, 2000c), the following model parameters are chosen: Δx=5 m, Δt=250 $year$. Fig. 1.2 shows the change in chloride content as a function of time. As can be seen, molecular diffusion smoothens the contrast in concentration, though it is a slow process.

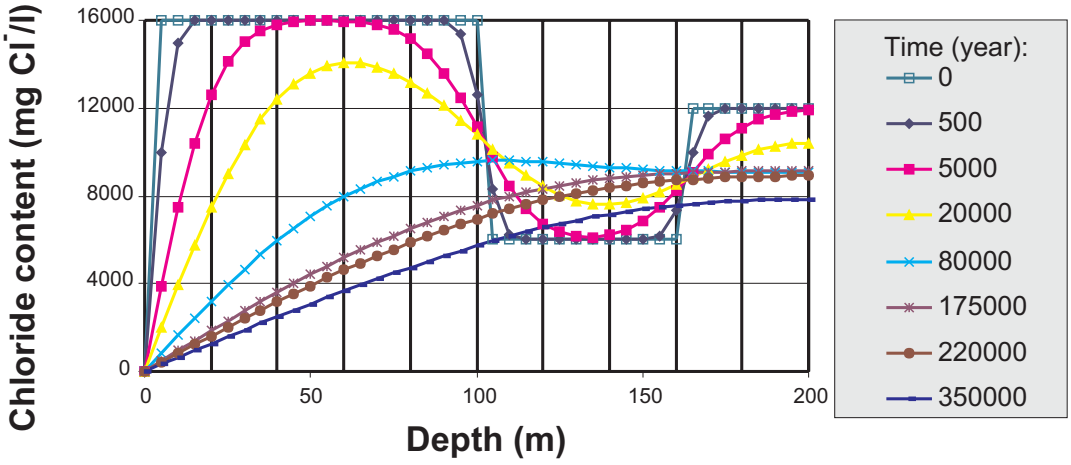

Figure 1.2: Change in chloride concentration in $mg\ Cl^-/l$ as a function of time in a layered aquifer due to molecular diffusion.

Chapter 2

Characteristics of the groundwater system

2.1 Chemical characteristics of water

2.1.1 Densities

Density should be considered to be a function of pressure, temperature of the fluid and concentration of dissolved solids:

$$\rho = f(p, T, S) \tag{2.1}$$

where:

- ρ = density (kg/m^3),
- p = pressure ($M\,L^{-1}\,T^{-2}$),
- T = temperature (^oC),
- S = salinity[1] or total dissolved solids (TDS) (mg/l).

The influence of pressure can be neglected under the given circumstances for most hydrogeologic systems. Furthermore, the influence of temperature on density is of minor importance with respect to the influence of dissolved solids concentration within many hydrogeologic systems, see fig. 2.1. Therefore, the density of groundwater is often only related to the concentration of dissolved solids in the groundwater, whereas the temperature is considered to be constant. In general, when the quality of groundwater is in question, the salinity or total dissolved solids TDS is considered. An advantage of using TDS is that a rapid determination of TDS is possible by measuring the electrical conductivity of a groundwater sample.

The concentration of dissolved solids is subdivided into negative (anions) and positive ions (cations), see table 2.1. For instance, ocean water consists of 11 main components: Since in coastal groundwater chloride (Cl^-) is the predominant negative ion, which is moreover investigated intensively, the interest is often focused on the chloride distribution. When, in fact, only changes in the chloride distribution are simulated, the distribution of all dissolved solids is meant. In other words, the distribution of chloride ions is considered to represent the distribution of all dissolved solids. As such, a proportional distribution of all dissolved solids, which is present in ocean water, is also assumed to be present in groundwater under consideration.

[1]The salinity is the concentration of dissolved solids in water, expressed in ($M\,L^{-3}$) (mg/l), *p.p.t.* (*parts per thousand*) or *p.p.m.* (*parts per million*).

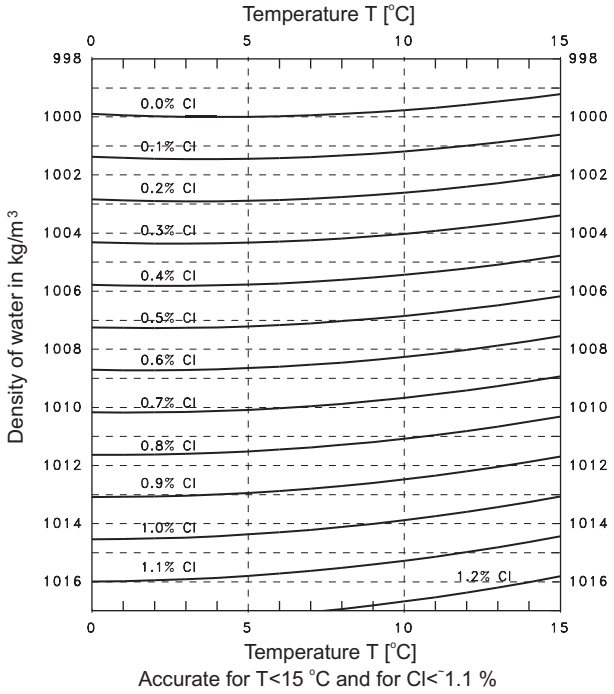

Figure 2.1: Density of water as a function of the chlorinity and temperature (ILRI, 1972).

Table 2.1: Composition of ocean water. The three components with low concentrations are Strontium ($\pm$ 8 mg/l), Borium ($\pm$ 5 mg/l) and Fluoride ($\pm$ 1 mg/l).

Ions		mg/l
negative ions	Cl^-	19,000
	SO_4^{-2}	2700
	HCO_3^-	140
	Br^-	65
total negative ions		21,905
positive ions	Na^+	10,600
	Mg^{+2}	1270
	Ca^{+2}	400
	K^+	380
total positive ions		12,650
Total Dissolved Solids		34,555

The applied classification of fresh, brackish and saline groundwater based on chloride concentrations according to Stuyfzand (1993) is presented in table 2.2. Obviously, there are various other classification systems possible, e.g. because the definition for fresh groundwater depends on the application of the groundwater. For instance, the drinking water standard in the European Community equals 150 $mg\ Cl^-/l$ (Stuyfzand, 1986), while according to the World Health Organisation, a convenient chloride concentration limit is 200

Table 2.2: Classification into eight main types of fresh, brackish or saline groundwater depending on the basis of chloride concentration, after Stuyfzand (1993).

Main type of groundwater	Chloride concentration ($mg\ Cl^-/l$)
oligohaline	0 - 5
oligohaline-fresh	5 - 30
fresh	30 - 150
fresh-brackish	150 - 300
brackish	300 - 1000
brackish-saline	1000 - 10,000
saline	10,000 - 20,000
hyperhaline or brine	$\geq$ 20,000

$mg\ Cl^-/l$ (Custodio *et al.*, 1987). A chloride concentration equal to 300 $mg\ Cl^-/l$ indicates the taste limit of human beings according to ICW (1976), while Todd (1980) gives 100 $mg\ Cl^-/l$ as the limit when salt can be tasted. Livestock can endure higher concentrations: up to 1500 $mg\ Cl^-/l$ may be accepted, in case the chloride concentration stays constant.

2.1.2 Equation of state

Numerous conversion formulas relating density to chloride concentration, salinity, temperature and pressure, can be found in literature, see e.g. Sorey (1978), Weast (1982), Voss (1984), Holzbecher (1998). For example, eqn. 2.2 gives an equation of state with a linear relation between chlorinity and density.

$$\rho(C) = \rho_f \left(1 + \alpha \frac{C_{(i,j)}}{C_s}\right) \tag{2.2}$$

where

- $\rho(C)$ = density of groundwater ($M\,L^{-3}$),
- ρ_f = reference density, usually the density of fresh groundwater (without dissolved solids) at mean subsoil temperature ($M\,L^{-3}$),
- ρ_s = density of saline groundwater at mean subsoil temperature ($M\,L^{-3}$),
- $\alpha = (\rho_s - \rho_f)/\rho_f$ = relative density difference ($-$),
- $C_{(i,j)}$ = chloride concentration or the so-called *chlorinity* ($mg\ Cl^-/l$). The salinity S is related to the chlorinity C by the formula: $C = 0.554\ S$,
- C_s = reference chloride concentration ($mg\ Cl^-/l$). In eqn. 2.2, a linear relation exists between ρ_s and C_s.

The following data can be applied for sea (ocean) water: $\rho_f = 1000\ kg/m^3$; $\rho_s = 1025\ kg/m^3$; thus $(\rho_s - \rho_f)/\rho_f = 0.025$; C_s = 19,300 $mg\ Cl^-/l$; and TDS = 34,500 mg/l. The TDS in oceans can be higher, due to, among others, a high degree of evaporation

and oceanic currents, and consequently, the density is higher than $\rho_s = 1025\ kg/m^3$. For instance, the chloride concentration in the Mediterranean Sea can be as high as 22,000 $mg\ Cl^-/l$ (ρ=1028 kg/m^3), and the TDS of the Red Sea and some areas of the Mediterranean can reach some 45,000 mg/l (the Dead Sea even reaches ρ=1200 kg/m^3).

Knudsen developed in 1902 the following formula:

$$\rho_{(S,T)} = 1000 + 0.8054S - 0.0065(T - 4 + 0.2214S)^2 \tag{2.3}$$

Expression 2.3 (see fig. 2.1) gives a rather good approximation for the density as a function of salinity and temperature, at a (constant) pressure of 1 atmosphere and for temperatures $< 15\ ^oC$ and salinity values $<$ 20,000 mg/l or $<$ 20 ppt. Sorey (1978) gives a temperature-dependent formula:

$$\rho_{(T)} = \rho_f \left[1 - \beta_T(T - T_0) - \gamma_T(T - T_0)^2\right] \tag{2.4}$$

or

$$\rho_{(T)} = 1000 \left[1 - 3.17 \times 10^{-4}(T - 4) - 2.56 \times 10^{-6}(T - 4)^2\right] \tag{2.5}$$

Hassanizadeh (1997) gives a formula which depends on temperature T, pressure p and salt mass fraction ω:

$$\rho_{(T,p,\omega)} = \rho_f e^{-\alpha(T-T_0)+\beta(p-p_0)+\gamma\omega} \tag{2.6}$$

where

- α=2 $\times$ 10^{-4} per ^oKelvin,
- β=4.45 $\times$ 10^{-10} ($m\,s^2\,kg^{-1}$),
- γ=0.7 ($-$).

Note that at high pressures, this equation is not applicable. Finally, in SUTRA (Voss, 1984) two formulas are given:

$$\text{Temperature } T \text{ dependent:} \quad \rho_{(T)} = \rho_f + \frac{\partial\rho}{\partial T}(T - T_0) \tag{2.7}$$

$$\text{Concentration } C \text{ dependent:} \quad \rho_{(C)} = \rho_f + \frac{\partial\rho}{\partial C}(C - C_0) \tag{2.8}$$

where

- ρ_f= density of fresh water ($kg\,m^{-3}$),
- $\frac{\partial\rho}{\partial T}$= a constant value of density change with temperature, e.g. -0.375 ($kg\,m^{-3}\,^oC$). Range: 20 ^oC-60^oC,
- T_0= base fluid temperature (^oC),
- C=mass fraction of total dissolved solids. The mass fraction of seawater, C_s, equals 0.0357 $\frac{kg(dissolvedsolids)}{kg(seawater)}$,
- $\frac{\partial\rho}{\partial C}$= a constant value of density change with concentration, e.g. 700 ($kg\,m^{-3}$) or $\frac{kg(seawater)^2}{kg(dissolvedsolids)m^3}$.

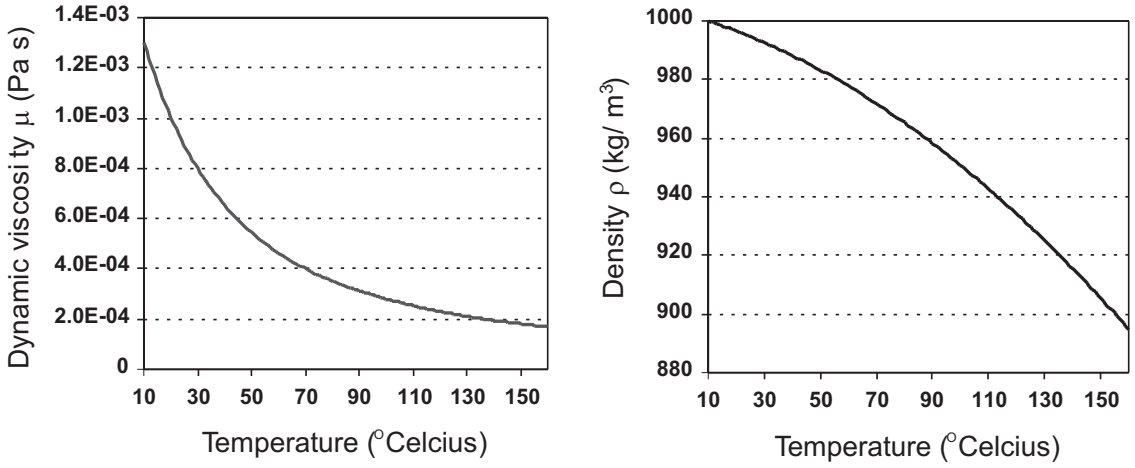

Figure 2.2: Dynamic viscosity (Huyakorn & Pinder, 1977) and density of water (Sorey, 1978) as a function of temperature (Smith & Chapman, 1983).

2.1.3 Dynamic viscosity

In case of temperature gradients, it is also important to know that the dynamic viscosity highly depends on the temperature (Huyakorn & Pinder, 1977), see also table 2.3 and fig. 2.2:

$$\mu = f(T) \cong (2.394 \times 10^{-5}) \times 10^{\frac{248.37}{T+133.15}}\ kg/ms \tag{2.9}$$

Note that this equation should only be applied for $T < 100\ ^oC$. For example, temperature in the top layers in the Netherlands is about 9 to 10 ^oC, whereas the gradient is about 3 ^oC per 100 m, which means the hydraulic conductivity at a depth of 100 m is about 8 % higher than at ground surface. Note that the dynamic viscosity μ is relatively insensitive to pressure. Furthermore, the dynamic viscosity also depends on the solute concentration, though only for very high solute concentrations.

Table 2.3: Variation of the dynamic viscosity μ with temperature T at a pressure of 100 kPa (1 *bar*) (Verruijt, 1970; Bear, 1972; Voss, 1984; CRC, 1994).

Temperature T	Dynamic viscosity μ $(kg/m\,s)$	
(^oC)	Verruijt, Bear, CRC	Eqn. 2.9
0	1.79×10^{-3}	1.76×10^{-3}
5	1.52×10^{-3}	1.50×10^{-3}
10	1.31×10^{-3}	1.30×10^{-3}
15	1.14×10^{-3}	1.14×10^{-3}
20	1.00×10^{-3}	1.00×10^{-3}
40	0.65×10^{-3}	0.65×10^{-3}
70	0.41×10^{-3}	0.40×10^{-3}
100	0.28×10^{-3}	0.28×10^{-3}

2.2 Equation of motion: Darcy's law

The equation of motion for three-dimensional (laminar) groundwater flow in an anisotropic non-homogeneous porous medium in the principal directions is described by Darcy's law (e.g. Bear, 1972):

$$q_x = -\frac{\kappa_x}{\mu}\frac{\partial p}{\partial x} \qquad q_y = -\frac{\kappa_y}{\mu}\frac{\partial p}{\partial y} \qquad q_z = -\frac{\kappa_z}{\mu}(\frac{\partial p}{\partial z} + \rho g) \tag{2.10}$$

where

- q_x, q_y, q_z = Darcian specific discharges in the principal directions ($L\,T^{-1}$),
- $\kappa_x, \kappa_y, \kappa_z$ = principal intrinsic permeabilities (L^2),
- μ = dynamic viscosity of water at point $[x, y, z]$ ($M\,L^{-1}\,T^{-1}$),
- p = pressure ($M\,L^{-1}\,T^{-2}$),
- ρ = density of groundwater at point $[x, y, z]$ ($M\,L^{-3}$),
- g = gravitational acceleration ($L\,T^{-2}$),
- $\rho g = \gamma$ = specific weight ($M\,L^{-2}\,T^{-2}$).

Darcy's law is only valid in the case of laminar flow: viz. at relatively low velocities when water particles move more or less parallel to each other. In other words, Darcy's law is valid as long as the so-called Reynolds number Re $(-)$ does not exceed some value between 1 and 10:

$$\text{Reynolds number:} \qquad Re = \frac{\rho q R}{\mu} < 1 - 10 \tag{2.11}$$

where R is the hydraulic radius of the pore (L). The groundwater system is basically a combination of rock (sediment) matrix and water. The size and shape of the voids of the matrix and viscosity and density of the pore water are determining factors for the hydraulic conductivity k ($L\,T^{-1}$).

If ρ is constant, then the hydraulic conductivities of groundwater in the principal directions would be defined as follows:

$$k_x = \frac{\kappa_x \rho g}{\mu} \qquad k_y = \frac{\kappa_y \rho g}{\mu} \qquad k_z = \frac{\kappa_z \rho g}{\mu} \tag{2.12}$$

2.2.1 Permeability and hydraulic conductivity

The intrinsic permeability κ largely depends on the size of the pores through the effective porosity n_e. A commonly-used equation is that of Kozeny-Carmen to clearly demonstrate the relation between κ and n_e:

$$\text{Kozeny-Carmen:} \qquad \kappa = c\,d^2\frac{n_e^3}{(1-n_e)^2} \qquad (m^2) \tag{2.13}$$

where

Table 2.4: Values for the hydraulic conductivity k and the intrinsic permeability κ. In conclusion: fine sand 1-10 m/day and clay 10^{-5}-10^{-4} m/day.

Soil	k **(m/s)**	κ **(m^2)**
Unconsolidated deposits		
Clay	$<10^{-9}$	$<10^{-17}$
Sandy clay	10^{-9}-10^{-8}	10^{-16}-10^{-15}
Silt	10^{-8}-10^{-7}	10^{-15}-10^{-14}
Peat	10^{-9}-10^{-7}	10^{-16}-10^{-14}
Very fine sand	10^{-6}-10^{-5}	10^{-13}-10^{-12}
Fine sand	10^{-5}-10^{-4}	10^{-12}-10^{-11}
Coarse sand	10^{-4}-10^{-3}	10^{-11}-10^{-10}
Sand with gravel	10^{-3}-10^{-2}	10^{-10}-10^{-9}
Gravel	$>10^{-2}$	$>10^{-9}$
Rocks		
Unfractured rocks	$<10^{-9}$	$<10^{-17}$
Sandstone	10^{-10}-10^{-6}	10^{-17}-10^{-13}
Limestone & dolomite	10^{-9}-10^{-6}	10^{-16}-10^{-13}
Fractured rocks	10^{-8}-10^{-4}	10^{-15}-10^{-11}
Permeable basalt	10^{-7}-10^{-2}	10^{-14}-10^{-9}
Karst limestone	10^{-6}-10^{-2}	10^{-13}-10^{-9}

- c = a coefficient depending on the structure of the pores, e.g. c=1/180 $(-)$,
- d = main grain size (diameter of the pore) (L),
- n_e = effective porosity $(-)$.

Table 2.4 shows some values for k and κ. It can be deduced that the permeability varies with depth due to increasing pressure or effective stress. Though exact relations are difficult to obtain as in situ data are scarce and upscaling of data from laboratory-scale experiments is somewhat unreliable, a correlation between permeability κ and depth z becomes widely accepted. For instance, the following equation is given for the permeability as a function of depth in the continental crust (Manning & Ingebritsen, 1999):

$$\log \kappa = -14 - 3.2 \log z \tag{2.14}$$

where z is the depth in kilometres (L). In addition, porosity can also be specified as a function of depth:

$$n_e = n_{e,0} \exp^{-\beta z} \tag{2.15}$$

where $n_{e,0}$ and β are fit-coefficients. Bethke (1985) presented some values for different types of sedimentary rocks. For instance, he used $n_{e,0}$=0.5 and β=0.5 for sands and $n_{e,0}$=0.6 and β=0.6 for shales. For the Slochteren Formation in the Netherlands, $n_{e,0}$=0.43 and β=0.3445 were used (Verweij, 1999).

The influence of density differences on the hydraulic conductivity is of little practical importance with regard to the accuracy of the determination of the permeability itself. More

important may be the phenomenon of changes in the hydraulic conductivity in case e.g. fresh groundwater is replaced by saline water. Irreversible changes in hydraulic conductivity may occur, as has been reported in several publications (e.g. Mehnert & Jennings, 1985; Goldenberg, Mandel & Magaritz, 1986).

2.3 Equation of continuity

Eqn. 2.16 describes the non-steady three-dimensional mass flow in a small element of a saturated anisotropic, porous medium (e.g. Bear, 1972; van der Heide & Boswinkel, 1982):

$$-\left[\frac{\partial(\rho_i q_x)}{\partial x}+\frac{\partial(\rho_i q_y)}{\partial y}+\frac{\partial(\rho_i q_z)}{\partial z}\right]=\frac{\partial(n_e\rho_i)}{\partial t}+W'(x,y,z,t) \tag{2.16}$$

where

- t = time (T),
- n_e = effective porosity of the medium ($-$),
- $W'(x,y,z,t)$ = source function, which describes the mass flux of the fluid into (negative sign) or out of (positive sign) the system ($M\,L^{-3}\,T^{-1}$).

2.4 Equation of solute transport

When solute concentration affects the density of groundwater, the flow of groundwater is density dependent. In addition, when fresh, brackish and saline groundwater is present, also the transport of solutes, and subsequently, the variation of densities should be taken into account. For that, the advection-dispersion equation describes the transport of solutes and change in density. In addition, an equation of state converts solute concentration to density. This concept is applicable in coastal aquifers where mostly non-uniform density distributions occur. Note that the advection-dispersion equation and the groundwater flow equation are coupled with each other through the effective velocity, the concentration and the density.

In this section, the advection-dispersion equation is briefly described. In the lecture notes of Groundwater Modelling I (Oude Essink, 2000c), this equation is described as:

$$R_d\frac{\partial C}{\partial t}=\frac{\partial}{\partial x_i}(D_{ij}\frac{\partial C}{\partial x_j})-\frac{\partial}{\partial x_i}(C\,V_i)+\frac{(C-C')\,W}{n_e b}-R_d\,\lambda\,C \tag{2.17}$$

where

- $R_d = 1+(\rho_b/n_e)K_d$ = retardation factor governing linear sorption ($-$). K_d is the distribution coefficient ($M^{-1}\,L^3$) and ρ_b is the bulk density of the porous material ($M\,L^{-3}$),
- C = concentration of the dissolved solids ($M\,L^{-3}$),
- D_{ij} = coefficient of hydrodynamic dispersion ($L^2\,T^{-1}$),

- $V_i = q_i/n_e$ = effective velocity of the groundwater in the direction of x_i ($L\,T^{-1}$),
- C' = concentration of the dissolved solids in a source or sink ($M\,L^{-3}$),
- $W(x, y, z, t)$ = general term for sources and sinks ($L\,T^{-1}$),
- n_e = effective porosity of the medium ($-$),
- λ = first-order rate constant, governing hydrolysis and decay (T^{-1}). Radioactive decay rates are often expressed as half-lives ($t_{1/2}$), where the half-life is the time required for the concentration to decrease to one-half of the original value: $t_{1/2} = (\ln 2)/\lambda$,
- b = saturated thickness of the aquifer (L).

With regard to the transport of a conservative[2] solute, viz. salt or Cl^-, R_d=1 and λ=0:

$$\frac{\partial C}{\partial t} = \frac{\partial}{\partial x_i}(D_{ij}\frac{\partial C}{\partial x_j}) - \frac{\partial}{\partial x_i}(C\,V_i) + \frac{(C - C')\,W}{n_e b} \tag{2.18}$$

The first term on the right hand side represents the change in concentration of solutes due to hydrodynamic dispersion. The second term represents the effect of advective transport which is the movement of solutes attributed to transport by flowing groundwater. The third term represents the contribution and removal of solutes due to fluid sources and sinks.

Hydrodynamic dispersion

Hydrodynamic dispersion D_h is defined as the combined effect of two processes:

$$D_h = D + D_m \tag{2.19}$$

where

- D ($L^2\,T^{-1}$) = mechanical (or convective) dispersion coefficient. This process is caused by velocity variations at the microscopic scale, see fig. 2.3. The spreading depends on both fluid flow and the characteristics of the pore system through which the flow takes place,
- D_m ($L^2\,T^{-1}$) = molecular diffusion coefficient. This process is caused by the random movement of molecules in a fluid and depends on concentration gradients, the properties of the fluid and the soil. For a conservative solute as chloride, the molecular diffusion D_m for porous media is approximately 10^{-9} m^2/s at a temperature of 25 ^oC.

Under normal groundwater flow conditions, molecular diffusion is of marginal importance with respect to mechanical dispersion. In fact, the subdivision of the hydrodynamic dispersion into mechanical dispersion and molecular diffusion is artificial. The mechanical

[2] A solute is conservative when no chemical reactions such as adsorption and radioactive decay are taking place.

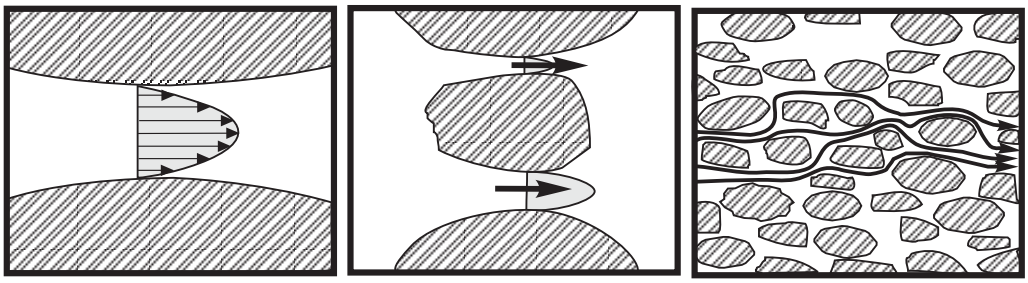

Figure 2.3: Causes of dispersion on microscale.

dispersion coefficient, which is a second-rank symmetrical tensor, is given by Scheidegger (1961):

$$D_{ij} = \alpha_{ijmn} \frac{V_m V_n}{|V|} \tag{2.20}$$

or

$$D_{ij} = \alpha_T |V| \delta_{ij} + (\alpha_L - \alpha_T) \frac{V_i V_j}{|V|} \tag{2.21}$$

where

- D_{ij} = coefficient of mechanical dispersion ($L^2 T^{-1}$),
- α_{ijmn} = *geometrical dispersivity tensor* of the aquifer (L),
- V_m, V_n = components of the real velocity in m and n direction ($L T^{-1}$),
- $|V|$ = magnitude of the real velocity ($L T^{-1}$),
- $\delta_{ij} = 1$ if $i = j$ and $\delta_{ij} = 0$ if $i \neq j$.

Scheidegger defines the dispersivity tensor for an isotropic aquifer in terms of two constants:

$$\begin{aligned} D_L &= \alpha_L |V| \\ D_T &= \alpha_T |V| \end{aligned} \tag{2.22}$$

where

- α_L = longitudinal dispersivity of the aquifer (L),
- α_T = transversal dispersivity of the aquifer (L).

For example, the components of hydrodynamic dispersion (in the principal directions) for two-dimensional and three-dimensional flow in an isotropic aquifer, considering mechanical

dispersion as well as molecular diffusion D_m, are as follows:

$$
\begin{array}{lcl}
 & two-dimensional & \\
D_{xx} & = & \alpha_L \frac{(V_x)^2}{|V|} + \alpha_T \frac{(V_z)^2}{|V|} + D_m \\
D_{zz} & = & \alpha_T \frac{(V_x)^2}{|V|} + \alpha_L \frac{(V_z)^2}{|V|} + D_m \\
D_{xz} & = & D_{zx} \;=\; (\alpha_L - \alpha_T) \frac{V_x\, V_z}{|V|}
\end{array}
\tag{2.23}
$$

$$
\begin{array}{lcl}
 & three-dimensional & \\
D_{xx} & = & \alpha_L \frac{(V_x)^2}{|V|} + \alpha_T \frac{(V_y)^2}{|V|} + \alpha_T \frac{(V_z)^2}{|V|} + D_m \\
D_{yy} & = & \alpha_T \frac{(V_x)^2}{|V|} + \alpha_L \frac{(V_y)^2}{|V|} + \alpha_T \frac{(V_z)^2}{|V|} + D_m \\
D_{zz} & = & \alpha_T \frac{(V_x)^2}{|V|} + \alpha_T \frac{(V_y)^2}{|V|} + \alpha_L \frac{(V_z)^2}{|V|} + D_m \\
D_{xy} & = & D_{yx} \;=\; (\alpha_L - \alpha_T) \frac{V_x\, V_y}{|V|} \\
D_{xz} & = & D_{zx} \;=\; (\alpha_L - \alpha_T) \frac{V_x\, V_z}{|V|} \\
D_{yz} & = & D_{zy} \;=\; (\alpha_L - \alpha_T) \frac{V_y\, V_z}{|V|}
\end{array}
\tag{2.24}
$$

The exact determination of the hydrodynamic dispersion is very difficult, if not impossible, as it depends on many features (e.g. scale effect, fingering, transient effects (Anderson & Woessner, 1992)). In fact, the more one knows about the hydraulic conductivity and porosity distribution, and subsequently, the exact velocity distribution, the more the hydrodynamic dispersion value will converge to the value of molecular diffusion. As such, one should model the heterogeneous and anisotropic medium as accurately as possible. However, as it is not possible to determine the exact hydraulic conductivity distribution as well as the velocity distribution, the exact value of the dispersion coefficient cannot be given. For this reason, the mechanical dispersion, which is inserted in the model, may (somewhat) be increased to take into account these uncertainties in the subsoil parameters. The less one knows, the higher the model dispersivities must be.

Gelhar *et al.* (1992) reviewed 59 different field sites in order to classify the dispersivity data into three reliability classes (see fig. 2.4). The representative scale of the cases ranges from 10^{-1} to 10^{5} m. They found that for these cases, the longitudinal dispersivity ranges from 10^{-2} to 10^{4} m. In conclusion, the variation in dispersivity reflects the influence of different degrees of aquifer heterogeneity at different field sites. They concluded that in general, longitudinal dispersivities in the lower part of the indicated range are more likely to be realistic for field applications. Therefore, the so-called *scale-dependency* of dispersivities ($\alpha_L = 0.1\,L$, where L is the traveled distance of the contaminant), determined from field data, should be reviewed critically. Furthermore, they indicated that there is a need for long-term, very large-scale experiments extending to several kilometres.

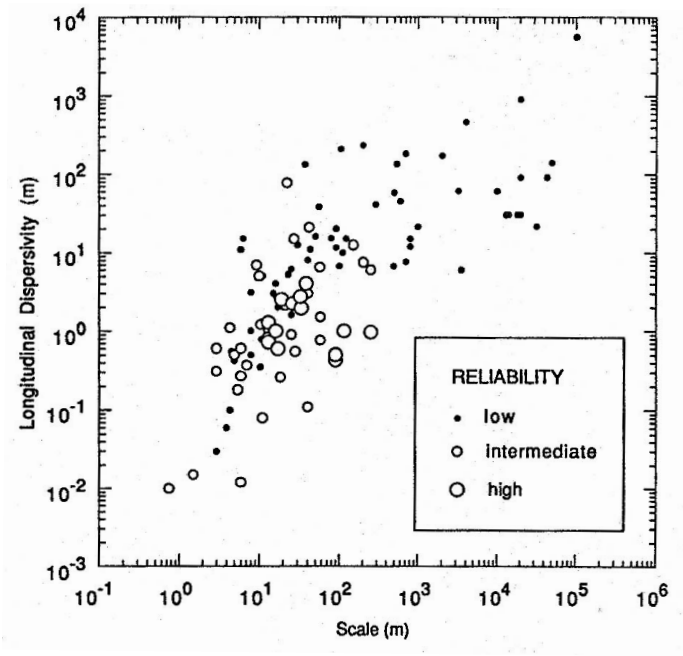

Figure 2.4: Longitudinal dispersivity versus scale with data classified by reliability (Gelhar *et al.*, 1992).

In contrast with some field sites in especially the U.S.A. (see, e.g. the cases in Gelhar *et al.*, 1992), the best estimates of the longitudinal dispersivities in Dutch and Belgian large-scale aquifer systems with Holocene and Pleistocene deposits of marine and fluviatile origin appear to yield rather small values. This observation is based on various case studies, such as Lebbe (1983), Kooiman *et al.* (1986), Stuyfzand (1991); Walraevens *et al.* (1993); and Oude Essink (1996).

For more information about hydrodynamic dispersion and values of dispersivities, see the lecture notes of Groundwater Modelling I (Oude Essink, 2000c).

2.5 Boussinesq approximation

The Boussinesq approximation[3] leads to a substantial simplification of the governing differential equations for salt water intrusion (and heat transport). The most simplified form is that changes in density can be neglected (in the balance equations such as the continuity eqn. 2.16) except from the buoyancy term ρg in Darcy's law in the z-direction (eqn. 2.10) (Holzbecher, 1998). As such, only the Darcian discharge couples the groundwater flow equation and the solute transport.

The Oberbeck-Boussinesq approximation is valid provided that the density variations (due to concentration or temperature changes) remain small to moderate in comparison with the reference density ρ throughout the considered hydrogeologic system (Nield &

[3]Actually, Oberbeck already considered this simplification in 1879, long before Boussinesq did (1903): as such, it is also called the Oberbeck-Boussinesq approximation.

Bejan, 1992). As such, for high concentration brines or high temperature gradients, the approximation is not valid anymore.

2.6 Brine groundwater

When high-concentration situations are considered, e.g. in rock salt formations, the mass density and the viscosity of the flowing fluid is obviously influenced by changes in concentration. In addition, theoretical studies have shown that Darcy's law and Fick's law have cross-coupling terms[4] (Hassanizadeh, 1986). Here, the equations are given for situations where temperature effects are negligible and the brine components do not react or adsorb (Hassanizadeh & Leijnse, 1988):

Equations for the fluid:

$$n_e \frac{\partial \rho}{\partial t} + \nabla \cdot (\rho q) = 0 \tag{2.25}$$

$$q = -\frac{\kappa}{\mu} \cdot (\nabla p - \rho g) - \mathsf{D}^f \cdot \nabla \omega \tag{2.26}$$

Equations for salt:

$$n_e \rho \frac{\partial \omega}{\partial t} + \rho q \cdot \nabla \omega + \nabla \cdot J = 0 \tag{2.27}$$

$$J = -\rho D \cdot \nabla \omega - \omega K^s \cdot (\nabla p - \rho g) \tag{2.28}$$

Equations of state (see also eqn. 2.6):

$$\rho = \rho_f e^{\beta(p-p_0)+\gamma\omega} \tag{2.29}$$

$$\mu = \mu_0(1 + \mathrm{m}(\omega)) \tag{2.30}$$

where

- ρ = fluid mass density ($M\,L^{-3}$),
- D^f = coefficient of density flow in the modified Darcy's equation ($L^2\,T^{-1}$),
- ω = salt mass fraction = ρ^s/ρ ($M\,M^{-1}$),
- ρ^s = mass concentration of pure salt component of the brine ($M\,L^{-3}$),
- J= diffusive-dispersive mass flux vector of the solute ($M\,L^{-2}\,T^{-1}$),
- K^s = pressure diffusion (-dispersion) coefficient in the modified Fick's equation ($M\,L^{-3}$),
- $\mathrm{m}(\omega) = 1.85\ \omega$ -4.10 ω^2 +44.50 ω^3 ($-$),
- $D = n_e D_{mol} + \alpha_T\,|q|\,\delta_{ij} + (\alpha_L - \alpha_T)\,\frac{q_i q_j}{|q|}$,
- $\delta_{ij} = 1$ if $i = j$ and $\delta_{ij} = 0$ if $i \neq j$.

[4]There is an analogy with heat and mass transfer (double-diffusive concevtion) from a cross-coupling term point of view. The so-called Soret effect refers to mass flux produced by a temperature gradient, and the Dufour effect refers to heat flux produced by a concentration gradient (Nield & Bejan, 1992).

Chapter 3

Freshwater head

3.1 Introduction

The relation between the pressure and the so-called piezometric head (or hydraulic head) is as follows (if the atmospheric pressure equals zero): piezometric head is the sum of the elevation head z and the pressure head h, see fig. 3.1:

$$\phi = \frac{p}{\rho g} + z \tag{3.1}$$

or

$$p = \rho g \left(\phi - z\right) \tag{3.2}$$

where

- ϕ = piezometric head (L),
- $h = \frac{p}{\rho g}$ = pressure head (L),
- z = elevation with respect to the reference level (L).

In most cases of groundwater flow, the piezometric head is used to determine the direction of flow and velocities. Applying Darcy's law expressed in piezometric heads as a representative for pressure is advantageous in many cases. However, one should be careful in coastal areas

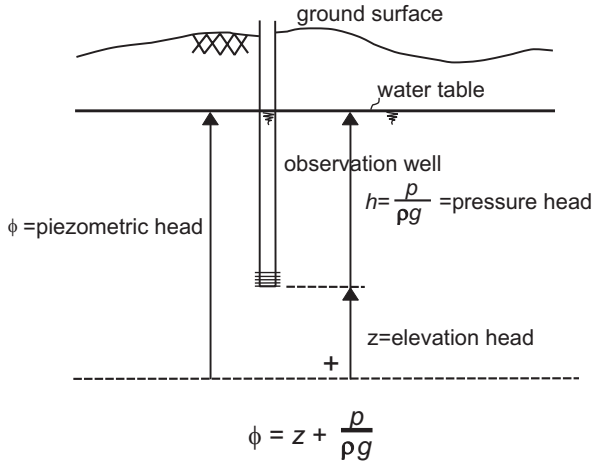

Figure 3.1: Definition of the piezometric head.

where density differences may occur. In these cases pressure should be used or, alternatively, piezometric heads should be adapted.

If a non-uniform density distribution is considered, the approach is somewhat different. In these cases, piezometric heads are often converted to pressures. It is also possible to convert piezometric heads of fresh, brackish and saline groundwater into so-called freshwater heads ϕ_f, in order to be able to compare levels with each other. The conversion into (fictive) freshwater head is as follows:

$$\phi_f = z + h_f \Longleftrightarrow \phi_f = z + \frac{p}{\rho_f g} \tag{3.3}$$

where

- ϕ_f = freshwater head of the observation well with respect to the reference level (L),
- z = elevation head (L),
- h_f=$\frac{p}{\rho_f g}$= pressure head (L),
- ρ_f = density of fresh water ($M\,L^{-3}$),
- g = acceleration of gravity ($L\,T^{-2}$).

Let us assume the presence of fresh, brackish and saline water in the subsoil (fig. 3.2) under hydrostatic conditions. If the screen of an observation well is positioned in the fresh water zone, the piezometric head as observed in the well, will be different from the observation in case the screen is in the saline zone. However this is only appearance. The difference is due to the fact that in the first case the column of water in the well is fresh, in the second case the pressure at the screen is represented by a (shorter) column of saline water with a higher density. Fig. 3.2 shows how observations may change, related to screen position and density profile. To make those levels with different densities comparable, they are expressed in a reference density, mostly of fresh water. First, the length of the column of water in the observation well is converted into a column of fresh water:

$$h_f = \frac{\rho}{\rho_f} h = (1 + \alpha) h \tag{3.4}$$

In this case the expression for the freshwater head (ϕ_f) becomes:

$$\phi_f = z + h_f \Longleftrightarrow \phi_f = z + \frac{\rho}{\rho_f} h \tag{3.5}$$

In this formula z is the elevation head, viz. the position of the screen, related to a reference level.

3.2 Horizontal flow

If horizontal flow is to be calculated, the pressure in a horizontal plane should be known. This means, from the pressure at the position of the screen (which can be obtained from

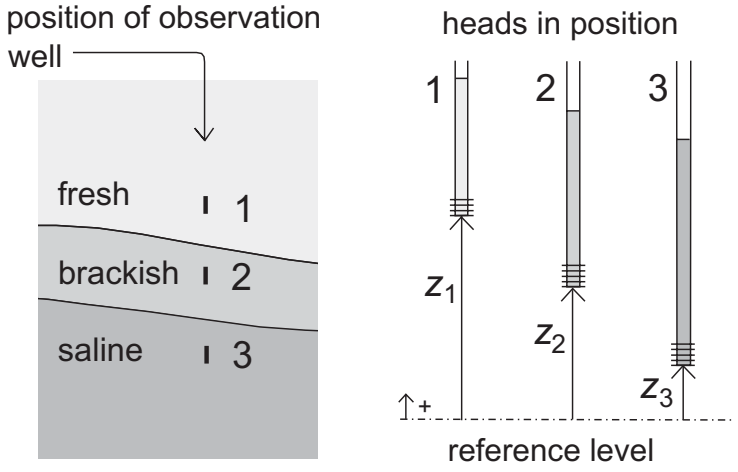

Figure 3.2: Piezometric heads at the same location, but at different depths with different densities.

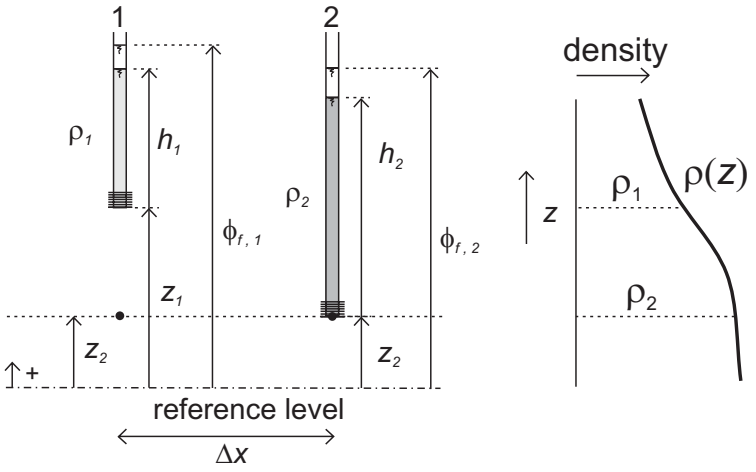

Figure 3.3: Determination of the horizontal flow component at the plane $z = z_2$.

the length of the water column), the pressure at that plane, e.g. at z_2, has to be computed (fig. 3.3):

$$p_1^{at\ z=z_2} = \rho_1 g h_1 + \int_{z_2}^{z_1} \rho(z) g dz \tag{3.6}$$

$$p_2^{at\ z=z_2} = \rho_2 g h_2 \tag{3.7}$$

$$\phi_{f,1}^{at\ z=z_2} = z_2 + \frac{\rho_1}{\rho_f} h_1 + \frac{1}{\rho_f g} \int_{z_2}^{z_1} \rho(z) g dz \tag{3.8}$$

$$\phi_{f,2}^{at\ z=z_2} = z_2 + \frac{\rho_2}{\rho_f} h_2 \tag{3.9}$$

To achieve this, the density profile should be known. Once pressure differences occur in that plane, there is groundwater flow, which can be computed applying Darcy's law:

$$q^{at\ z=z_2} \cong -k_x \frac{\phi_{f,2}^{at\ z=z_2} - \phi_{f,1}^{at\ z=z_2}}{\Delta x} \tag{3.10}$$

3.3 Vertical flow

To determine the magnitude of vertical flow in case of fresh and saline groundwater, one has to check whether or not the groundwater system is in a hydrostatic situation. Assume e.g. two observation wells at one location, one above an aquitard at z_1 and the other at z_2 below the aquitard with different densities (see fig. 3.4). If we had to check whether or not there is vertical flow through the aquitard, we could compute the pressure at e.g. z_p from the observation at the well screens z_1 and z_2, making use of the density distribution which should be known. For instance, the hydrostatic pressure at e.g. z_p is computed starting from the pressure at the screen at level z_1, which can be obtained from the observation. By integrating the specific weight ($\rho(z)gdz$) from z_1 to z_p, the pressure at level z_p can be determined. The same procedure accounts for the well screen z_2 up to z_p. In terms of freshwater heads:

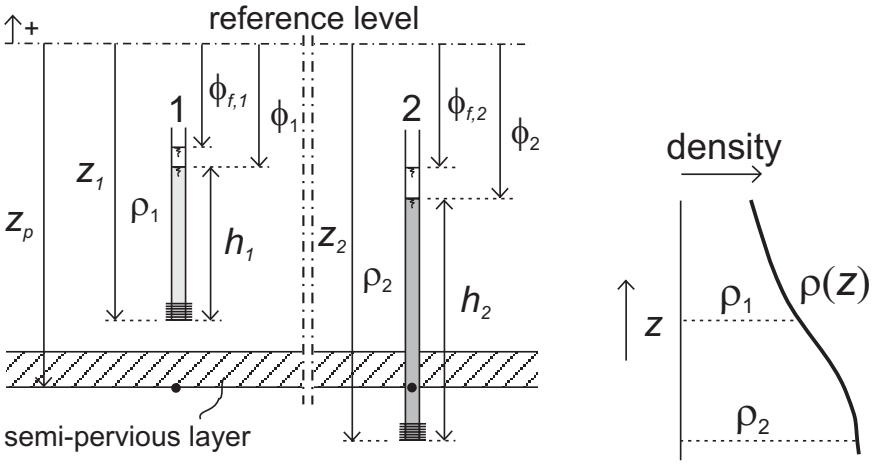

Figure 3.4: Determination of the vertical flow component. Note that the observations are located in one well.

$$\phi_{f,1}^{at\ z=z_p} = z_p + \frac{\rho_1}{\rho_f} h_1 + \frac{1}{\rho_f g} \int_{z_p}^{z_1} \rho(z) g dz \tag{3.11}$$

$$\phi_{f,2}^{at\ z=z_p} = z_p + \frac{\rho_2}{\rho_f} h_2 - \frac{1}{\rho_f g} \int_{z_2}^{z_p} \rho(z) g dz \tag{3.12}$$

By comparing the result of the computations for $\phi_{f,1}$ and $\phi_{f,2}$ at the position z_p, it can be deduced whether there is vertical flow and the direction, upward or downward. The magnitude and direction follows from Darcy's law:

$$q^{at\ z=z_p} \cong \frac{\phi_{f,2}^{at\ z_p} - \phi_{f,1}^{at\ z_p}}{c} \tag{3.13}$$

a. if $\phi_{f,2}^{\mathrm{at}\ z_p} < \phi_{f,1}^{at\ z_p}$ then downward flow occurs,

b. if $\phi_{f,2}^{\mathrm{at}\ z_p} = \phi_{f,1}^{at\ z_p}$ then no vertical flow occurs,

c. if $\phi_{f,2}^{\mathrm{at}\ z_p} > \phi_{f,1}^{at\ z_p}$ then upward flow occurs.

Example 3.1: is there vertical flow through the aquitard?

Consider the following situation in fig. 3.5. As the density in the two observations differs, it cannot be deduced directly that the groundwater flow through the aquitard is downwards. First, the piezometric heads must be converted to freshwater heads. Suppose that the vertical flow is downwards: this means that the aquitard contains fresh groundwater, $\rho = 1000$ kg/m^3. The freshwater heads are as follows:

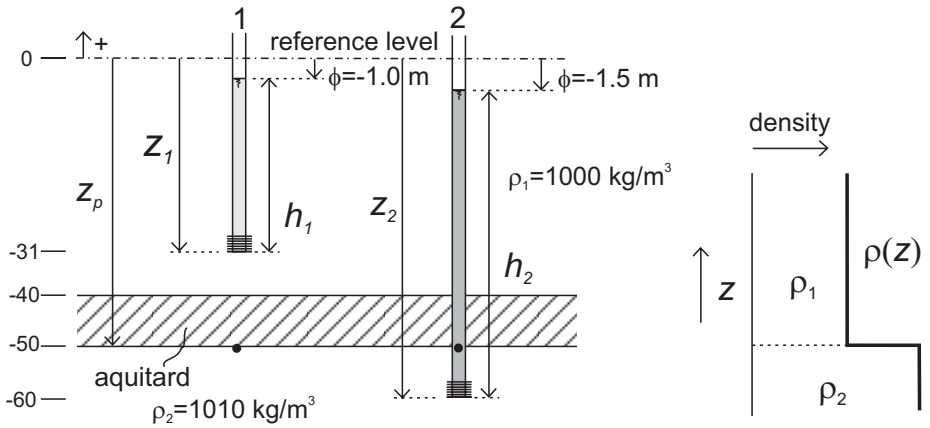

Figure 3.5: Vertical flow through an aquitard.

$$\phi_{f,1}^{z=-50} = -50 + \frac{1000}{1000}30 + \frac{1}{1000g}\int_{-50}^{-31} 1000g\,dz \tag{3.14}$$

$$= -50 + 30 + 19 = -1.0 \text{ m} \tag{3.15}$$

$$\phi_{f,2}^{z=-50} = -50 + \frac{1010}{1000}58.5 - \frac{1}{1000g}\int_{-60}^{-50} 1010g\,dz \tag{3.16}$$

$$= -50 + 59.085 - 1.01(-50 + 60) = -1.015 \text{ m} \tag{3.17}$$

Now, it can be deduced that there is a small groundwater flow downwards. The supposition that the aquitard contains fresh groundwater is okay. However, if the result of the calculation would indicate upward flow, the supposition is wrong. Then, the aquitard is supposed to contain saline groundwater. After recalculating the freshwater heads, the following two situations can occur:

1. the flow appears to be upward, which means that the aquitard indeed contains saline groundwater.
2. the flow is now downwards, which means that the supposition of a saline aquitard is wrong. As such, the conclusion is that the interface between fresh and saline groundwater is positioned **in** the aquitard, and there is no vertical flow.

Exercise 3.1: vertical flow through the aquitard ?

Does vertical flow occur through the resistance layer as schematised in the situation given in fig. 3.6 ? Note that both observation wells are located at one place.

Exercise 3.2: Determination of vertical groundwater flow through the aquitards.

Calculate the vertical groundwater flow through the two aquitards (e.g. clayey layers) for the schematisation as given in fig. 3.7.

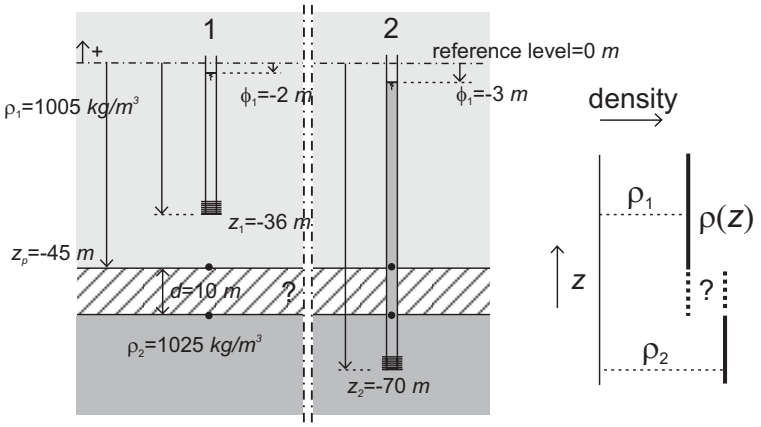

Figure 3.6: Exercise 3.1: vertical flow through the aquitard ?

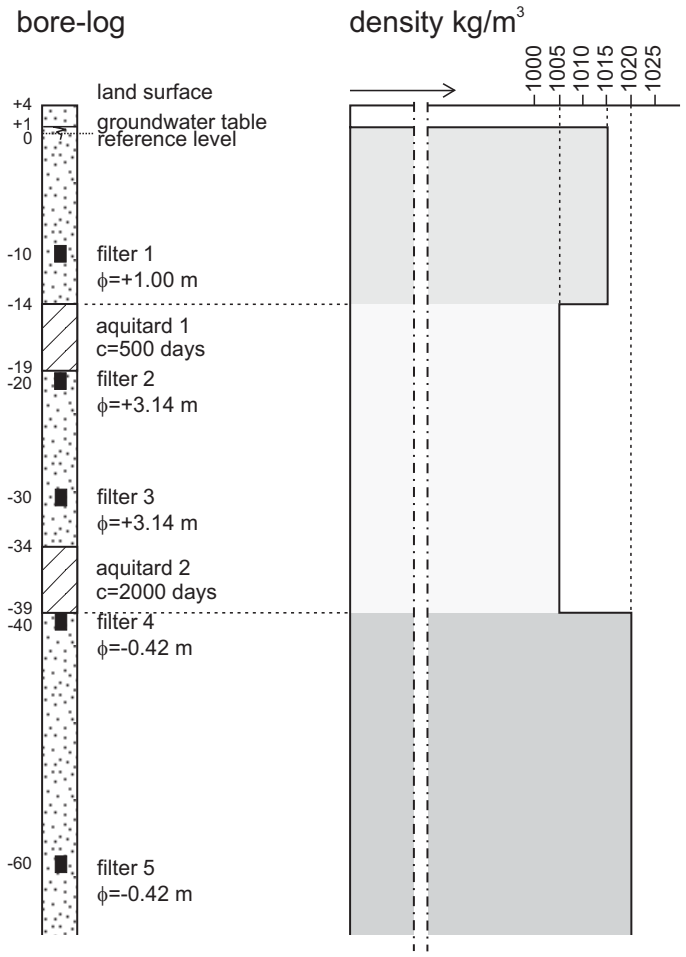

Figure 3.7: Exercise 3.2: determination of vertical groundwater flow through the aquitards (van Dam, 1992).

Chapter 4

The concept of a fresh-saline interface

Although the differences in density appear to be small, they have a significant effect on piezometric heads and thus on the groundwater system. In many approaches, only fresh groundwater is considered in coastal aquifers, so no density differences are taken into account. In reality, however, density flow may highly affect groundwater flow in these coastal aquifers. In this chapter, a straightforward concept is applied which takes into account density flow in a simple way: the interface approximation based on the Badon Ghijben-Herzberg principle.

4.1 Badon Ghijben-Herzberg principle

The Badon Ghijben (1889)-Herzberg (1901) principle[1] (BGH) describes the position of an interface between fresh and saline groundwater (fig. 4.1). Eqn. 4.2 represents the Badon Ghijben-Herzberg principle:

pressure saline groundwater=pressure fresh groundwater

$$\rho_s H g = \rho_f (H + h) g \Longleftrightarrow \rho_s H = \rho_f H + \rho_f h \tag{4.1}$$

$$h = \frac{\rho_s - \rho_f}{\rho_f} H \Longleftrightarrow h = \alpha H \tag{4.2}$$

[1] In 1889, the Dutchman Badon Ghijben, who did research for the public water supply in a dune area for the city of Amsterdam and in 1901, independently, the German Herzberg developed the equilibrium equation for this phenomenon in groundwater. Note that the American of French birth Du Commun already referred to this principle in 1828.

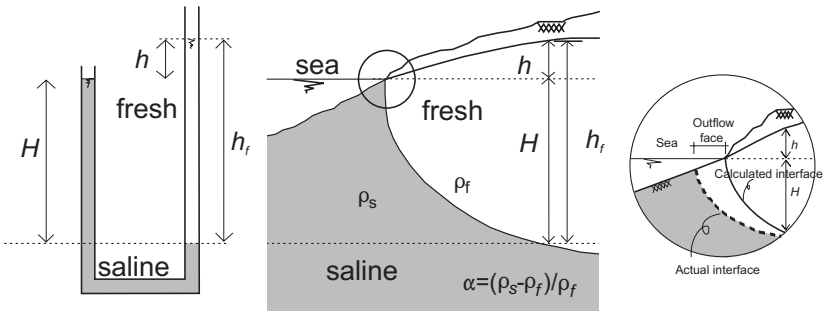

Figure 4.1: The Badon Ghijben-Herzberg principle: a fresh-salt interface in an unconfined coastal aquifer.

For ρ_s=1025 kg/m^3 and ρ_f=1000 kg/m^3, the relative density difference $\alpha = 40$. The equation is correct if there is only horizontal flow in the fresh water zone and the saline water is stagnant. Though the position of the interface is not correct at the outflow zone, the use of the equation still gives a rather good approximation of the real situation.

The Badon Ghijben-Herzberg principle was originally formulated for the situation that the transition zone between fresh and saline groundwater is only a small percentage of the thickness of the saturated freshwater body (thus, mostly in the order of several metres). Under these circumstances, a fresh-salt interface should be applied. This situation occurs in unspoiled sand-dune areas or (coral) islands, where the freshwater lens evolves by natural groundwater recharge. In addition, the principle can only be applied in case the vertical flow component in the freshwater body is negligible. In reality, however, such systems seldom occur. Most systems are not hydrostatic (the Dupuit-Forcheimer condition[2] should not be applied), and as a result, the formula leads to (small) errors, especially in the vicinity of the outflow zone. Nevertheless, though the position of the interface is not completely correct, the use of the equation still gives a rather good approximation of the real situation.

As a matter of fact, the principle should only be applied under the following conditions:

- the aquifer is homogeneous,
- hydrodynamic dispersion is negligible,
- vertical flow in the aquitard, horizontal flow is negligible,
- horizontal flow in the aquifer, vertical flow is negligible,
- saline groundwater is at rest: $q_s = 0$.

In the following, analytical formulae for the interface between fresh and saline groundwater are presented for unconfined, confined and semi-confined aquifers, illustrated with some simple examples. For more information, see van Dam (1983, 1992). These analytical solutions increases the understanding of groundwater flow and fresh groundwater resources in coastal areas.

4.2 Unconfined aquifer (1D situation)

Freshwater lenses have evolved in unconfined (phreatic, water table) aquifers due to natural groundwater recharge (see fig. 4.2). The three governing equations are (van Dam, 1992):

$$\text{(I) Darcy:} \qquad q = -k(H+h)\frac{dh}{dx} \tag{4.3}$$

$$\text{(II) Continuity:} \qquad dq = f\,dx \tag{4.4}$$

$$\text{(III) BGH:} \qquad h = \alpha H \tag{4.5}$$

where

[2] Dupuit indicated that for flow towards a well in the center of a circular island in a unconfined aquifer the following assumptions hold: (1) the flow is horizontal, (2) the velocity over the depth of flow is uniform, and (3) the velocity at the free surface is a derivative of the radius towards the well instead of the flow path towards the well.

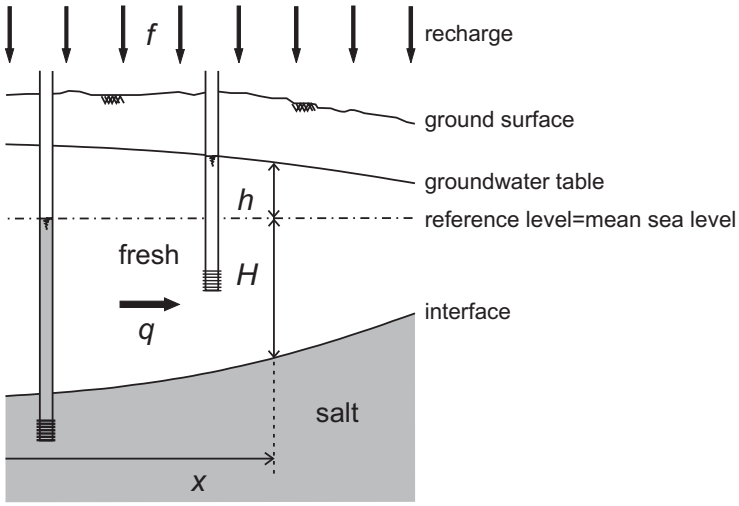

Figure 4.2: The fresh-salt interface in an unconfined aquifer.

- q = groundwater flow per unit coast length ($L^2\,T^{-1}$),
- H = depth of the fresh-salt interface below mean sea level (L),
- f = natural groundwater recharge ($L\,T^{-1}$),
- x = horizontal position (distance from the axis of symmetry) (L),
- α = relative density difference $(\rho_s - \rho_f)/\rho_f$ $(-)$,
- h = piezometric head of fresh water with respect to mean sea level (L).

Combining the equations gives:

$$dq = f\,dx \Longleftrightarrow q = fx + C_1 \tag{4.6}$$

$$-k(H+h)\frac{dh}{dx} = fx + C_1 \Longleftrightarrow -k(H+\alpha H)\alpha\frac{dH}{dx} = fx + C_1 \tag{4.7}$$

$$H\,dH = -\frac{fx + C_1}{k(1+\alpha)\alpha}dx \Longleftrightarrow \frac{1}{2}H^2 = \frac{-\frac{1}{2}fx^2 - C_1x + C_2}{k(1+\alpha)\alpha} \tag{4.8}$$

The analytical formulae are as follows:

$$H = \sqrt{\frac{-fx^2 - 2C_1x + 2C_2}{k(1+\alpha)\alpha}} \tag{4.9}$$

$$h = \alpha H \tag{4.10}$$

$$q = fx + C_1 \tag{4.11}$$

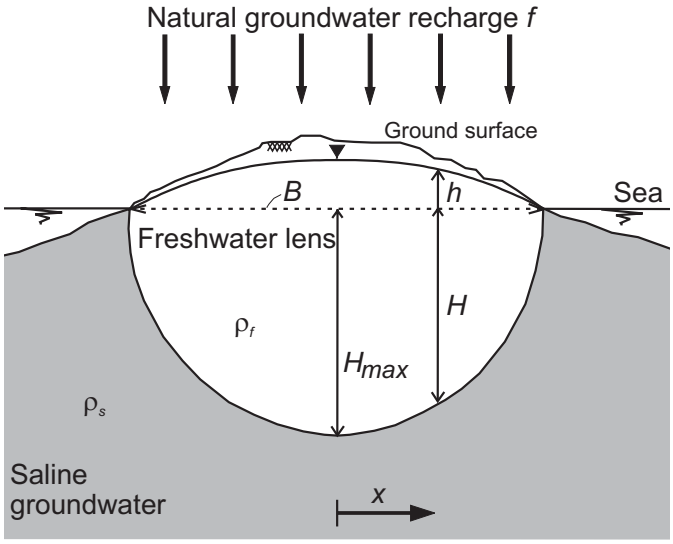

Figure 4.3: The fresh-salt interface in an elongated island.

Example 4.1: elongated island

A one-dimensional phreatic groundwater flow is considered through an elongated island or a strip of sand-dunes where a freshwater lens has evolved due to natural groundwater recharge (see fig. 4.3). The boundary conditions are:

$$x = 0 : q = 0 \longrightarrow C_1 = 0 \tag{4.12}$$

$$x = 0.5B : H = 0 \longrightarrow C_2 = fB^2/8 \tag{4.13}$$

The depth of the fresh-salt interface becomes:

$$H = \sqrt{\frac{f(0.25\,B^2 - x^2)}{k\,(1+\alpha)\,\alpha}} \tag{4.14}$$

where B=width of sand-dunes (L). As can be seen, the depth of the fresh-salt interface H is proportional to the width B of the sand-dune area. The volume of water in the freshwater lens, which has the shape of an ellipse[3], is equal to:

$$V = \frac{1}{4}\pi(1+\alpha)H_{max}Bn_e \tag{4.15}$$

Note that the α in $(1+\alpha)$ accounts for the volume of water in the phreatic part of the lens. The characteristic time $\mathcal{T}$ is defined as:

$$\mathcal{T} = \frac{\text{volume of water in lens}}{\text{inflow of water}} = \frac{\frac{1}{4}\pi(1+\alpha)H_{max}Bn_e}{fB} \tag{4.16}$$

$$\mathcal{T} = \frac{\pi n_e B}{8}\sqrt{\frac{(1+\alpha)}{k\,f\,\alpha}} \tag{4.17}$$

For example, if B=2000 m, α=0.025, k=10 m/day and f=1 mm/day, then the deepest position of the interface H_{max} (in the middle of the lens) is 62.5 m and the highest phreatic groundwater level 1.56 m. With a porosity n_e equal to 0.35, the volume V=52,396 m^3/m' and $\mathcal{T}$=47.8 $year$. This means that, without outflow of groundwater at the edges, it takes 47.8 years before the entire freshwater lens would be filled.

[3]The surface of an ellipse is equal to $\frac{1}{4}\pi ab$, where a and b are the two main diametres. If a=B and b=$2H_{max}$, the surface of the entire ellipse becomes $\frac{1}{2}\pi H_{max}B$.

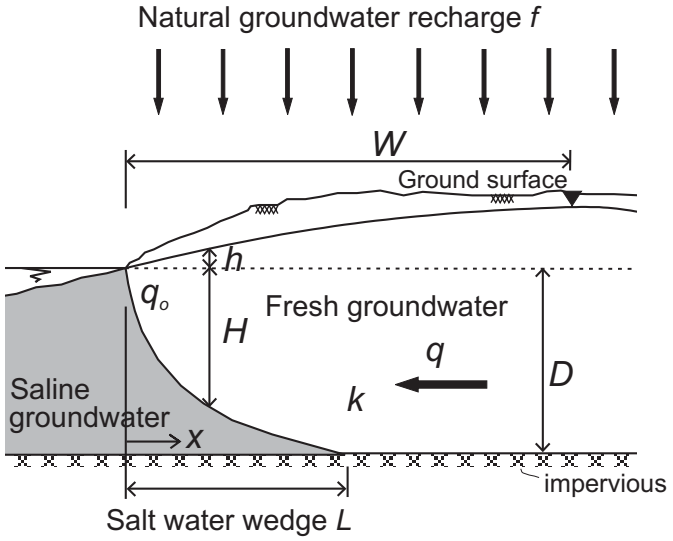

Figure 4.4: Salt water wedge in a shallow unconfined aquifer.

Example 4.2: salt water wedge

In many shallow phreatic aquifers, the freshwater body originally touches the impervious base, thus creating a salt water wedge of length L, see fig. 4.4. The corresponding boundary conditions are:

$$x = 0 : q = q_0 \qquad (q_0 = -fW) \longrightarrow C_1 = q_0 \tag{4.18}$$

$$x = 0 : H = 0 \longrightarrow C_2 = 0 \tag{4.19}$$

where

- W = width of the coastal aquifer up to the water divide (L),
- q_0 = natural groundwater outflow at the coastline x=0 (negative sign) ($L^2\,T^{-1}$).

Saline groundwater is stagnant. The length of the salt water wedge L is:

$$x = L : H = D \tag{4.20}$$

where D = thickness of the aquifer (L). The equations of this case become:

$$\begin{aligned} H &= \sqrt{\frac{-f\,x^2 - 2\,q_0\,x}{k\,(1+\alpha)\,\alpha}} \\ h &= \alpha\,H \\ q &= f\,x + q_0 \\ q_0 &= -fW \\ L &= -\frac{q_0}{f} - \sqrt{(\frac{q_0}{f})^2 - \frac{k}{f}\,D^2\,(1+\alpha)\alpha} \end{aligned} \tag{4.21}$$

For example, if W=3000 m, f=1 mm/day, α=0.020, k=20 m/day and D=50 m, then the length of the salt water wedge L is 175.1 m.

4.3 Unconfined aquifer (axial-symmetric situation)

The three equations for the axial-symmetric situation, that is a circular sandy island with recharge, are (van Dam, 1992):

$$\text{(I) Darcy:} \qquad Q = -2\pi r k(H+h)\frac{dh}{dr} \tag{4.22}$$

$$\text{(II) Continuity:} \qquad dQ = f2\pi r dr \Longleftrightarrow Q = f\pi r^2 + C_1 \tag{4.23}$$

$$\text{(III) BGH:} \qquad h = \alpha H \Longleftrightarrow \frac{dh}{dr} = \alpha\frac{dH}{dr} \tag{4.24}$$

Combining these equations gives:

$$-2k(H+\alpha H)\alpha\frac{dH}{dr} = fr + \frac{C_1}{\pi r} \tag{4.25}$$

$$HdH = -\frac{fr + \frac{C_1}{\pi r}}{2k(1+\alpha)\alpha}dr \Longleftrightarrow \frac{1}{2}H^2 = \frac{-\frac{1}{2}fr^2 - \frac{C_1}{\pi}\ln r + C_2}{2k(1+\alpha)\alpha} \tag{4.26}$$

$$H = \sqrt{\frac{-fr^2 - \frac{2C_1}{\pi}\ln r + 2C_2}{2k(1+\alpha)\alpha}} \tag{4.27}$$

Example 4.3: sandy island

The boundary conditions for a sandy circular island are:

$$r = 0 : Q = 0 \longrightarrow C_1 = 0 \tag{4.28}$$

$$r = R : H = 0 \longrightarrow C_2 = 0.5fR^2 \tag{4.29}$$

Eqn. 4.27 gives, together with these boundary conditions, the formula for the axial-symmetric situation:

$$H = \sqrt{\frac{f(R^2 - r^2)}{2\,k\,(1+\alpha)\,\alpha}} \tag{4.30}$$

where

- R = radius of the sandy island (L),
- r = distance from the centre of the circular island (L).

For example, if R=3000 m, α=0.02 (ρ_s=1020 kg/m^3), k=25 m/day and f=0.5 mm/day, then the deepest position of the interface H_{max} (at r=0 m) is 66.4 m and the highest groundwater level 1.33 m. The content of water in this freshwater lens[4], is equal to:

$$I = \frac{2}{3}\pi(1+\alpha)H_{max}R^2 n_e \tag{4.31}$$

Note that the α in $(1+\alpha)$ accounts for the volume of water in the phreatic part of the lens. The characteristic time $\mathcal{T}$ is defined as:

$$\mathcal{T} = \frac{\text{volume of water in lens}}{\text{inflow of water}} = \frac{\frac{2}{3}\pi(1+\alpha)H_{max}R^2 n_e}{f\pi R^2} \tag{4.32}$$

$$\mathcal{T} = \frac{\pi\sqrt{2}n_e R^3}{3}n_e\sqrt{\frac{f\,(1+\alpha)}{k\,\alpha}} \tag{4.33}$$

For example, if R=5000 m, α=0.02, k=50 m/day and f=500 $mm/year$, then the deepest position of the interface H_{max} (in the middle of the lens) is 129.5 m. With a porosity n_e equal to 0.35, the content I=2.42 $\times$ 10^9 m^3 and $\mathcal{T}$=61.6 $year$. This means that, without outflow of groundwater at the edges, it takes 61.6 years before the entire freshwater lens would be filled.

[4]The content of a ellipsoid is equal to $\frac{4}{3}\pi abc$, where a, b and c are the three main radia. If a=H_{max} and b=c=R, than the content of the ellipsoid becomes $\frac{4}{3}\pi H_{max}R^2$.

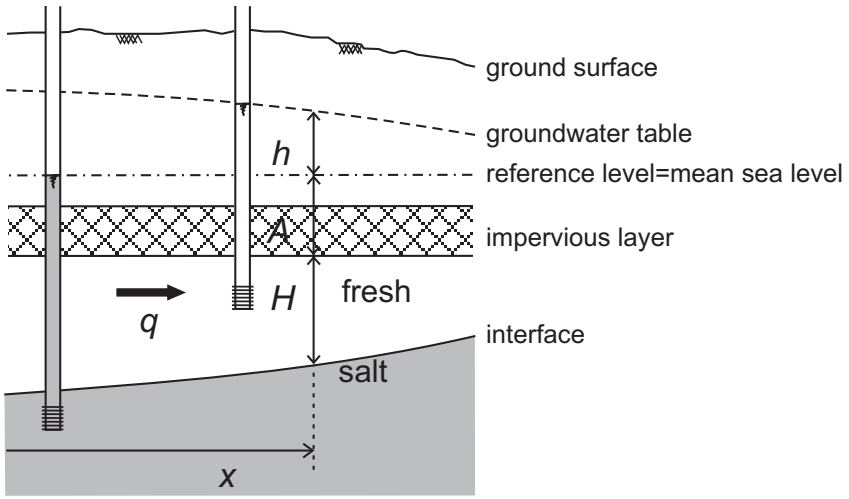

Figure 4.5: The fresh-salt interface in a confined aquifer.

4.4 Confined aquifer (1D situation)

A confined aquifer is enclosed by two aquicludes. The three equations involved are (see fig. 4.5):

$$\text{(I) Darcy:} \qquad q = -kH\frac{dh}{dx} \tag{4.34}$$

$$\text{(II) Continuity:} \qquad q = q_0 \tag{4.35}$$

$$\text{(III) BGH:} \qquad h = \alpha(H + A) \tag{4.36}$$

where

- q_0 = fresh groundwater flow from recharge in the uplands, per unit coast length ($L^2\,T^{-1}$),
- A = height of the sea level with respect to the top of the aquifer (L).

Combining the equations:

$$-kH\frac{dh}{dx} = q_0 \Longleftrightarrow HdH = -\frac{q_0}{k\alpha}dx \tag{4.37}$$

$$\frac{1}{2}H^2 = -\frac{q_0 x}{k\alpha} + C \Longleftrightarrow H = \sqrt{-\frac{2q_0 x}{k\alpha} + 2C} \tag{4.38}$$

Example 4.4: salt water wedge in a confined aquifer

The freshwater body touches the impervious base, thus creating a salt water wedge (fig. 4.6). The corresponding boundary condition is:

$$x = 0 : H = 0 \longrightarrow C = 0 \tag{4.39}$$

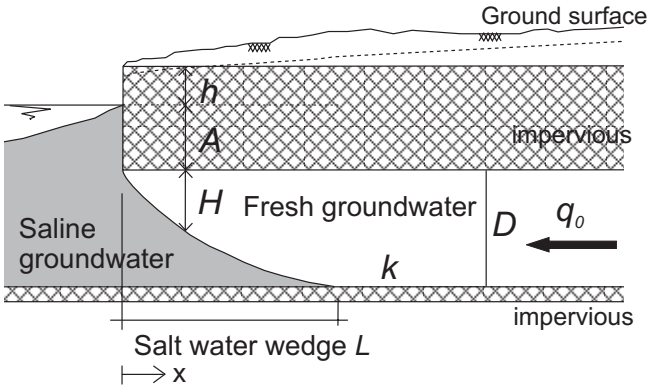

Figure 4.6: The salt water wedge in a confined coastal aquifer.

The following formula can be applied to determine the length of the salt water wedge L:

$$x = L : H = D \tag{4.40}$$

Inserting these two equations in eqn. 4.38 gives:

$$\begin{aligned} H &= \sqrt{\frac{-2\,q_0\,x}{k\,\alpha}} \\ h &= \alpha\,(H + A) \\ q &= q_0 \\ L &= -\frac{k\,D^2\,\alpha}{2\,q_0} \end{aligned} \tag{4.41}$$

where

- D = saturated thickness of the confined aquifer (L).

As can be seen, the length of the salt water wedge is determined (inversely proportional) by the fresh groundwater flow q_0, since all other parameters remain constant. The fresh groundwater flow could differ due to changes in recharge in the uplands. Possible causes of reduced recharge are changes in the hydrologic regime (e.g. climate change) or human activities such as groundwater extraction. For example, if D=40 m, α=0.025, k=25 m/day and q=-fW= -1 mm/day $\times$ 2000 m=-2 m^2/day, then the length of the salt water wedge L is 250 m.

Intermezzo II: the outflow of fresh groundwater

In theory, the depth of the interface H below the impervious aquitard at x=0 equals zero (see eqn. 4.39 and fig. 4.6). Based on eqn. 4.34, this means that the gradient of the freshwater head must be infinite large in order to obtain an outflow q_0. In reality, this situation does not occur. In fact, there exists a value for H >0 to assure outflow of fresh water towards the sea.

Glover (1959) obtained an analytical solution for the exact position of the interface, which causes a shift of the interface in x-direction (fig. 4.7):

$$H = \sqrt{-\frac{2q_0}{k\alpha}\left(x - \frac{q_0}{2k\alpha}\right)} \tag{4.42}$$

$$\text{for } x = 0 : H_0 = \frac{q_0}{k\alpha} \tag{4.43}$$

The outflow length x_0 is as follows:

$$\text{for } H = 0 : x_0 = \frac{q_0}{2k\alpha} \tag{4.44}$$

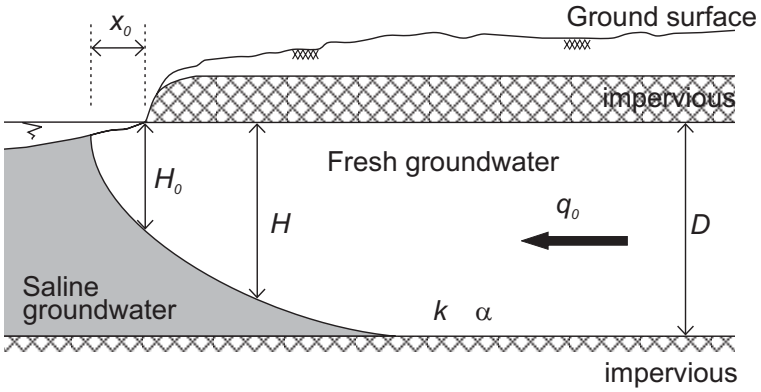

Figure 4.7: The outflow of fresh groundwater in a confined aquifer.

4.5 Confined aquifer (axial-symmetric situation)

The three equations for the axial-symmetric situation, that is a circular sandy island with a circular line of injection wells, are (van Dam, 1992):

$$\text{(I) Darcy:} \qquad Q = -2\pi r k H \frac{dh}{dr} \tag{4.45}$$

$$\text{(II) Continuity:} \qquad Q = Q_0 \tag{4.46}$$

$$\text{(III) BGH:} \qquad h = \alpha(H + A) \Longleftrightarrow \frac{dh}{dr} = \alpha \frac{dH}{dr} \tag{4.47}$$

Combining these equations gives:

$$-2\pi r k H \alpha \frac{dH}{dr} = Q_0 \Longleftrightarrow H dH = \frac{-Q_0}{2\pi k \alpha r} dr \tag{4.48}$$

$$\frac{1}{2}H^2 = \frac{-Q_0 \ln r}{2\pi k \alpha} + C \Longleftrightarrow H = \sqrt{\frac{-Q_0 \ln r}{\pi k \alpha} + 2C} \tag{4.49}$$

4.6 Semi-confined aquifer (1D situation)

A semi-confined (leaky) aquifer is bounded by aquitards (semi-pervious layers). The aquitard has a hydraulic resistance which suppresses vertical groundwater flow. The three equations involved are (see fig. 4.8) (van Dam, 1992):

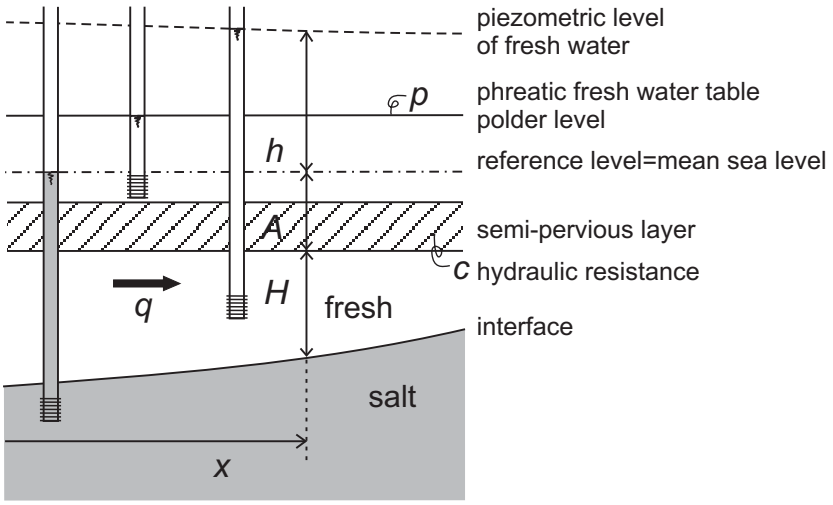

Figure 4.8: The fresh-salt interface in a semi-confined aquifer.

$$\text{(I) Darcy:} \quad q = -kH\frac{dh}{dx} \Longleftrightarrow \frac{dq}{dx} = -k\left(H\frac{d^2h}{dx^2} + \frac{dH}{dx}\frac{dh}{dx}\right) \tag{4.50}$$

$$\text{(II) Continuity:} \quad dq = -\frac{h-p}{c}dx \Longleftrightarrow \frac{dq}{dx} = -\frac{h-p}{c} \tag{4.51}$$

$$\text{(III) BGH:} \quad h = \alpha(H+A) \Longleftrightarrow \frac{dh}{dx} = \alpha\frac{dH}{dx} \Longleftrightarrow \frac{d^2h}{dx^2} = \alpha\frac{d^2H}{dx^2} \tag{4.52}$$

where c the hydraulic resistance of the aquitard (T): $c = d/k_v$, where d is thickness of the aquitard (L) and k_v ($L\,T^{-1}$) is the vertical hydraulic conductivity. Combining the equations gives:

$$-k\left(H\alpha\frac{d^2H}{dx^2} + \frac{dH}{dx}\alpha\frac{dH}{dx}\right) = -\frac{\alpha(H+A)-p}{c} \tag{4.53}$$

$$H\frac{d^2H}{dx^2} + \left(\frac{dH}{dx}\right)^2 - \frac{H+A-\frac{p}{\alpha}}{kc} = 0 \tag{4.54}$$

$$H\frac{d^2H}{dx^2} + \left(\frac{dH}{dx}\right)^2 - \frac{H-E}{kc} = 0, \qquad \text{where} \quad E = \frac{p}{\alpha} - A \tag{4.55}$$

There exist 13 different analytical solutions for this problem (van Dam & Sikkema, 1982).

Example 4.5: equilibrium depth

One of these 13 solutions is the solution for the equilibrium depth:

$$H = E; \quad h = \alpha(E+A) = p; \quad q = 0 \tag{4.56}$$

For the other 12 solutions, the reader is referred to van Dam & Sikkema (1982) and Sikkema & van Dam (1982).

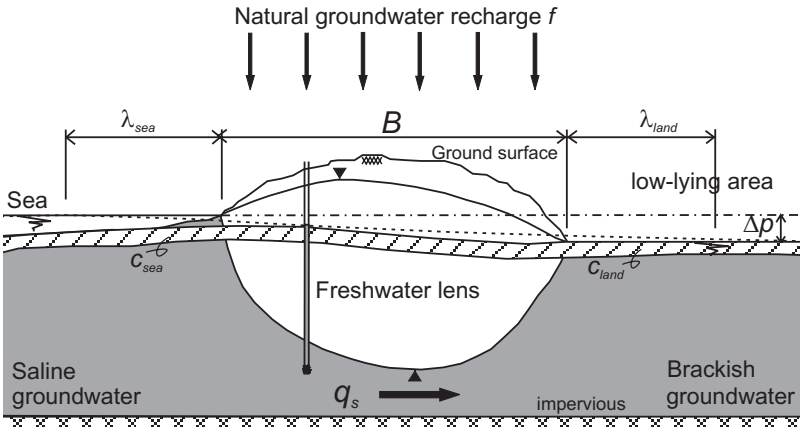

Figure 4.9: Salt water intrusion in a semi-confined aquifer.

Example 4.6: flow of saline groundwater underneath a lens

Up till now, saline groundwater is supposed to be stagnant. In this situation, however, saline groundwater is flowing. The flow of saline groundwater q_s underneath a freshwater lens depends on the characteristic length λ van Dam (1993), see fig. 4.9. An approximation of the saline groundwater flow q_s is:

$$q_s = kD_s \frac{\Delta p}{\lambda_{sea} + B + \lambda_{land}} \tag{4.57}$$

where

- kD_s = average transmissivity of the aquifer between impervious base and the freshwater lens ($L^2\,T^{-1}$),
- c_{sea}, c_{land} = hydraulic resistance of the aquitard at the seaside and the inland side respectively (T),
- λ_{sea}, $\lambda_{land} = \sqrt{kD_s c_{sea}}$, $\sqrt{kD_s c_{land}}$ = the characteristic lengths of the formation at the seaside and the inland side respectively (L),
- B = width of the sand-dunes (L).

Obviously, as the characteristic lengths are often in the order of kilometres, the aquitards considerably effect the flow of saline groundwater q_s.

4.7 Semi-confined aquifer (axial-symmetric situation)

The three equations for the axial-symmetric situation for a semi-confined aquifer are:

$$\text{(I) Darcy:} \qquad Q = -2\pi r k H \frac{dh}{dr} \tag{4.58}$$

$$\frac{dQ}{dr} = -2\pi k \left(rH\frac{d^2h}{dr^2} + r\frac{dH}{dr}\frac{dh}{dr} + H\frac{dh}{dr} \right) \tag{4.59}$$

$$\text{(II) Continuity:} \qquad dQ = -2\pi r \frac{h-p}{c} dr \tag{4.60}$$

$$\frac{dQ}{dr} = -2\pi r \frac{h-p}{c} \tag{4.61}$$

(III) BGH: $$h = \alpha(H+A) \tag{4.62}$$

$$\frac{dh}{dr} = \alpha\frac{dH}{dr} \Longleftrightarrow \frac{d^2h}{dr^2} = \alpha\frac{d^2H}{dr^2} \tag{4.63}$$

Combining the equations gives:

$$-2\pi k\left(rH\alpha\frac{d^2H}{dr^2} + r\frac{dH}{dr}\alpha\frac{dH}{dr} + H\alpha\frac{dH}{dr}\right) = -2\pi r\frac{\alpha(H+A)-p}{c} \tag{4.64}$$

$$rH\frac{d^2H}{dr^2} + r\left(\frac{dH}{dr}\right)^2 + H\frac{dH}{dr} - r\frac{(H+A)-\frac{p}{\alpha}}{kc} = 0 \tag{4.65}$$

$$rH\frac{d^2H}{dr^2} + r\left(\frac{dH}{dr}\right)^2 + H\frac{dH}{dr} - r\frac{H-E}{kc} = 0, \quad \text{where} \quad E = \frac{p}{\alpha} - A \tag{4.66}$$

This equation cannot be solved easily. However, one simple solution is the solution for the equilibrium depth (see also eqn. 4.56):

$$H = E; \quad h = \alpha(E+A) = p; \quad Q = 0 \tag{4.67}$$

4.8 Evolution of a freshwater lens in a phreatic aquifer

There exist analytical solutions for the evolution of a freshwater lens in a phreatic aquifer. Boekelman & Grakist (1973), Boekelman (1998) considered a transient interface between fresh and saline groundwater in a phreatic aquifer, for both a two-dimensional as well as an axial-symmetric situation.

4.8.1 Two-dimensional situation

For the two-dimensional situation, an elongated island or strip of sand-dunes is considered with a freshwater lens evolving due to natural groundwater recharge (see fig. 4.10). The governing equations for this situation are:

(I) Darcy: $$q = -k(H+h)\frac{\partial h}{\partial x} \tag{4.68}$$

(II) Continuity: $$\frac{\partial q}{\partial x} = f - n_e\frac{\partial H}{\partial t} - n_e\frac{\partial h}{\partial t} \tag{4.69}$$

(III) BGH: $$h = \alpha H \tag{4.70}$$

where n_e is the effective porosity $(-)$. Note that in eqn. 4.69 two transient terms are considered. Combination of these three equations gives:

$$\frac{2n_e}{k\alpha}\frac{\partial H}{\partial t} - \frac{2f}{k\alpha(1+\alpha)} - \frac{\partial^2 H^2}{\partial x^2} = 0 \tag{4.71}$$

This is not a linear differential equation. Hence, the equation cannot be solved analytically. However, an approximate solution is possible assuming that at each moment in time the

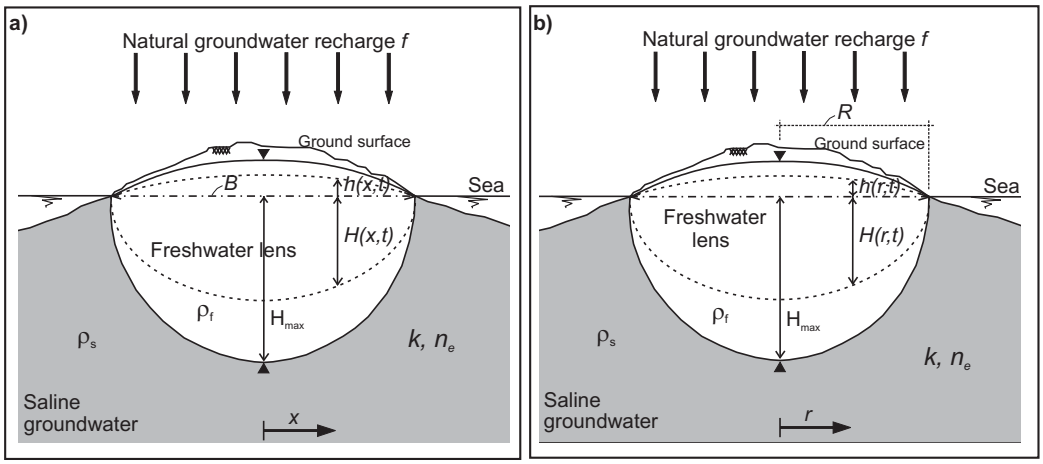

Figure 4.10: The transient interface in: **a)** an elongated island (2D) and **b)** a circular island (3D).

shape of the lens is conformable to the shape of the lens in the steady-state situation ($t \rightarrow \infty$). If so, the only difference is a time dependent factor $F(t)$. This results in eqn. 4.72:

$$H(x,t) = F(t)\sqrt{\frac{f(0.25B^2 - x^2)}{k(1+\alpha)\alpha}} \tag{4.72}$$

$$\text{for } t = \infty : F(t) = 1 \tag{4.73}$$

$$\text{for } t = 0 : F(t) = 0 \tag{4.74}$$

If eqn. 4.72 is introduced into eqn. 4.71, the best overall solution is found by integrating between $x = 0$ and $x = 0.5B$. This leads to a solution for $F(t)$ which satisfies the differential equation on an average. This leads to the following formula for $F(t)$ (Boekelman, 1998):

$$F(t) = \tanh(t/\tau) \tag{4.75}$$

where

$$\tau = \frac{\pi n_e B}{8}\sqrt{\frac{(1+\alpha)}{kf\alpha}} \tag{4.76}$$

The factor τ is a time constant (unit T) which contains the physical characteristics of the area. Note that τ equals the characteristic time $\mathcal{T}$ in eqn. 4.17. For instance, for $t = \tau$ and 3τ, $\tanh(t/\tau) \approx 0.761$ respectively ≈ 0.995. This implies that at $t = 3\tau$, the shape of the freshwater lens has nearly reached the steady-state situation. Boekelman also obtained formulas for the specific discharge q and the growth of the freshwater lens. Based on the thickness of the freshwater lens H, the evolution of the storage in the freshwater lens was determined:

$$V(t) = f\,B\,\tau\tanh(t/\tau) \tag{4.77}$$

The steady-state storage of the freshwater lens (at $t \rightarrow \infty$) is equal to:

$$V_\infty = fB\tau = \frac{\pi n_e B^2}{8}\sqrt{\frac{f(1+\alpha)}{k\alpha}} \tag{4.78}$$

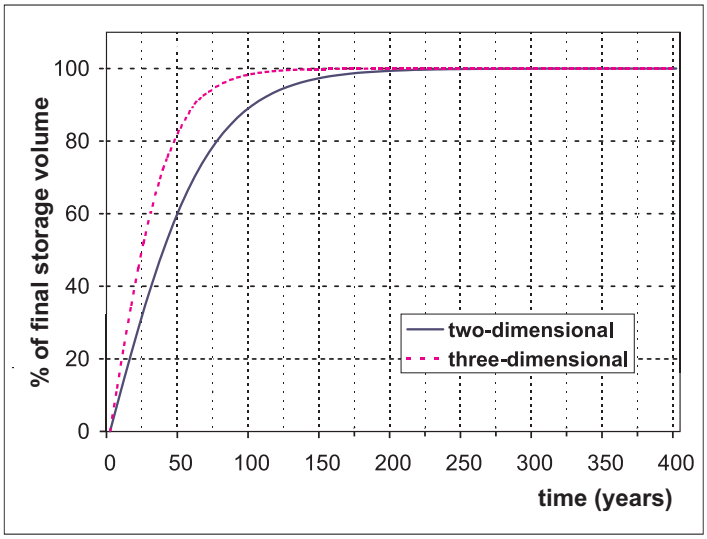

Figure 4.11: Evolution of the storage of the freshwater lens in a: **a)** two-dimensional and **b)** axial-symmetric situation.

This formula obviously corresponds with the straight formula based on the form of the lens which is an ellipse: $V_\infty = \pi n_e(1+\alpha)H_{max}B/4$, where H_{max}=maximum depth of the freshwater lens (m).

Example 4.7: Evolution of a freshwater lens in two-dimensions

For example, the following parameter set can be assumed (see fig. 4.10): α=0.025, B=4000 m, f=0.36 m/yr, k=20 m/day, n_e=0.35 and no hydrodynamic dispersion. With these values, H_{max}=87.7 m, the time constant τ equals 25073 $days$ or 68.6 $years$ and V_∞=98.85 $\times$ 10^3 m^3.

In fig. 4.11, the increase in storage of the freshwater lens can be seen. At the initial situation, the aquifer contains only saline groundwater. The analytical solution suggests a one-dimensional aquifer where vertical groundwater flow is neglected. In reality, however, the outflow of fresh groundwater, equal to $0.5Bf$ at each side, has to exit the aquifer at $x = 0.5B$ with very high vertical velocities. This problem of the outflow of fresh groundwater is not considered in the analytical situation (Glover (1959) suggested to apply a so-called outflow width equal to $0.25Bf/\alpha k$), see also Intermezzo II (page 36).

4.8.2 Axial-symmetric situation

Boekelman & Grakist (1973), Boekelman (1998) also considered a transient interface between fresh and saline groundwater in an axial-symmetric phreatic aquifer: an axial-symmetric situation. The equations are similar. In a circular sandy island, a freshwater lens is evolving due to natural groundwater recharge (see fig. 4.10). The governing equations for this situation are:

$$\text{(I) Darcy:} \qquad Q = -2\pi rk(H+h)\frac{\partial h}{\partial r} \tag{4.79}$$

$$\text{(II) Continuity:} \qquad \frac{\partial Q}{\partial r} = 2\pi fr - 2\pi r n_e \frac{\partial H}{\partial t} - 2\pi r n_e \frac{\partial h}{\partial t} \tag{4.80}$$

(III) BGH: $$h = \alpha H \tag{4.81}$$

Note that eqn. 4.80 comprises two transient terms. Combination of these equations gives:

$$\frac{2n_e}{k\alpha}\frac{\partial H}{\partial t} - \frac{2f}{k(1+\alpha)\alpha} - \frac{\partial^2 H^2}{\partial r^2} - \frac{1}{r}\frac{\partial H^2}{\partial r} = 0 \tag{4.82}$$

To solve this non-linear equation, again an approximate solution can be found assuming that at each moment in time the shape of the lens is conformable to the shape of the lens in the steady-state situation ($t \rightarrow \infty$). If so, the only difference is a time dependent factor $F(t)$. This results in eqn. 4.83:

$$H(r,t) = F(t)\sqrt{\frac{f(R^2 - r^2)}{2k(1+\alpha)\alpha}} \tag{4.83}$$

$$\text{for } t = \infty : F(t) = 1 \tag{4.84}$$

$$\text{for } t = 0 : F(t) = 0 \tag{4.85}$$

Now eqn. 4.83 is introduced into eqn. 4.82 and -to find the best overall solution- integrated over the whole area: from $r = 0$ to $r = R$. This leads to the following formula for $F(t)$ (Boekelman, 1998):

$$F(t) = \tanh(t/\tau) \tag{4.86}$$

where

$$\tau = \frac{\sqrt{2}n_e R}{3}\sqrt{\frac{(1+\alpha)}{kf\alpha}} \tag{4.87}$$

The time constant τ (unit of time) again comprises the characteristics of the area. Note that τ equals the characteristic time $\mathcal{T}$ in eqn. 4.33. At $t = 3\tau$, the shape of the freshwater lens has nearly reached the steady-state situation. Boekelman (1998) also obtained formulas for the discharge Q and the growth of the freshwater lens.

Based on the thickness of the freshwater lens H, the evolution of the freshwater storage in the lens was determined:

$$V(t) = \pi f R^2 \tau \tanh(t/\tau) \tag{4.88}$$

The steady-state storage of the freshwater lens (at $t \rightarrow \infty$) is equal to:

$$V_\infty = \pi f R^2 \tau = \frac{\pi\sqrt{2}n_e R^3}{3}\sqrt{\frac{f(1+\alpha)}{k\alpha}} \tag{4.89}$$

This formula obviously corresponds with the straightforward formula based on the shape of the lens: $V = 2\pi/3 n_e(1+\alpha)H_{max}R^2$, where H_{max}=$H(0,\infty)$=maximum depth of the freshwater lens (m).

Example 4.8: Evolution of a freshwater lens in an axial-symmetric situation

For example, for the following parameters: α=0.025, R=2000 m, f=0.36 m/yr, k=20 m/day, n_e=0.35 and no hydrodynamic dispersion, the maximum depth of the lens $H_{max} = H(0,\infty)$=62.02 m; the time constant τ=15049 *days* or 41.20 *years* and $V(t)$=186.4 $\times$ 10^6 $\times$ $\tanh(t/\tau)$ m^3. In fig. 4.11, the increase in storage of the freshwater lens as a function of time can be seen.

The evolution of the lens was compared with the results of a numerical computer code MOCDENS3D (Oude Essink, 1998b) and showed a good agreement, see fig. 6.14 in section 6.5.4, page 77.

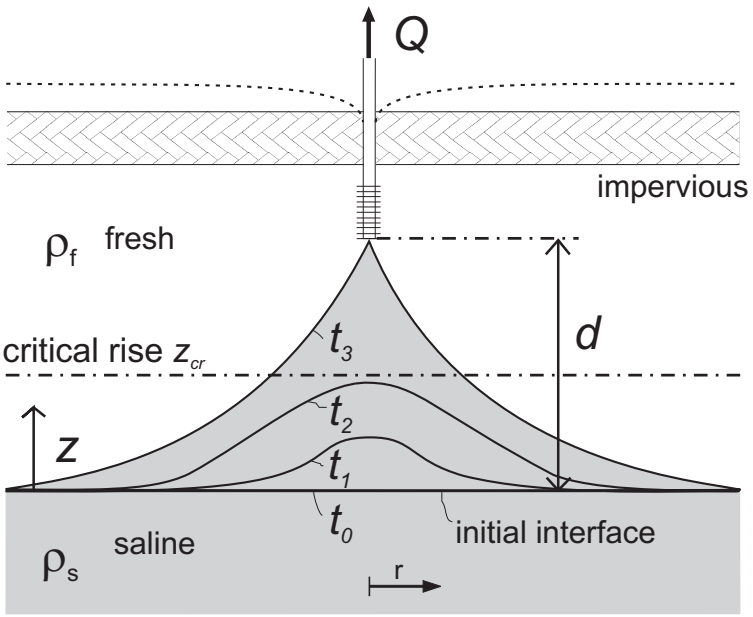

Figure 4.12: Upconing of saline groundwater under a pumping well.

4.9 Upconing of saline groundwater

In areas where saline groundwater is present below fresh groundwater, the interface between fresh and saline groundwater may rise when piezometric heads are lowered due to well extraction. This phenomenon is called interface upconing (see fig. 4.12). Especially in overpumped areas, e.g. in a semi-arid zone as the Gaza Strip, upconing of saline groundwater has become a serious threat to domestic water supply. Solutions are often difficult to invoke as water is scarce in these areas and illegal extractions are not easily to be stopped. As a result of the extraction and the lowering of the piezometric heads in the fresh and saline groundwater zone, the interface will rise. In case of a continuous extraction of fresh water, the interface will rise until it reaches the pumping well. From that moment on, the quality of the extracted groundwater deteriorates, and the pumping has to stop. In order to avoid or to limit these negative effects, one should keep the extraction rate, and so the lowering of the piezometric head, below a certain limit. After reducing the extraction significantly, the interface may descend to its original position, though at a very slow pace. Another solution is to replace the extraction well to a location where saline groundwater is positioned at greater depth from the well.

Fig. 4.12 shows the movement of the interface as a function of time t. An analytical solution exists to approximate the upconing of the interface underneath a pumping well (Bear & Dagan, 1964; Dagan & Bear, 1968; Schmorak & Mercado, 1969):

$$z(r,t) = \frac{Q}{2\pi\alpha k_x d}\left[\frac{1}{(1+R'^2)^{1/2}} - \frac{1}{[(1+\gamma')^2+R'^2]^{1/2}}\right] \tag{4.90}$$

$$R' = \frac{r}{d}\frac{k_z}{k_x}^{1/2} \qquad \gamma' = \frac{\alpha k_z}{2n_e d}t \tag{4.91}$$

where

- $z(r,t)$ = rise of interface above its initial position at place r and time t (L),
- Q = extraction rate of the well $(L^3\,T^{-1})$,
- $\alpha = (\rho_s - \rho_f)/\rho_f$ = relative density difference $(-)$,
- d = distance between well screen and the initial position of fresh-saline interface at t=0 (L),
- k_x = horizontal hydraulic conductivity $(L\,T^{-1})$,
- k_z = vertical hydraulic conductivity $(L\,T^{-1})$,
- n_e = effective porosity $(-)$,
- t = time elapsed since start of pumping (T).

For upconing of the interface directly underneath the pumping well, the equation becomes:

$$z(0,t) = \frac{Q}{2\pi\alpha k_x d}\left[1 - \frac{1}{1+\gamma'}\right] \tag{4.92}$$

The ultimate position of the interface, at $t \to \infty$, equals:

$$z(r, t\to\infty) = \frac{Q}{2\pi\alpha k_x d}\left[\frac{1}{(1+R'^2)^{1/2}}\right] \tag{4.93}$$

and directly underneath the pumping well:

$$z(0, t\to\infty) = \frac{Q}{2\pi\alpha k_x d} \tag{4.94}$$

Now, a so-called critical rise $z_{cr} = \theta d$ of the interface is introduced. In case the upconed interface passes z_{cr}, it will reach the pumping well with a sudden jump. Thus, assuming an abrupt interface such that the salinisation of the pumping well occurs only for $z > z_{cr}$, the maximum permissible pumping rate without pumping of saline groundwater is given by:

$$Q_{max} \le z_{cr} 2\pi\alpha k_x d \quad \text{or} \quad Q_{max} \le 2\pi\alpha k_x \theta d^2 \tag{4.95}$$

In literature, the value for θ varies from 0.25 to 0.6. So with respect to upconing a well-distributed system of shallow wells with small extraction rates is advantageous. Relatively small extractions cause little upconing and shallow well screens offer a better starting position against salinisation.

4.10 Effect of a relative sea level rise

Changes in global mean sea level (M.S.L.) will probably directly affect the coastal surface water system, rivers and estuaries, as well as the coastal aquifers. Here, the impacts of a relative sea level rise on the coastal surface water system, rivers and estuaries, and coastal aquifers are discussed:

- The coastal surface water system will directly sense the impacts of sea level rise. Increases in storm surges, wave attack, flooding, and collapses of coastal protection defences could directly induce the inundation of populated areas and loss of lives must be feared. Furthermore, in the medium term, sea level rise would cause an increase in coastal erosion. If no compensating measures such as sand-suppletion are taken, it could result in severe shoreline retreat. Shoreline retreat will also affect coastal aquifers (see fig. 4.13), e.g., by reducing the width of the sand-dunes along the coastline where fresh groundwater resources are situated and by diminishing the length over which natural groundwater recharge occurs. Both events may lead to a decrease in fresh groundwater resources.

- Rivers and estuaries will experience an increased salt water intrusion in case of sea level rise, if the river bed elevation can not match with sea level rise. Because the sediment load at many river mouths is reduced significantly these last decades among others due to human activities (building dams, sand-mining), quite some rivers and estuaries are expected to have an increased salt water intrusion. This could threaten adjacent aquifers along rivers and estuaries from which groundwater is extracted. Furthermore, the backwater effect of sea level rise would also decrease the safety against flooding over large distances upstream the river mouth. Especially areas adjacent to rivers with valley slopes only slightly steeper than river slopes have to be protected by embankments.

- Coastal aquifers within the zone of influence of M.S.L. can be threatened by sea level rise (see fig. 4.13). Intrusion of salt water is accelerated into these aquifers, which could result in smaller freshwater resources (Oude Essink, 1999b, 2000a). Furthermore, seepage will increase quantitatively in those areas and this seepage could contain more saline groundwater. In consequence, crops may suffer from salt damage and fertile agriculture land might change into barren land. In addition, the mixing zone between fresh and saline groundwater will be shifted further inland. Extraction wells, which were previously located beyond the salinisation zone, will then be situated in areas where upconing of brackish or saline groundwater can easily occur. This can be considered as one of the most serious effects of sea level rise for every coastal aquifer where groundwater is heavily exploited.

It is important to recognise that impacts of sea level rise must be considered in relation to impacts of human activities. It is very likely that not sea level rise, but human activities will cause a severe salinisation of most coastal aquifers in the future. A reason for this assumption can, among others, be deduced from the time lag between causes and effects. Sea level rise takes place progressively. The time characteristic of sea level rise is in the order of decades. On the other hand, the time characteristic of human activities, such as

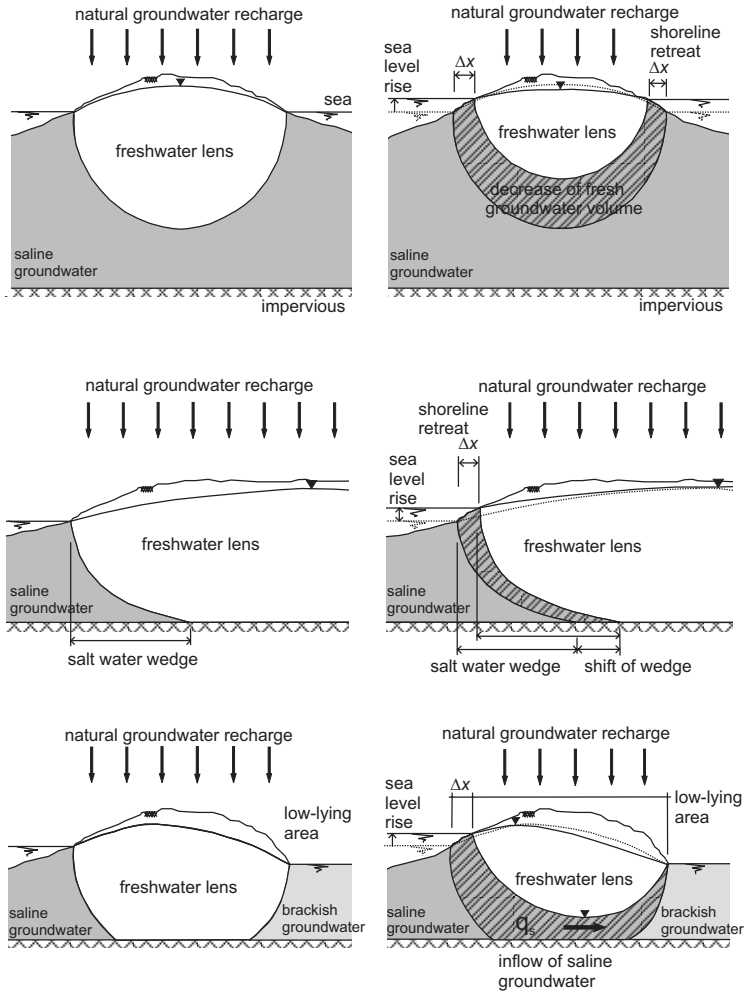

Figure 4.13: Effects of a sea level rise on coastal aquifers.

groundwater extraction projects, is in the order of years. Before negative impacts, such as upconing, are recognised, it may be too late to take countermeasures.

Exercise 4.1: Freshwater lens in an one dimensional situation.

Consider an infinite long strip of sand-dune with a cross-section as given in fig. 4.14. The sea level is constant.

1. Derive the global analytical equations for h, H and q (thus including the constants $C1$ and $C2$) for the interface between fresh and saline in a phreatic aquifer (one-dimensional situation), as shown in the figure.
2. Determine the shape of the freshwater lens (viz. H and h as a function of x), based on the answer of question 4.1.1 and the parameters in the figure.
3. Determine h and H in the middle of the dune and q at the boundary of the freshwater lens.
4. Explain what will happen with the freshwater lens if no recharge occurs during a long period.
5. Now assume an aquiclude (impervious layer) at a depth D of 146 m below mean sea level. Where ('at x=...') will the freshwater lens reach this aquiclude ?

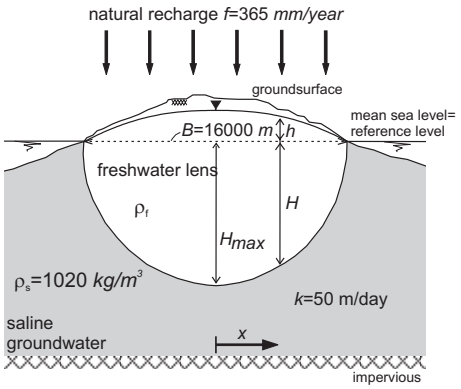

Figure 4.14: Exercise 4.1: freshwater lens in an one dimensional situation.

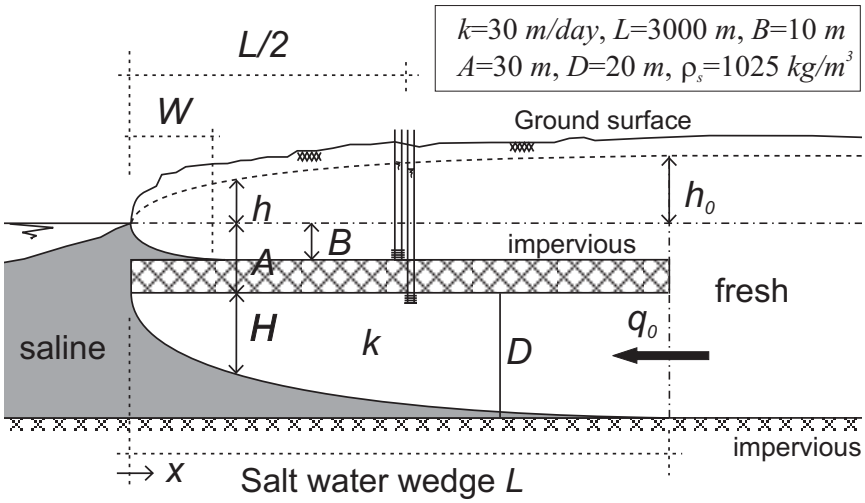

Figure 4.15: Exercise 4.2: Freshwater lenses in a hydrogeologic setting.

Exercise 4.2: Freshwater lenses in a hydrogeologic setting.

1. How large must h_0 be in order to avoid salt water intrusion in the freshwater system (for the system $x > L$) ?
2. What is the specific recharge q_0 in this situation through the deep aquifer ?
3. Now the upper phreatic aquifer will be considered: what will be the size of the salt water wedge W, knowing the size of h_0 from question 1 ?
4. What will be the difference in freshwater head at $x = L/2$ between the confined and phreatic aquifer?

Solution 4.2: Freshwater lenses in a hydrogeologic setting.

1. h_0=1.25 m.
2. q_0=-0.05 m^3/m'/day.
3. W=319.5 m.
4. $\Delta\phi$=0.40 m.

Chapter 5

Control of salt water intrusion

It takes a considerable time before the salinisation of the subsoil of groundwater systems due to the negative effects of human activities (e.g. dramatic lowering of the piezometric heads due to excessive overpumping) is actually observed. The main reason is that in the salinisation process enormous volumes of fresh groundwater have to be replaced by saline groundwater.

Besides technical countermeasures as described below, other instruments are available to cope with salt water intrusion problems. For instance, an intensive cooperation between (local) authorities and water users is essential to control the extraction per capita. Educating, training, informing the water users, and participation of water users in regularly decisions could be very effective in coming to a lower water use. In addition, groundwater extractions could be restricted through a system of permits. It may be necessary to reduce agricultural activities and move to other places. A shift to more salt resistent crops could enlighten the need to extract groundwater of high quality. Finally, in some areas (e.g. tropical islands), desalinisation of saline water could relieve the stress on groundwater resources though at the expense of high energy costs.

5.1 Countermeasures to control salt water intrusion

As countermeasures to control the salt water intrusion probably also need a long time to become effective, they should be taken in due time.

In general, the salinisation may be substantial in coastal groundwater flow systems where the existing piezometric heads are lower than a few metres above $M.S.L.$ In those cases, countermeasures should be applied to reduce salt water intrusion. The following countermeasures against the salinisation process can be considered (see fig. 5.1):

1. application of freshwater injection barriers, e.g. through injection or (deep-well) infiltration of fresh (purified sewage) water near the shoreline. This is already applied in Israel, at Long Island and in Los Angeles.

2. extraction of saline and brackish groundwater. However, this could regrettably result in undesirably low piezometric heads, especially in shallow coastal groundwater systems. Furthermore, the disposal of the extracted saline or brackish groundwater could meet with problems.

3. modifying pumping practice and/or well system through reduction of withdrawal rates and/or adequate relocation of extraction wells. The desired extraction rate

should preferably be extracted by well-distributed shallow wells to prevent excessive upconing. In most situations, groundwater withdrawal for domestic, agricultural and industrial water supply has not been reduced during periods of droughts, so that salt water intrusion tends to occur anyway.

4. land reclamation, thus creating a foreland where a freshwater body may develop, which could delay the inflow of saline groundwater.

5. increase of (artificial) recharge in upland areas to enlarge the outflow of fresh groundwater through the coastal groundwater system, and thus, to reduce the length of the salt water wedge.

6. creation of physical barriers, such as sheet piles, clay trenches and injection of chemicals. This solution is only applicable in shallow aquifers and at high cost. A small physical barrier by injecting pumping cement grout has been implemented at Okinawa-Jima Island in Japan.

The present countermeasures to prevent and/or retard salt water intrusion due to the negative effects of human activities resemble the possible solutions to counteract the effects of a relative sea level rise on the salinisation process. In fact, sea level rise is basically the same as equally lowering the land surface and thus the phreatic groundwater level. Nowadays, dramatic lowering of the piezometric heads due to excessive overpumping already occurs in many groundwater systems around the world, see table 1.2. It is obvious that, for those systems, the impact of a (relatively small) sea level rise (e.g. 0.5 *m per century*) on the groundwater system will be of marginal importance compared to the effect of an increase in withdrawal rate.

The economic feasibility of countermeasures should be investigated. For instance, it is recommended to derive the optimum position of well lines and rates of extraction or infiltration. Moreover, the countermeasures should be adapted and optimised in the course of the realisation of the measure, based on changes in the salinity of the subsoil.

5.2 Monitoring of salt water intrusion

Monitoring[1] of the quality of groundwater on a regular basis is important in areas where salt water intrusion may be expected. The conventional way is to use the results of groundwater sample analyses. Besides this, geophysical exploration techniques have proven to be very useful. Geo-electrical sounding is used for regional exploration of subsurface layering. The result obtained is a subdivision of the subsoil into layers with different specific electrical resistivity values. The specific resistivity values of layers are strongly affected by the salinity of the pore water, making geo-electrical sounding very useful with regard to salinisation.

Well systems in coastal areas, used for the extraction of drinking water, have to be safeguarded and need extra attention. The conventional way is to set up a network of observation wells around the well system and to analyse groundwater samples and piezometric heads. These wells should be located at different levels and at such a distance that in case

[1] This section is written by R.H. Boekelman, Delft University of Technology, Civil Engineering, Hydrology and Ecology.

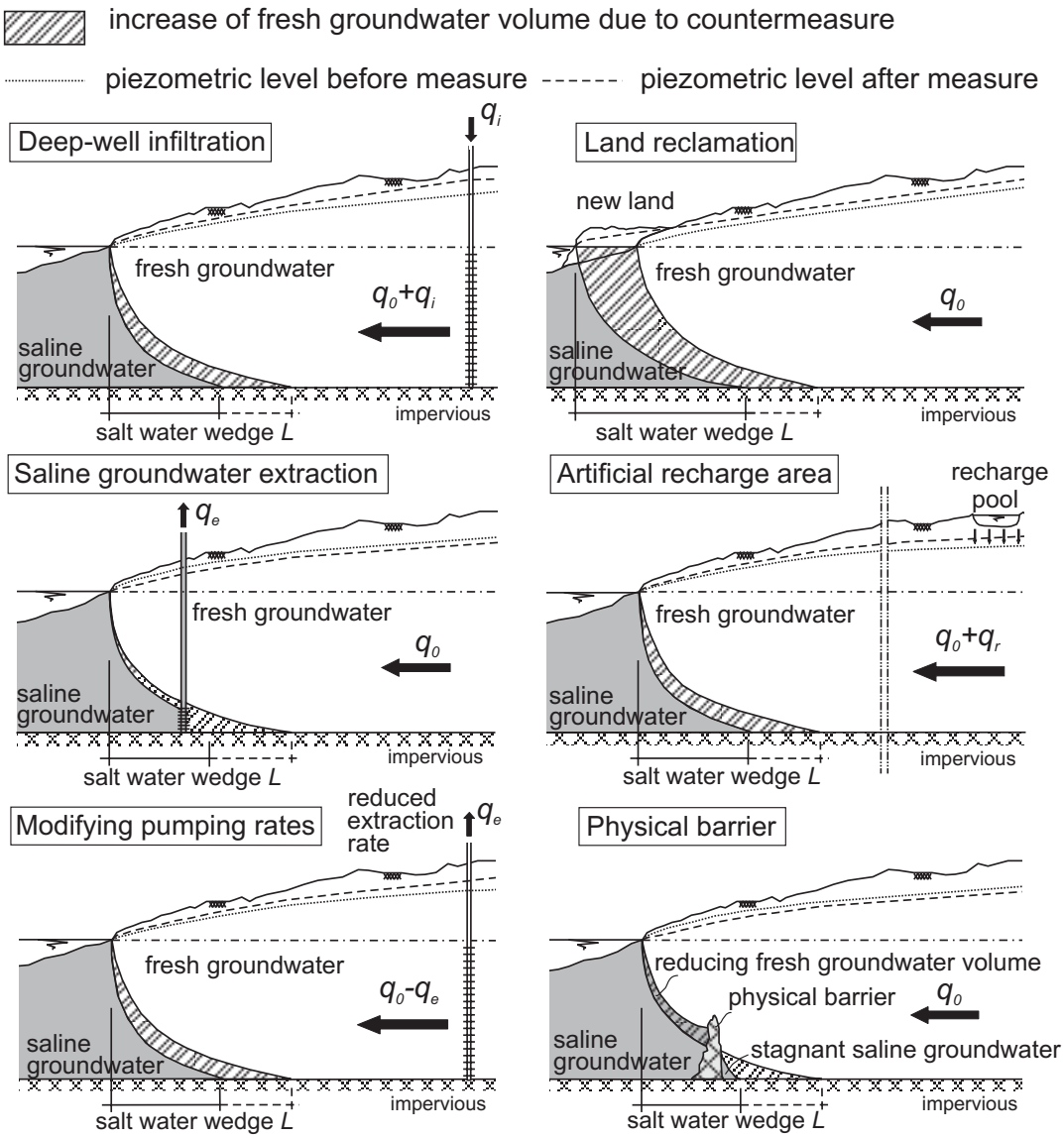

Figure 5.1: Countermeasures to control salt water intrusion.

of salinisation the eventual progression of the saline front can be observed and appropriate and timely countermeasures can be taken. If saline water is already present in deeper layers also observation wells will have to be situated under the extraction wells and deep enough to detect upconing already at an early stage. Gradients in piezometric head indicating flow from saline parts of the hydrogeological system towards the extraction wells should be avoided; see fig. 5.2. In this case, flow lines through the transition zone will always carry brackish water to the extraction system and may lead to abandoning of wells.

At present very often a special application of an electrical resistivity method is used in combination with observation wells. The system includes a multistrand cable, an electrical resistivity meter and a switch. The cable is installed vertically in the subsoil, mostly taped

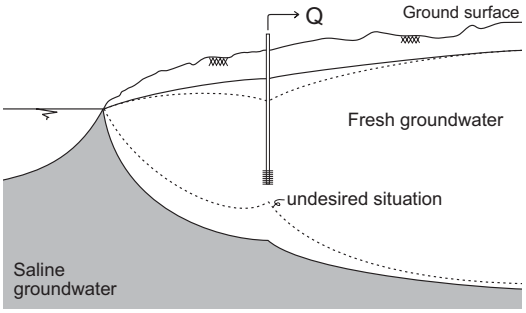

Figure 5.2: Piezometric heads in a coastal aquifer due to pumping.

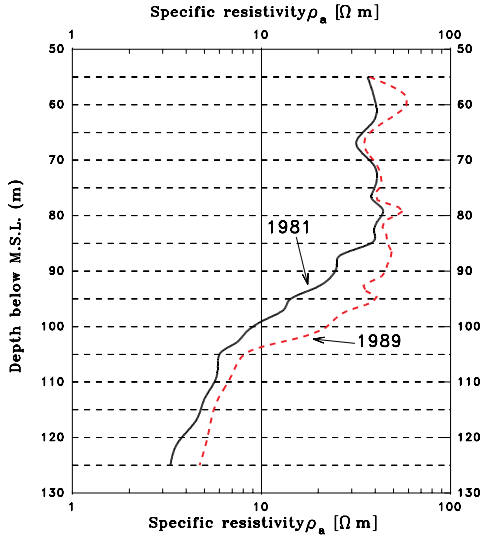

Figure 5.3: Measurements of a Permanent Electrode System, showing desalinisation effects (Singh *et al.*, 1990). Resistivity values $> 35\ \Omega m$ indicate the presence of groundwater with a chloride content of $\sim 300\ mg/l$; ρ_a-values $< 5\ \Omega m$ represent brackish groundwater ($\sim 5500\ mg\ Cl^-/l$).

to the tube of an observation well. On the outside of the cable and at regular intervals pairs of electrodes are applied. The system applies a 4-electrode measuring system: 2 current electrodes (C) and 2 potential electrodes (P), with one pair (C, P) at the surface and the other pair (C, P) in the subsoil. Switching from one pair of electrodes to the next results in resistivity values related to depth. Low specific resistivity values indicate salinisation. This so-called Permanent Electrode System (PES) offers the possibility to repeat measurements as often as desirable and is very well suited for automation. Fig. 5.3 shows the results of two measurements in a deep polder in The Netherlands. The graphs indicate clearly desalinisation effects of inflow of fresh groundwater from a bounding area over a period of 8 *years*. The transition zone between fresh and saline groundwater has been moved down some 10 m.

Chapter 6

Numerical modelling

6.1 Introduction

In the past, the behaviour of density dependent groundwater flow has been investigated by means of analogue models as well as by means of analytical models. However, since computers appeared on the scene, numerical models gained ground. At present, a large number of numerical models is available, capable of handling fresh and saline groundwater flow in aquifer systems[1].

Reviews of literature on fresh and saline groundwater and available computer codes and models are given in e.g. Reilly & Goodman (1985), Custodio *et al.* (1987), and Bear *et al.* (1999). In addition, all Salt Water Intrusion Meeting-proceedings comprise a large number of case studies with different kinds of models (see e.g. SWIM-Delft'86, SWIM-Barcelona'92, SWIM-Malmö'96 and SWIM-Gent'98).

6.1.1 Interface model versus solute transport model

Interface models are based on the assumption that an interface between fresh and saline groundwater represents the actual situation: the well-known *Badon Ghijben-Herzberg principle*. The straightforward interface models can be applied as an educational means to gain a clear insight into the behaviour of fresh and saline groundwater in coastal aquifer systems. As such, interface models are still widely applied. Nevertheless, restrictions on the applicability of the principle should be considered:

a. First, the principle only approximates the actual occurrence of fresh, brackish and saline groundwater in the subsoil. In fact, the brackish zone between fresh and saline groundwater should only be schematised by an interface when the maximum thickness of the brackish zone is in the order of several metres only. This condition applies only in rare situations where the freshwater lens is evolved by natural recharge, as occurs in sand-dune areas or in (coral) islands.

b. Second, the principle assumes a hydrostatic equilibrium, whereas in reality the aquifer system might considerably deviate from this equilibrium situation. In those cases, e.g. in freshwater bodies near the shoreline, the Badon Ghijben-Herzberg principle

[1]The U.S. Geological Survey is the leading institute in developing groundwater flow models (http://water.usgs.gov/software/ground_water.html). Some distributors of affordable computer codes are the International Ground Water Modeling Center (http://www.mines.edu/research/igwmc/), the Scientific Software Group (http://www.scisoftware.com/), Geotrans (http://www.geotrans.com/), and Waterloo Hydrogeologic (http://www.flowpath.com/).

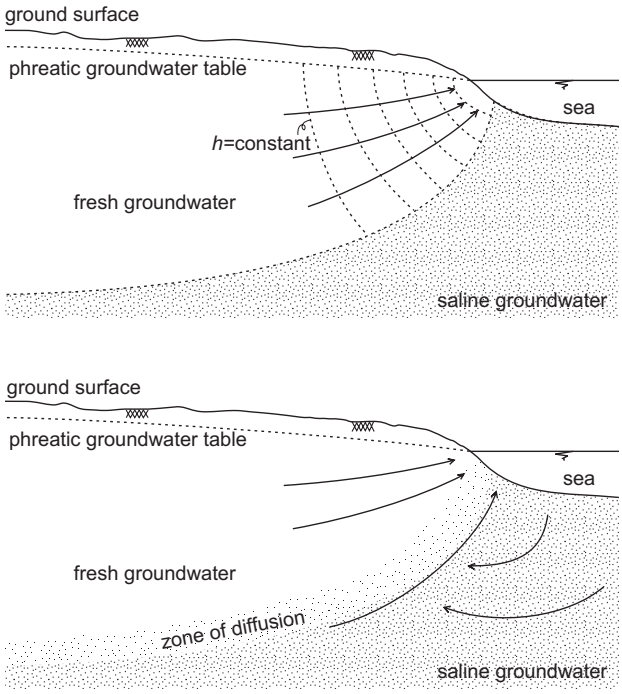

Figure 6.1: Salt water intrusion in a coastal aquifer: **a)** balance between fresh water and static salt water and **b)** circulation of salt water from the sea to the zone of diffusion and back to the sea (modified from Henry, 1964).

should not be applied, because the computed position of the interface deviates from the actual position as the coast is approached.

In many coastal aquifer systems, a relatively broad transition zone[2] (fig. 6.1) between fresh, brackish and saline groundwater is present because of various processes during geological history (e.g. regressions, transgressions). In addition, the transition zone is also increasing as a result of the circulation of brackish water due to inflow of saline groundwater (mixing with fresh groundwater due to hydrodynamic dispersion), the tidal regime and human activities, such as (artificial) recharge and groundwater extraction at high and variable rates (Cooper, 1964). For example, this situation occurs in Dutch hydrogeologic cross-sections with Holocene and Pleistocene deposits of marine and fluviatile origin (Meinardi, 1973; Maas, 1989). Under such conditions, more sophisticated models are required than just models with expressions for interfaces: models which take into account variable densities and the transport of solutes. These models are referred to as solute transport models or salt water intrusion models. They apply the advection-dispersion equation to convert solute concentration (or total dissolved solids) to density through the equation of state. They are able to simulate, among others, salt water intrusion in coastal aquifers where mostly non-uniform density distributions occur; changes in solute concentration (e.g. near pumping wells due to upconing); and changes in storages of freshwater in sand-dune areas. As solute transport models usually apply numerical schemes, they can also be utilised to simulate

[2]Other terms are mixing zone, zone of dispersion or brackish zone.

aquifer systems with complex hydrogeologic geometries and inversions of fresh and saline groundwater caused by (pre)historic events.

6.1.2 Two-dimensional versus three-dimensional models

Two-dimensional groundwater flow models, which also simulate solute transport, require quite some effort before they are completely understood. Although they can be applied in various situations, the practical application is rather limited. The most important restriction of these models is obviously that only cross-sections can be simulated. Therefore, a proper cross-section should be carefully selected.

In many cases, however, groundwater flow perpendicular to the coastline is disturbed in such a way that the schematisation and modelling of the actual situation by a cross-section cannot be allowed any more. Such situations occur for instance in polder areas where the controlled phreatic groundwater levels lead to radial flow patterns, in areas with complex hydrogeologic geometries or in the vicinity of singular wells where groundwater is extracted or infiltrated. Under those circumstances, 3D models should be applied to simulate density dependent groundwater flow. Obviously, 3D models naturally require even more effort to be understood, implemented and utilised effectively than 2D models. For instance, the problems that arise to visualise 3D groundwater flow and solute transport on a (2D) monitor should not be underestimated. The practical application of 3D salt water intrusion models on a broad scale is still at an early stage of development.

6.2 Problems with 3D modelling of salt water intrusion

Though 3D modelling of salt water intrusion in hydrogeologic systems is technically possible, a number of practical problems arises (Oude Essink & Boekelman, 1996):

1. the data availability problem,
2. the computer problem,
3. the numerical dispersion problem.

6.2.1 The data availability problem

A numerical model of salt water intrusion in a coastal hydrogeologic system must be calibrated and verified with available groundwater data in order to prove its predictive capability, accuracy and reliability. Characteristic groundwater data are: subsoil parameters (e.g. the hydraulic conductivity, the exact position of aquitards; the effective porosity; the anisotropy, and the hydrodynamic dispersion), groundwater extraction rates, and salinity and piezometric head distributions as a function of space and time. Regrettably, in many cases reliable and sufficient data are scarce. The availability of enough reliable data is obviously even more pinching for 3D models than for 2D models. As such, the application of 3D computer codes is restricted seriously. Some common problems are:

- Upscaling of data from 1D and 2D to 3D
  In fact, the collection of data is one- or two-dimensional. Geohydrologic information

is mostly obtained from a point source (e.g. groundwater level from a observation well) or from a line source (geohydrologic information from a geohydrologic column). This information must be extrapolated or interpolated to a 3D distribution of subsoil parameters. This upscaling obviously faces difficulties.

- Long time series of hydrochemical constituents
  Another problem is that the calibration of groundwater flow models with salinities changing over time and space is still rather laborious. As the flow of groundwater and subsequently the transport of hydrochemical constituents are slow processes, it takes quite some years before a salinisation can be detected. As such, relative long time series of monitored salinities (of some tens of years or even more) are necessary in order to accurately calibrate 3D salt water intrusion in large-scale coastal hydrogeologic systems. Unfortunately, these time series are available only occasionally and reliable measurements are scarce in many cases. As a consequence, the calibration will be less reliable. One has to collect many data during many years before a good calibration can be achieved.

As a remedy for the data availability problem, the collection and the analysis of reliable groundwater data should be intensified, varying from subsoil parameters to records of solute concentrations and piezometric heads as functions of time and space. The present salinisation process should be monitored as a function of time to detect long-term changes. The geometry and geohydrologic parameters of the coastal hydrogeologic systems should be determined and described, particularly for those hydrogeologic systems which are vulnerable and sensitive to natural and man-induced processes.

In addition, to solve the data availability problem to a certain extent, so-called Geohydrologic Information Systems can be very useful. In these systems, all relevant geohydrologic data can be stored. By analysing these systems, areas with a lack of data can be detected immediately. In 1990, research institutes, governmental organizations and drinking water companies in the Netherlands started the development of a so-called REgional Geohydrologic Information System (REGIS). In REGIS, a database is available to supply all types of relevant geohydrologic information, such as geo-electric data, groundwater levels (observation well data), chemical data, geohydrologic columns, topographic information, pumping and borehole test data, locations of contaminants, etc. Now, the system is operational and has already proven to be profitable.

However, it has to be accepted that the availability of data will always lag behind the developments in computer possibilities, and thus, will always restrict practical applications to a certain extent.

6.2.2 The computer problem

Until some years ago, 3D modelling of salt water intrusion in large-scale coastal hydrogeologic systems was not really possible due to shortcomings in computer possibilities[3]. The required number of elements to model large-scale coastal hydrogeologic systems is

[3]Three-dimensional modelling of oil and gas reservoir behaviour by the petroleum industry is already taking place for many years: apparently, the benefit of predicting reliable oil and gas reservoirs has been higher.

enormous, e.g. several hundreds of thousands of elements. Two major reasons restricting application are the memory problem (limited memory to store data of a 3D model) and the speed problem (limited computer speed to execute a (transient) 3D model). This situation is changing very fast:

- The memory problem
  A computer system with sufficient random access memory (RAM) is required to store data and arrays during the execution of the model. Until the late 1980's, most FORTRAN compilers accessed only 640 Kb of RAM, which is the standard memory limit of DOS. As such, the possibility to store large amounts of data was limited. So, the arrays which represent the parameters and the number of elements should not be dimensioned too large. The problem of insufficient memory has recently been solved. Since the late 1980's, much more memory is available on the personal computer: the so-called Extended Memory RAM (EM RAM). Executables of computer codes can address this EM RAM beyond the usual 640 Kb RAM-limit of DOS through sophisticated compilers (e.g. the Lahey Fortran compiler F77L-EM/32 in combination with the Lahey/Ergo/Phar-Lab 386 Operating System). As such, even stand-alone personal computers can accommodate a much larger number of elements than under 640 Kb of conventional RAM.

  Nowadays, the EM RAM in a computer can be increased without high costs. Standard computer systems contain several (tens of) Mb of EM RAM, so the memory problem has been disposed for 2D and some 3D problems. Anyway, the application on a broad scale of 3D models for extensive and complex geometries is still in an early stage.

- The speed problem
  The length of time necessary to execute the computations with the computer program for a given set of input data of a geohydrologic problem is the so-called execution time. This execution time depends on four factors:

  a. the speed of the computer
     Nowadays, new stand-alone (personal or mini) computer systems with fast processors (disk-speed) open the application of 3D modelling of large-scale geometries.

  b. the size of the model
     The number of elements and type of the governing equations being solved determines the size of the model. The larger the number of elements, the longer the execution time will be.

  c. the efficiency of the compiler
     To execute the model, an executable file of the computer code must be produced by an appropriate compiler. A compiler reads the source code and generates machine language statements for the computer hardware. Some compilers go through commands and information more efficiently than others. For example, the Lahey Fortran compiler (e.g. F77L-EM/32) is capable of a very rapid compilation of FORTRAN-codes under DOS environment.

  d. the type of the output device
     Some models ask for keyboard input during the execution or frequently write to

the screen printer or even an output file. These actions increase the execution time (massive output files of several Mb's may increase the execution time substantially). The output devices can be reduced by setting the printing options to minimal output.

6.2.3 The numerical dispersion problem

Numerical approximations of the derivatives of the non-linear solute transport equation may introduce truncation errors and oscillation errors (see fig. 6.2). As such, these errors limit the techniques that solve the partial differential equation. The truncation error has the appearance of an additional dispersion-like term, the so-called *numerical dispersion*, which may dominate the numerical accuracy of the solution. Oscillations may occur in the solution of the solute transport equation as a result of over and undershooting of the solute concentration values. If the oscillation reaches unacceptable values, the solution may even become unstable. There is a close relation between numerical accuracy (numerical dispersion) and stability (oscillation) (Peaceman, 1977; Pinder & Gray, 1977). In fact, numerical dispersion acts to stabilize the solution of the solute transport equation. Numerical dispersion spreads the sharp front by generating a solution which applies a greater dispersion than the hydrodynamic dispersion. In order to suppress the numerical dispersion, the numerical scheme (spatial as well as temporal) can be adapted. Meanwhile, this scheme may lead to over and undershooting, and subsequently, oscillation may be amplified. For these reasons, the discretisation scheme should be chosen carefully in order to control both numerical accuracy and stability. The interest is focussed on the spatial discretisation which is largely responsible for the numerical dispersion.

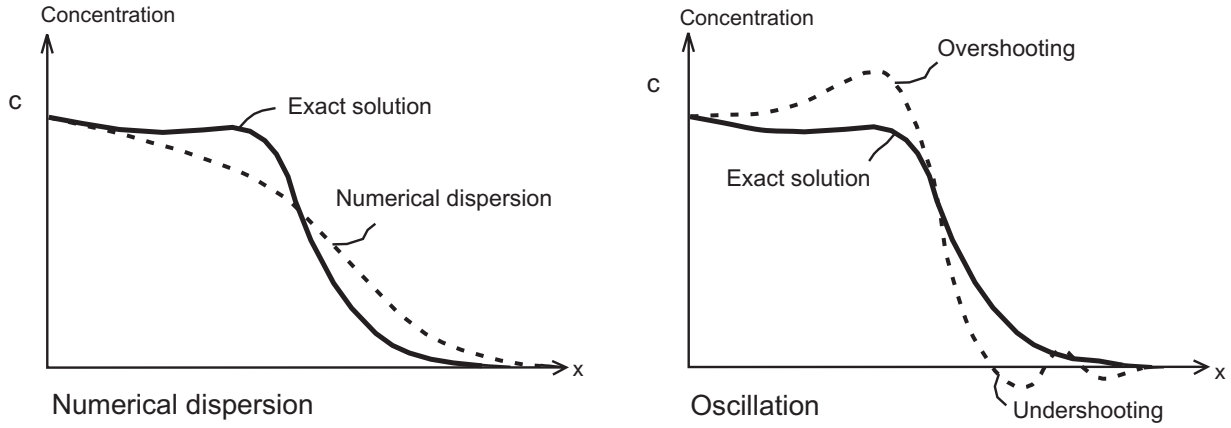

Figure 6.2: Schematisation of numerical dispersion and oscillation.

Analysis of the truncation error

In order to quantify numerical accuracy, an eigenvalue analysis of the advection-dispersion equation should be performed[4]. Such an analysis will demonstrate the importance of the

[4]In addition, a stability analysis should determine the stability condition (e.g. Peaceman, 1977).

dimension of the element (see e.g. Frind & Pinder, 1983). Which of the terms of the advection-dispersion equation is more dominant depends on the relative size of the advective and dispersive fluxes at the level of the discretisation element (Kinzelbach, 1987a). The grid Peclet number can be applied to assess the most dominant process. For small grid Peclet numbers ($Pe_{grid} < 1$) the dispersive fluxes (viz. the parabolic nature of the advection-dispersion equation) prevails, whereas for great grid Peclet numbers ($Pe_{grid} > 2$) the advective fluxes (the hyperbolic nature) dominates. In field problems, advective transport of solute mostly dominates over dispersive transport. Numerical solving (by means of the standard finite element method and the finite difference method) of an equation with a hyperbolic nature is more difficult than solving an equation with a parabolic nature.

A one-dimensional schematisation of the standard advection-dispersion equation is often applied to demonstrate, in case of the finite difference method[5], in a simple way the principle of assessing truncation errors (e.g. Bear & Verruijt, 1987). Approximations of the first-order derivatives generate errors in the order of magnitude of the second-order derivatives. This is shown by using Taylor series expansions (e.g. Lantz, 1971; INTERCOMP, 1976; Bear & Verruijt, 1987). The truncation errors depend on the chosen numerical approximation scheme (e.g. backward, central or forward difference in space and time). For the analysis of the truncation error, the so-called *grid Peclet number* Pe_{grid} is defined:

$$Pe_{grid} = \left| \frac{V \Delta x}{D_h} \right| \tag{6.1}$$

where

- Pe_{grid} = grid Peclet number $(-)$,
- V = effective velocity of groundwater $(L\,T^{-1})$,
- Δx = dimension of the element (L),
- D_h = hydrodynamic dispersion $(L^2\,T^{-1})$.

Grid Peclet numbers (and Courant numbers[6]) have been mentioned in various quantitative descriptions. Whether or not the numerical dispersion is suppressed, depends on the discretisation technique applied (e.g. Jensen & Finlayson, 1978; Voss & Souza, 1987). In summary, it appears that in order to obtain real and distinct eigenvalues, the spatial discretisation should meet the condition (Daus *et al.*, 1985):

$Pe_{grid} \leq 2$	Finite difference algorithm, central in space
$Pe_{grid} \leq 2$	Finite element algorithm, linear basic functions
$Pe_{grid} \leq 4$	Finite element algorithm, quadratic basic functions

(6.2)

As can be deduced, this grid Peclet number imposes that the dimension of the element should be not greater than a few times the magnitude of the longitudinal dispersivity that

[5]The analysis of (truncation and oscillation) errors caused by numerical dispersion and oscillation by means of central finite difference approximations for the finite difference method is similar for the finite element method (Pinder & Gray, 1977; Kinzelbach, 1987a).

[6]The Courant condition Co, $\frac{V \Delta t}{\Delta x}$, is physically interpreted as the ratio of the advective transport distance during one time step to the spatial discretisation.

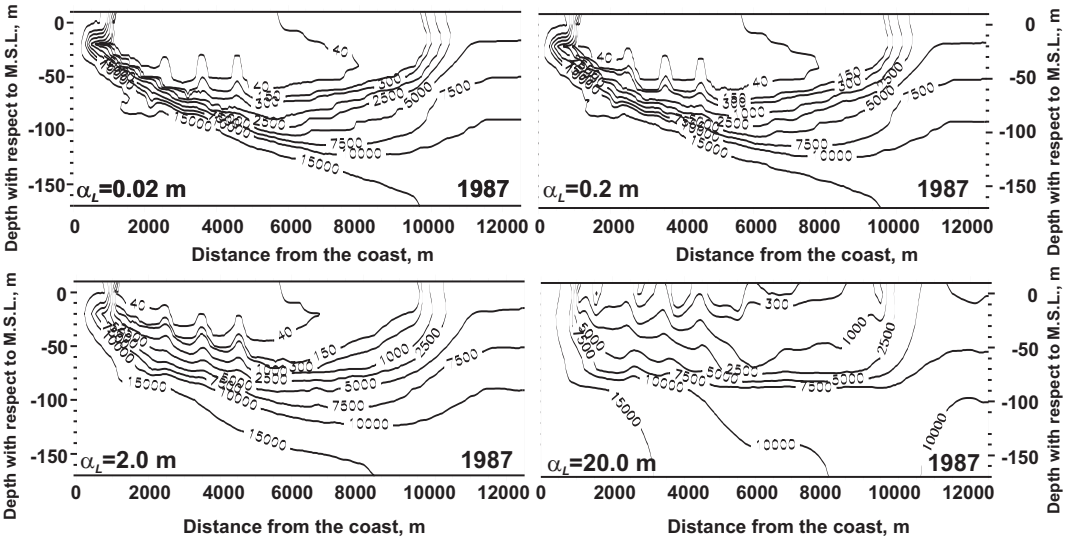

Figure 6.3: Chloride distributions (in $mg\ Cl^-/l$) in 1987 in a cross-section of the sand-dune area of Amsterdam Waterworks, the Netherlands, calculated with MOC (Konikow & Bredehoeft, 1978) (adapted for density differences to model vertical cross-sections (Oude Essink, 1996)) for four different longitudinal dispersivities: α_L=0.02 m, α_L=0.2 m, α_L=2.0 m and α_L=20.0 m. A thick freshwater lens is only simulated for small dispersivities.

represents hydrodynamic dispersion, as otherwise numerical dispersion will occur. When the dimension of the hydrogeologic system in question is large and the (longitudinal) dispersivity is small (e.g. in the order of decimetres for Holocene and Pleistocene deposits of marine and fluviatile origin), the dimensions of the elements must be in the order of (tens of) metres.

As such, computer codes, of which the solution of the advection-dispersion equation is based on standard finite element or finite difference techniques, cannot yet be applied to model large-scale coastal hydrogeologic systems. The reason is that these codes must satisfy a condition of spatial discretisation, characterised by the grid Peclet number, in order to suppress truncation and oscillation errors. Both widely used methods have in common that they produce poor results at great (grid) Peclet numbers. As such, it is peculiar that this well-known fact does not have a broader attention in numerical modelling practices of groundwater contaminant transport (Uffink, 1990).

The dispersion coefficient

For information about hydrodynamic dispersion and values of dispersivities, see subsection 2.4, page 17 or the lecture notes of Groundwater Modelling I (Oude Essink, 2000c).

Computations have indicated that if a great hydrodynamic dispersion (that means great dispersivities) is simulated during long simulation times, unrealistic solutions are generated (Oude Essink, 1996). In fig. 6.3, the effect of the longitudinal dispersivity α_L is evaluated by comparing the results of simulations with four different values of α_L: 0.02 m, 0.2 m, 2.0 m and 20.0 m. The chloride distributions of the cross-section are given after a simulation time

of 134 years: from 1854 till the end of 1987. The cross-section is situated in a sand-dune area along the Dutch coast where a freshwater lens has been formed. The calculated chloride distribution matches the observed distribution best if small longitudinal dispersivities are applied, namely α_L=0.02 m and α_L=0.2 m. By contrast, the case with α_L=2.0 m shows a freshwater lens that is too thin, whereas the case with α_L=20.0 m does not simulate a freshwater lens any more: the aquifer system only consists of a large brackish zone. This situation does not occur in reality.

The dimension of the element

If mechanical dispersion dominates over molecular diffusion, the hydrodynamic dispersion D_h in eqn. 6.1 can be expressed as D_h=$\alpha_L\,|V|$, and thus, eqn. 6.2 becomes:

$$\begin{aligned} &\Delta x \leq 2\,\alpha_L && \text{Finite difference algorithm, central in space} \\ &\Delta x \leq 2\,\alpha_L && \text{Finite element algorithm, linear basic functions} \\ &\Delta x \leq 4\,\alpha_L && \text{Finite element algorithm, quadratic basic functions} \end{aligned} \tag{6.3}$$

Note that there are acceptable solutions obtained with values up to $\Delta x < 10\,\alpha_L$[7]. As such, this restriction is not very compulsory. Under those circumstances, the solution can still be satisfactory though in some places over and undershooting (viz. oscillation) may occur.

From the formulations in eqn. 6.3 can be deduced that the application to model salt water intrusion in large-scale coastal hydrogeologic systems is restricted for 2D or especially 3D computer codes which are based on the standard the finite element method and the finite difference method (see fig. 6.4). Because, as a matter of fact, the restriction means that the dimension of the element may not be larger than four times the magnitude of the longitudinal dispersivity. Unfortunately, the longitudinal dispersivity is for many aquifer systems in the order of (at maximum) metres, and thus the dimension of the element should also be in the order of (tens) of metres. Consequently, a very large number of elements is necessary to model large-scale areas of various square kilometres. For the time being, the allowed number of elements is restricted by computer memory capacity and execution time. In conclusion, when standard the finite element method and the finite difference method are applied, 3D modelling of salt water intrusion of coastal aquifer systems is, for the time being, only possible on the scale of small geometries, such as small islands.

Remedy for the numerical dispersion problem

To avoid the numerical dispersion problems associated with standard finite element and finite difference solutions of the advection-dispersion equations, particle tracking solutions should be used, such as the method of characteristics (particle tracking for advection with a finite difference solution of the dispersion part) or the random walk method (to reproduce a Gaussian distribution of particles to simulate dispersion).

Note that research is taken place to develop more effective solution techniques based on the finite element method with the purpose to reduce numerical dispersion (Sudicky, 1989; Esch, van, personal communication, 1996).

[7]Sudicky (1989) even obtained highly accurate solutions for grid Peclet numbers in excess of 30 for the finite element method, based on a Laplace transformation of the temporal derivatives.

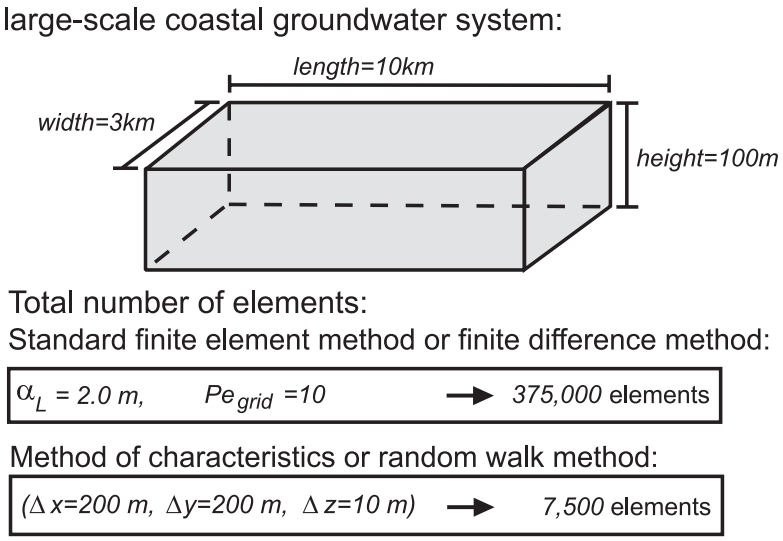

Figure 6.4: Effect of the longitudinal dispersivity α_L on the total number of elements which are required to simulate a large-scale coastal aquifer by means of a model based on the standard finite element or finite difference method and a model based on the method of characteristics or the random walk method (viz. no effect of α_L !).

6.3 Some computer codes

Here follows a summary of some computer codes which can simulate density dependent groundwater flow and solute transport in order to model salt water intrusion.

6.3.1 SUTRA

SUTRA[8] is a two-dimensional finite element code (a three-dimensional version is on its way). The manual of SUTRA is well-documented (Voss, 1984). The code has been applied successfully for the simulation of salt water intrusion in various types of profiles, which is demonstrated in a large number of publications, such as Voss & Souza (1987) and Souza & Voss (1987). Gradually, SUTRA has become a widely accepted groundwater flow model throughout the world, and accordingly, it has a prosperous future in store in the field of two-dimensional modelling of solute transport in density dependent (coastal) hydrogeologic systems. It can simulate density dependent groundwater flow with (thermal) energy transport or chemically reactive (single-species) solute transport. The SUTRA flow simulation can be applied for areal and for cross-sectional modelling of saturated groundwater systems, and for cross-sectional modelling of unsaturated zone flow. It applies a weighted residual numerical method combining Galerkin finite-elements with integrated finite differences to solve groundwater flow and transport equations (either energy or solute). As SUTRA is a finite element model, the system is represented by nodes and (quadrilateral) elements. The applied temporal discretisation is based on a backward finite-difference approximation for

[8] http://www.scisoftware.com/products/sutra_overview/sutra_overview.html, http://magma.Mines.EDU/igwmc/software/igwmcsoft/sutra.htm

the time derivatives.

A unique aspect of SUTRA is the availability of a flow-direction-dependent longitudinal dispersion form (besides the flow-direction-independent form) which allows the longitudinal dispersivity to vary with direction. Longitudinal dispersivities should be in the order of the size of either the largest hydrogeologic or flow inhomogeneities along the transport reach or of that of the distance between those inhomogeneities, whichever is the greater value.

Narrow transition zones require a careful choice of spatial and temporal discretisation. Voss & Souza (1987) stated that oscillations in the numerical method do not occur if the following expression is obeyed:

$$Pe_{grid} = \frac{|V|\,\Delta x_i}{(\alpha_L\,|V| + D_m)} < 4 \tag{6.4}$$

where

- Δx_i = longest distance between sides of an element (L),
- $|V|$ = magnitude of the real velocity ($L\,T^{-1}$),
- D_m = molecular diffusion ($L^2\,T^{-1}$).

This expression appears to be a severe restriction, see e.g. subsection 6.2.3. SUTRA may compute inaccurate solute distribution if longitudinal dispersivities are small.

6.3.2 HST3D

HST3D (Kipp, 1986)[9] a three-dimensional finite difference code that can simulate heat and solute transport. Modelling a large-scale coastal hydrogeologic system with a non-uniform density distribution with HST3D appears to be rather complicated when small longitudinal dispersivities should be applied. Large dispersivities (e.g. α_L=200 m if Δx= 250 m) have to be inserted into the model, as otherwise the solute transport equation does not converge to a solution. As a consequence of simulations with large dispersivities, excessive hydrodynamic dispersion created extensive and unrealistic brackish zones which do not agree with the actual situation. For this reason, HST3D is certain to be unsuitable in many cases.

6.3.3 SWICHA

SWICHA (Huyakorn *et al.*, 1987; Lester, 1991) (http://magma.Mines.EDU/igwmc/software/igwmcsoft/swicha.htm) is a three-dimensional finite element code. It can simulate variable density fluid flow and solute transport processes in saturated porous media. The applications range from simple one-dimensional to complex three-dimensional, coupled flow and solute transport. The groundwater flow and solute equations are solved by the Galerkin technique. An implicit Picard iterative scheme is applied to treat the non-linearity of the problems. For a transient solution of the salt water intrusion problem, the Crank-Nicolson time step scheme is applied to handle the temporal discretisation. Spatial discretisation is

[9] http://wwwbrr.cr.usgs.gov/projects/GW_Solute/hst/index.html,
http://www.scisoftware.com/products/hst3d_overview/hst3d_overview.html

performed using rectangular or triangular elements. The solute transport equation may not converge to a solution if a so-called *critical Peclet number* is exceeded in a element. In order to solve this problem, SWICHA offers a trick at the user's option: numerical dispersion (the so-called *artificial dispersion*) is added to the solute transport equation matrix. Then, spatial oscillations are suppressed and the critical Peclet number is no longer exceeded in that element. Subsequently, the solution will converge. It appears that convergence difficulties especially occur when small dispersivities are used, unless: (1) a lot of artificial dispersion is added to the matrix (then, the overall dispersion is great again), or (2) the grid is refined to avoid local numerical oscillations which come with the Galerkin technique.

6.3.4 METROPOL

METROPOL (Sauter *et al.*, 1993) (MEthod for the TRansport Of POLlutants) simulates three-dimensional groundwater flow with varying density and simultaneous transport of contaminants. It is based on the finite element method. METROPOL is developed by the Dutch National Institute of Public Health and Environmental Protection RIVM. It has been applied to simulate safety assessments of the geological disposal of radionuclear waste in (high-brine) salt formations.

6.3.5 SWIFT

SWIFT (Ward, 1991; Ward & Benegar, 1998) (Sandia Waste-Isolation Flow and Transport model)[10] is a three-dimensional code to simulate groundwater flow, heat (energy), brine and radionuclide transport in porous and fractured media. The equations for flow, heat and brine are coupled by fluid density, viscosity and porosity. The equations are solved by the finite difference method. In Ward & Benegar (1998) it is stated that though grid Peclet numbers greater than 4 may cause problems (e.g. oscillations), a value of 10 or more is sometimes acceptable.

6.3.6 FAST-C(2D/3D)

FAST-C(2D/3D) (Holzbecher, 1998) can be applied to model density driven flow in porous media using the streamfunction formulation. Density variations are caused by temperature or salinity gradients. The code is based on a finite difference discretisation, whereas the conjugate gradient method is employed as the equation solver. The three-dimensional version, FAST-C(3D), is based on the pressure formulation and needs additional testing. Steady state as well as transient modelling of confined aquifers is possible. Velocity dependent dispersion is taken into account. Holzbecher considers a vast number of temperature and saline problems to validate his code, such as steady and transient advection, Elder's problem, upconing of salt water, Henry's problem, Hydrocoin test case, etc.

[10] http://www.hsigeotrans.com/swift.html,
http://magma.Mines.EDU/igwmc/software/igwmcsoft/swift.htm

6.3.7 FEFLOW

FEFLOW (Diersch, 1996)[11] a three-dimensional computer code, which employs the finite element method. The governing partial differential equations describe groundwater flow, where differences in density affect the fluid flow. Advection, hydrodynamic dispersion as well as relatively simple chemical reactions (e.g. adsorption) are taken into account. Fluid density effects are caused by contaminant mass as well as temperature differences simultaneously, inducing thermohaline flow. Graphical tools for the visual analysis of the data are included. FEFLOW is verified with the free convection problems (Elder's and Bénard's problem), and for Henry's problem, upconing of saltwater and the Hydrocoin case (case 5, level 1).

6.3.8 D^3F

D^3F (Fein, *et al.*, 1998), which stands for Distributed Density Driven Flow, is the newest, sophisticated, computer code to simulate density-driven groundwater flow. It is based on the volume element method. Permeabilities, porosities, values for boundary and initial conditions can be defined as constants as well as simple spatial user-defined functions. In addition, a stochastic permeability distribution technique is available to consider small-scale heterogeneities. Fluid density and viscosity are functions of salt concentration and temperature. It consists of a pre-processor, the simulator itself and a post-processor. The code can be run on serial as well as massively parallel computers.

6.4 MOCDENS3D

The three-dimensional computer code MOC3D (Konikow *et al.*, 1996) is adapted for density differences: MOCDENS3D (Oude Essink, 1998a, 1998b, 1999a)[12]. As a result, it is possible to model transient three-dimensional groundwater flow in large-scale hydrogeologic systems where non-uniform density distributions occur. A special field of application is the simulation of salt water intrusion in coastal aquifers. The groundwater flow equation is solved by the MODFLOW module of MOCDENS3D. Density differences are taken into account through adding buoyancy terms to the RHS term of the basic groundwater flow equation of MODFLOW. The advection-dispersion equation is solved by the MOC module, using the method of characteristics. Advective transport of solutes is modelled by means of particle tracking and dispersive transport by means of the finite difference method. An advantage of applying the method of characteristics is that the condition of spatial discretisation is not strict. As a consequence, the displacement of fresh, brackish and saline groundwater in large-scale hydrogeologic systems can easily be modelled.

Note that other people have developed a density dependent version of the MODFLOW computer code in combination with a solute transport module. MOCDENS3D is just one of them. For instance, the Testing and Research Institute of the Netherlands Waterworks (KIWA) have developed a combination of MODFLOW (adapted for density differences) and the solute transport code MT3D96 (Schaars, 1996; Van Gerven & Schaars, 1998a; Gerven

[11] http://www.scisoftware.com/products/feflow_overview/feflow_overview.html
[12] http://www.geo.uu.nl/~goe/anima.htm

& Schaars, 1998b). In addition, SEAWAT, developed by Guo & Bennett (1998), has the same characteristics as the KIWA version.

6.4.1 Characteristics of MOCDENS3D

MOCDENS3D (in total some 15000 FORTRAN lines including remarks), which is in fact MOC3D (Konikow *et al.*, 1996) but now adapted for density differences, consists of two robust modules which are fully integrated with each other. First, it comprises a solute transport module, here called the MOC module[13], to displace the density field (originally, this module was applied to simulate ordinary solute transport). Second, it comprises a groundwater flow module, here called the MODFLOW module[14], adapted for density differences to compute transient density dependent groundwater flow. This feature is possible by inserting a so-called buoyancy term in the basic equation of the MODFLOW module, a relatively simple adaptation as can be seen in the following section. The velocity field distribution is obtained from the computed freshwater head distribution. Subsequently, the velocity field is used in the MOC module to simulate changes in density field. As such, the two modules are coupled with each other. Some characteristics of MOCDENS3D are:

- the code takes into account hydrodynamic dispersion (molecular diffusion as well as mechanical dispersion) and chemical reactions such as adsorption (by means of a retardation factor) and radioactive decay,

- solute transport is modelled through splitting up the advection-dispersion equation into two components: (a) an advective component which is solved by means of a particle tracking technique (the so-called Method Of Characteristics: MOC), and (b) a dispersive component which is solved by the finite difference method. Due to the splitting up, numerical dispersion can be kept within bounds, even if coarse elements and small longitudinal dispersivities are used. As such, numerical problems don't occur when elements measure e.g. 250*250*10 m in combination with a longitudinal dispersivity of α_L=1 m. Especially in this characteristic MOCDENS3D differs from codes which solve the partial differential equations with the standard finite element or finite difference methods. With these methods, severe numerical implications may occur when the spatial discretisation condition is not met. This spatial discretisation condition is characterised by the so-called grid-Peclet-number (Frind & Pinder, 1983; Daus *et al.*, 1985; Kinzelbach, 1987a, 1987b; and Oude Essink & Boekelman, 1996).

- the variation of the pore volume of the elements should be relatively small, as otherwise the demand of mass conservation of solute is violated too much[15]. This numerical characteristic is related to the particle tracking technique; as a matter of fact, the 3D

[13] MOC3D, version 1.1 of May 1997, is the 3D successor of MOC (Konikow & Bredehoeft, 1978).

[14] The MODFLOW module is just MODFLOW-96 (McDonald & Harbaugh, 1988; Harbaugh & McDonald, 1996), version 3.0 of December 1996, but now fully integrated in MOC3D.

[15] As a matter as fact, the density dependent groundwater flow equation in the MODFLOW module could be discretised for elements with a variable pore volume by taking into account density differences in horizontal direction, see e.g. Olsthoorn (1996). However, elements in the MOC module are considered to be uniform. Therefore, adaptation of density differences in horizontal direction is unnecessary and, as such, not applicable.

solute transport code MT3D (Zheng, 1990) suffers the same problem. The applied version of MOCDENS3D uses a uniform grid.

- though numerical dispersion is limited, deviations in the mass balance of solute transport still occur. A substantial difference between the initial mass (in the appearance of the concentration distribution) and the mass after a large number of particle displacements may arise, in particular when discretisation of the elements is coarse or when time steps are large.

6.4.2 Adaptation of the MODFLOW module for density differences

The groundwater flow equation in the MODFLOW module is as follows:

$$\sum Q_i = S_s \frac{\Delta\phi}{\Delta t} \Delta V \tag{6.5}$$

where

- S_s = specific storage of the porous material (L^{-1}),
- Q_i = total flow rate into the element ($L^3\,T^{-1}$),
- ΔV = volume of the element (L^3),
- $\Delta\phi$ = change in head over a time interval of length Δt (L).

The discretised groundwater flow equation for a uniform grid in MODFLOW is (McDonald & Harbaugh, 1988), see also the lecture notes of Groundwater Modelling I (Oude Essink, 2000c):

$$\begin{gathered} CV_{i,j,k-1/2}\phi^m_{i,j,k-1} + CC_{i-1/2,j,k}\phi^m_{i-1,j,k} + CR_{i,j-1/2,k}\phi^m_{i,j-1,k} \\ +(-CV_{i,j,k-1/2} - CC_{i-1/2,j,k} - CR_{i,j-1/2,k} \\ -CR_{i,j+1/2,k} - CC_{i+1/2,j,k} - CV_{i,j,k+1/2} + HCOF_{i,j,k})\phi^m_{i,j,k} \\ +CR_{i,j+1/2,k}\phi^m_{i,j+1,k} + CC_{i+1/2,j,k}\phi^m_{i+1,j,k} + CV_{i,j,k+1/2}\phi^m_{i,j,k+1} \\ = RHS_{i,j,k} \end{gathered} \tag{6.6}$$

where

- $HCOF_{i,j,k} = P_{i,j,k} - SC1_{i,j,k}/(t_m - t_{m-1})$,
- $RHS_{i,j,k} = -Q_{i,j,k} - SC1_{i,j,k}\phi^{m-1}_{i,j,k}/(t_m - t_{m-1})$, and
- $SC1_{i,j,k} = SS_{i,j,k}\Delta r_j \Delta c_i \Delta v_k$.

Note that CV, CC and CR are the hydraulic conductances in respectively the layer, column and row direction. The attention is focused in the vertical volume flow in element $[i, j, k]$, see fig. 6.5. First, the basic vertical Darcian velocity (specific discharge) is defined as follows (see also eqn. 2.10)

$$q_z = -\frac{\kappa_z}{\mu}\left(\frac{\partial p}{\partial z} + \rho g\right) \tag{6.7}$$

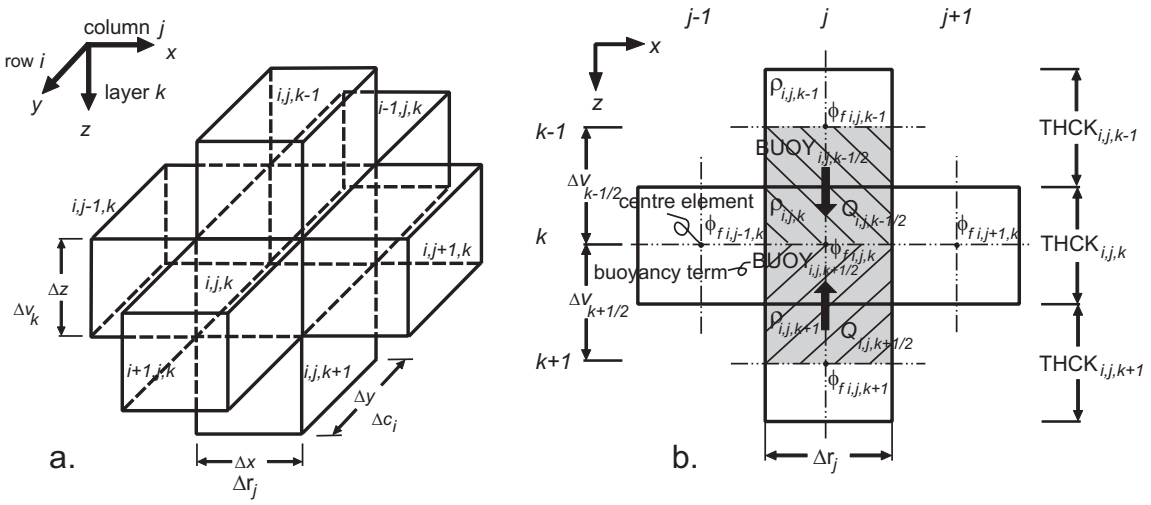

Figure 6.5: MODFLOW elements with corresponding density terms.

Under normal conditions, MODFLOW applies piezometric heads. However, here so-called equivalent freshwater heads[16] are used because density differences are taken into account. Introduction of this freshwater head ϕ_f gives:

$$\phi_f = \frac{p}{\rho_f g} + z \tag{6.8}$$

Inserting of eqn. 6.8 in eqn. 6.7 gives:

$$q_z = -\frac{\kappa_z \rho_f g}{\mu}\left(\frac{\partial \phi_f}{\partial z} + \frac{\rho - \rho_f}{\rho_f}\right) \tag{6.9}$$

In many cases small viscosity differences can be neglected if density differences are considered in normal hydrogeologic systems (Verruijt, 1980; Bear & Verruijt, 1987). Eqn. 6.9 can then be written as[17]:

$$q_z = -k_z\left(\frac{\partial \phi_f}{\partial z} + \frac{\rho - \rho_f}{\rho_f}\right) \tag{6.10}$$

where k_z=$\kappa_z \rho_f g/\mu$=hydraulic conductivity for fresh water and $(\rho - \rho_f)/\rho_f$=the so-called *buoyancy term*. Discretisation of this buoyancy term, which is required in the MODFLOW module, gives (see fig. 6.5):

$$BUOY_{i,j,k+1/2} = \left(\frac{(\rho_{i,j,k} + \rho_{i,j,k+1})/2 - \rho_f}{\rho_f}\right) \tag{6.11}$$

[16]Definition: fictive piezometric head as will be measured when the observation well is filled with fresh groundwater instead of saline or brackish.

[17]Note that in cases with high groundwater densities, such as brine transport in salt domes with densities up to 1200 kg/m^3, eqn. 6.9 instead of eqn. 6.10 should be applied. Moreover, additional cross-coupling terms for Darcy's and Fick's laws are necessary to take into account the dependency of fluid motion to brine transport, and vice versa (e.g. Hassanizadeh & Leijnse, 1988), see page 21. These terms are not included in MOCDENS3D. As such, under circumstances with high salt concentrations, sophisticated codes such as METROPOL should be applied ('though it's not often done').

The MOC module relates the density $\rho_{i,j,k}$ to the solute concentration $C_{i,j,k}$ in groundwater for each element through the equation of state:

$$\rho_{i,j,k} = \rho_f \left(1 + \frac{\rho_s - \rho_f}{\rho_f}\frac{C_{i,j,k}}{C_s}\right) \qquad \text{or} \qquad \rho_{i,j,k} = \rho_f \left(1 + \beta C_{i,j,k}\right) \tag{6.12}$$

where $C_{i,j,k}$=solute concentration in groundwater in element $[i,j,k]$ (in mg TDS/l); C_s=reference solute concentration in saline groundwater (e.g. 35000 $mg\ TDS/l$); β=coefficient of compositional expansion (e.g.=0.025/35000=7.14 $\times 10^{-7}$ l/mg TDS). Rewriting eqn. 6.10 in discretised terms of the MODFLOW module and using eqn. 6.11 gives for the flow at the top of element $[i,j,k]$:

$$q_{i,j,k-1/2} = KV_{i,j,k-1/2}\left(\frac{\phi_{f,i,j,k-1} - \phi_{f,i,j,k}}{\Delta v_{k-1/2}} + BUOY_{i,j,k-1/2}\right) \tag{6.13}$$

and for the flow at the bottom of element $[i,j,k]$ (the negative sign is for flow **into** the element $[i,j,k]$):

$$q_{i,j,k+1/2} = -KV_{i,j,k+1/2}\left(\frac{\phi_{f,i,j,k} - \phi_{f,i,j,k+1}}{\Delta v_{k+1/2}} + BUOY_{i,j,k+1/2}\right) \tag{6.14}$$

The vertical Darcian velocity q is multiplied by the area $\Delta r_j\ \Delta c_i$ to obtain the volume flow Q. The conductance value in vertical direction, $CV_{i,j,k-1/2} = KV_{i,j,k-1/2}\,\Delta r_j\,\Delta c_i/\Delta v_{k-1/2}$ (McDonald & Harbaugh, 1988) is used to rewrite eqn. 6.13:

$$Q_{i,j,k-1/2} = +CV_{i,j,k-1/2}\left(\phi_{f,i,j,k-1} - \phi_{f,i,j,k} + BUOY_{i,j,k-1/2}\Delta v_{k-1/2}\right) \tag{6.15}$$

Similar for eqn. 6.14:

$$Q_{i,j,k+1/2} = +CV_{i,j,k+1/2}\left(\phi_{f,i,j,k+1} - \phi_{f,i,j,k} - BUOY_{i,j,k+1/2}\Delta v_{k+1/2}\right) \tag{6.16}$$

In $Q_{i,j,k-1/2}$, the density contribution is positive ($+CV_{i,j,k-1/2}\,BUOY_{i,j,k-1/2}\,\Delta v_{k-1/2}$) whereas in $Q_{i,j,k+1/2}$ it is negative ($-CV_{i,j,k+1/2}\,BUOY_{i,j,k+1/2}\Delta v_{k+1/2}$). This is because the direction of flow at the bottom of element $[i,j,k]$ $Q_{i,j,k+1/2}$ is the opposite to the direction of the z-axis and the gravity. In the MOC module the thicknesses $THCK_{i,j,k}$ of all elements in the grid are known: consequently, $\Delta v_{k-1/2}$ and $\Delta v_{k+1/2}$ can be rewritten as $(THCK_{i,j,k-1} + THCK_{i,j,k})/2$ and $(THCK_{i,j,k} + THCK_{i,j,k+1})/2$, respectively (fig. 6.5).

Summarizing, three adaptations are necessary to make MOC3D suitable for density dependent groundwater flow:

a. subtract for each element the two buoyancy terms of the eqn. 6.15 and 6.16 from the right hand side term $RHS_{i,j,k}$ in eqn. 6.6 of the MODFLOW module for each time the groundwater flow equation is solved:

$$\begin{aligned} RHS^{new}_{i,j,k} \Longrightarrow RHS^{old}_{i,j,k} &- CV_{i,j,k-1/2}BUOY_{i,j,k-1/2}(THCK_{i,j,k-1} + THCK_{i,j,k})/2 \\ &+ CV_{i,j,k+1/2}BUOY_{i,j,k+1/2}(THCK_{i,j,k} + THCK_{i,j,k+1})/2 \end{aligned} \tag{6.17}$$

b. add the two buoyancy terms of the eqn. 6.15 and 6.16 to the volume flows $Q_{i,j,k-1/2}$ and $Q_{i,j,k+1/2}$ respectively. These flows are used in the MOC module to simulate solute transport by means of particle tracking:

$$Q^{new}_{i,j,k-1/2} \Longrightarrow Q^{old}_{i,j,k-1/2} + CV_{i,j,k-1/2} BUOY_{i,j,k-1/2} (THCK_{i,j,k-1} + THCK_{i,j,k})/2 \tag{6.18}$$

and

$$Q^{new}_{i,j,k+1/2} \Longrightarrow Q^{old}_{i,j,k+1/2} - CV_{i,j,k+1/2} BUOY_{i,j,k+1/2} (THCK_{i,j,k} + THCK_{i,j,k+1})/2 \tag{6.19}$$

c. transform piezometric heads h to freshwater heads ϕ_f:

$$h_{i,j,k} \Longrightarrow \phi_{f,i,j,k} \tag{6.20}$$

As a matter of fact, these adaptations have already been executed by Lebbe (1983) for the 2D solute transport code MOC (Konikow & Bredehoeft, 1978). Note again that ϕ_f has become a fictive freshwater head as density is taken into account. Therefore, streamlines (or velocity vectors) are not perpendicular to the freshwater head contour lines. However, in hydrogeologic systems with ordinary fresh groundwater nothing changes with respect to the original MODFLOW computations.

6.4.3 Size of the time step Δt

In case of groundwater flow with variable densities, the velocity field depends on the density distribution through the freshwater head distribution. When fresh, brackish and saline groundwater displace, the density distribution changes accordingly. After a while, the freshwater head distribution and velocity field should be computed once again, as otherwise the velocity field does not correspond with the current density distribution. Consequently, the size of the time step Δt for the groundwater flow equation should be known in advance, since it determines how often the velocity field is computed again. Therefore, it is important to determine the size of the time step Δt. This size depends on the pace of the solute process involved as a large time step could cause an unrealistic solution (e.g. see fig. 6.20). For instance, the time step Δt in large-scale hydrogeologic systems in coastal dune areas can be in the order of (several) years (Lebbe, 1983; Oude Essink, 1996), whereas near severe groundwater extractions the density distribution can change so fast that a smaller time step is needed (in the order of months). In MOCDENS3D, the size of the time step is manually determined. The so-called CFL (Courant-Friedrichs-Lewy) condition, which is applied by the MOC module for solute transport as a stability criterion (Konikow & Bredehoeft, 1978), could be utilized to estimate an acceptable size of the time step for the groundwater flow equation. The size of the time step is determined on the basis of experience and/or through trial-and-error (e.g. by means of several test computations: when the density distribution changes rapidly, small time steps are required).

6.4.4 Conversion to freshwater head

As a non-uniform density distribution in the groundwater system is modelled, the piezometric heads in fresh, brackish or saline groundwater must be converted into freshwater

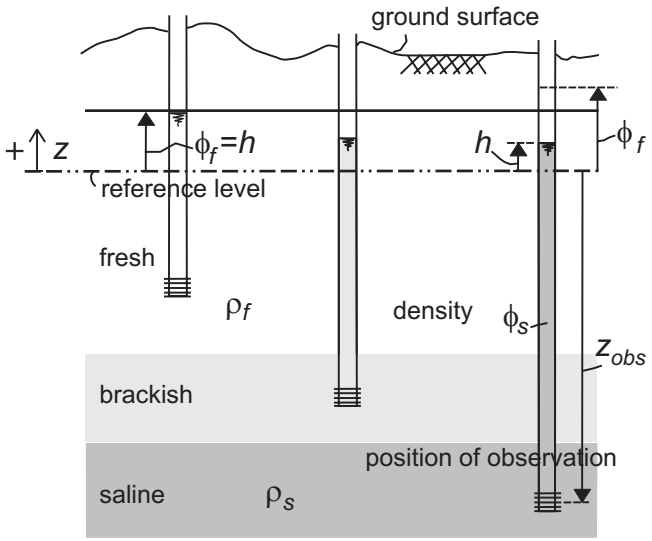

Figure 6.6: Conversion from observed piezometric level to freshwater head.

heads ϕ_f. The determination of the (fictive) freshwater head is as follows (see fig. 6.6):

$$\phi_f = (h - z_{obs}) \cdot \frac{\rho_{obs}}{\rho_f} + z_{obs} \tag{6.21}$$

where

- ϕ_f = freshwater head of the observation well with respect to the reference level (L),
- h = observed piezometric level relative to the reference level (L),
- z_{obs} = elevation of the point of observation relative to the reference level (L),
- ρ_{obs} = density of the water column in the observation well ($M\,L^{-3}$).

For example, at a vertical boundary with a constant piezometric level the freshwater head configuration can be assessed assuming that no vertical groundwater movements occur. This means the situation is supposed to be *hydrostatic*. If the piezometric level in the upper element, $\phi_{f,i,j,1}$, and the density distribution in vertical direction are known, the freshwater heads in all elements underneath the upper element can be determined. For each element at an increasing depth with respect to the reference level, e.g. *N.A.P.*, the freshwater head in the centre of the element $[i, j, k]$ is as follows:

$$\phi_{f,i,j,k} = \phi_{f,i,j,k-1} + BUOY_{i,j,k-1/2}(THCK_{i,j,k-1} + THCK_{i,j,k})/2 \tag{6.22}$$

where $\phi_{f,i,j,k}$ and $\phi_{f,i,j,k-1}$ are the freshwater heads respectively in the elements $[i, j, k]$ and $[i, j, k-1]$ (L).

6.4.5 Solute transport: the MOC3D module

The three-dimensional equation for solute transport in homogeneous isotropic porous media can be written as follows:

$$\frac{\partial C}{\partial t} = \frac{1}{n_e R_d}\frac{\partial}{\partial x_i}(n_e D_{ij}\frac{\partial C}{\partial x_j}) - \frac{V_i}{R_d}\frac{\partial C}{\partial x_i} + \frac{\sum[W(C-C')]}{n_e R_d} - \lambda C \tag{6.23}$$

where

- C = concentration of the dissolved solids ($M\,L^{-3}$),
- D_{ij} = coefficient of hydrodynamic dispersion ($L^2\,T^{-1}$),
- $V_i = q_i/n_e$ = effective velocity of the groundwater in the direction of x_i ($L\,T^{-1}$),
- $W(x, y, z, t)$ = general term for sources and sinks (T^{-1}),
- C' = concentration of the dissolved solids in a source or sink ($M\,L^{-3}$),
- n_e = effective porosity of the medium ($-$),
- $R_d = 1 + (\rho_b/n_e)K_d$ = retardation factor governing adsorption ($-$). K_d is the distribution coefficient ($M^{-1}\,L^3$) and ρ_b is the bulk density of the porous material ($M\,L^{-3}$),
- λ = first-order rate constant, governing hydrolysis and decay (T^{-1}). Radioactive decay rates are often expressed as half-lives ($t_{1/2}$), where the half-life is the time required for the concentration to decrease to one-half of the original value: $t_{1/2} = (\ln 2)/\lambda$.

Stability criteria

Three stability criteria determine the explicit numerical solution of the advection-dispersion equation. These criteria may require that the flow time step Δt, applied to solve the groundwater flow equation, must be subdivided into a number of smaller solute time steps Δt_s to accurately solve the advection-dispersion equation. During such a solute time step, particles are moved to new positions. The distance over which a particle is moved is proportional to the length of that solute time step and the velocity at the location of that particle. The three stability criteria of the advection-dispersion equation, which must all three be satisfied in MOCDENS3D, are:

1. The explicit solution of the hydrodynamic part of the advection-dispersion equation is stable, if:

$$\Delta t_s \leq \min_{(\text{over grid})}\left[\frac{0.5}{\frac{D_{xx}}{R_d(\Delta x)^2} + \frac{D_{yy}}{R_d(\Delta y)^2} + \frac{D_{zz}}{R_d(\Delta z)^2}}\right] \tag{6.24}$$

   This expression is called the Neumann-criterion. Thus, the smallest permissible time step Δt_s for solving the advection-dispersion equation occurs in the node that has the greatest value of $\frac{D_{xx}}{(\Delta x)^2} + \frac{D_{yy}}{(\Delta y)^2} + \frac{D_{zz}}{(\Delta z)^2}$.

2. Consider the mixing of groundwater of one concentration $C_{i,j}$ with injected or recharged (surface) water of a different concentration $C'_{i,j}$. The change in concentration in that specific source node is not allowed to exceed the difference between the concentration in the aquifer $C_{i,j}$ and the source concentration $C'_{i,j}$. This condition produces:

$$\Delta t_s \leq \min_{(\text{over grid})} \left[\frac{n_e \, R_d}{W_{i,j,k}} \right] \tag{6.25}$$

3. The last stability criterion for the maximum permissible time step Δt_s involves the particle movements to simulate advective transport:

$$\begin{aligned} \Delta t_s V_{x,particle} &\leq \zeta \Delta x \\ \Delta t_s V_{y,particle} &\leq \zeta \Delta y \\ \Delta t_s V_{z,particle} &\leq \zeta \Delta z \end{aligned} \tag{6.26}$$

where

- ζ = the maximum relative distance across an element, in which a particle is allowed to move during one solute time step Δt_s. It is usually a fraction of the grid dimension ($0 < \zeta \leq 1$) in order to ensure that the particle movements are controlled within one solute time step.

Obviously, this criterion is based on the Courant number Co. Rewriting equation 6.26 gives:

$$\begin{aligned} \Delta t_s &\leq \frac{\zeta \Delta x}{V_{x,max}} \\ \Delta t_s &\leq \frac{\zeta \Delta y}{V_{y,max}} \\ \Delta t_s &\leq \frac{\zeta \Delta z}{V_{z,max}} \end{aligned} \tag{6.27}$$

where $V_{x,max}, V_{y,max}, V_{z,max}$ are the maximum real velocities at a node or boundary of a element respectively in the x, y and z-direction.

Finally, the smallest solute time step Δt_s is applied which is determined by the equations 6.24, 6.25 and 6.27. If the flow time step Δt is greater than the smallest solute time step Δt_s, then the flow time step Δt is subdivided into the appropriate number of smaller time steps Δt_s required to solve the advection-dispersion equation. It may occur that the stability criteria are not so strict that the smallest required solute time step Δt_s is greater than the flow time step Δt. Then, Δt_s must be equal to Δt.

6.5 Examples of numerical modelling with MOCDENS3D

6.5.1 Introduction

Model testing comprises, besides comparison with the results of other models and with reality, model verification of problems for which analytical solutions exist. Numerical models, that simulate not only groundwater flow but also solute transport, can be tested or

validated[18] by various models with analytical solutions. Analytical solutions of solute transport can be complex, and therefore, mostly straightforward hypothetical cases are considered. For instance, analytical solutions are given for the one-dimensional form of the advection-dispersion equation by Ogata & Banks (1961), Shamir & Harleman (1966), Kinzelbach (1986, 1987a), Gelhar & Collins (1971), Freeze & Cherry (1979) and Uffink (1990). Bear (1972, 1979) has summarized examples of analytical solutions of the hydrodynamic dispersion with specific boundary and initial value problems.

First, the groundwater flow situation for a case with a vertical interface between fresh and saline groundwater will be discussed. Unfortunately, there are no analytical solutions for density dependent groundwater flow in combination with hydrodynamic dispersion but the one Henry developed in the 1960s (Henry, 1964).

6.5.2 Vertical interface between fresh and saline groundwater

In this example, groundwater flow due to density differences in a simple geometry will be considered (fig. 6.7a and table 6.1). In this homogeneous aquifer, saline groundwater at the right will flow underneath fresh groundwater at the left due to differences in density (fig. 6.8). In the beginning, the velocities at the interface between fresh and saline groundwater are large. As a function of time, the initial vertical interface is moving towards a horizontal position. Meanwhile, the velocities are reducing (fig. 6.9). Finally, the velocities reduce to zero, when the interface is in a steady state situation. Note that a Dirichlet boundary condition (constant freshwater head equal to 0 m) is present at the left boundary at x=0.00625 m and z=0.25625 m (for a grid of 80 $\times$ 40 elements), which causes a slight disturbance in the concentration distribution. In this example, some numerical dispersion occurs in a few elements near the interface.

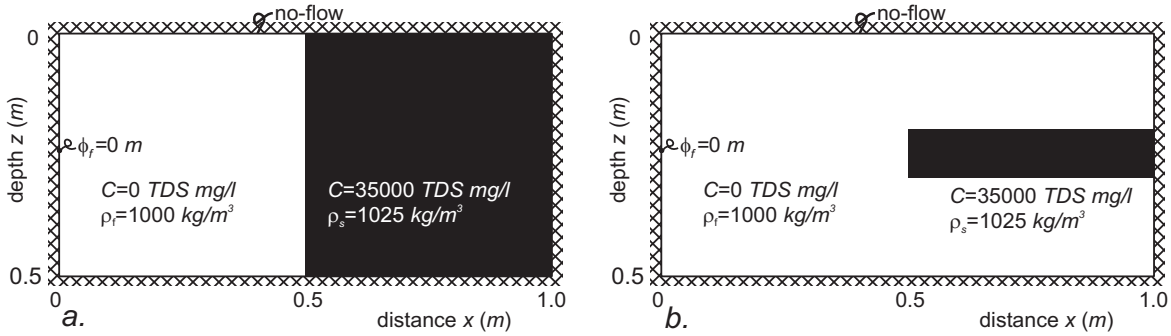

Figure 6.7: a. Geometry of a vertical interface between fresh and saline groundwater; and b. Saltwater pocket in a fresh groundwater environment.

The analytical solution of the initial absolute velocity difference left and right of the

[18]Often the testing of the computer codes for problems with known solutions is (erroneously) called *validation*. A mathematical model is said to be *validated*, if sufficient testing has been performed to show an acceptable degree of correlation (Huyakorn *et al.*, 1984). However, as a matter of fact, the models can only be *invalidated*, since the testing is only a limited demonstration of the reliability of the model (Konikow & Bredehoeft, 1992).

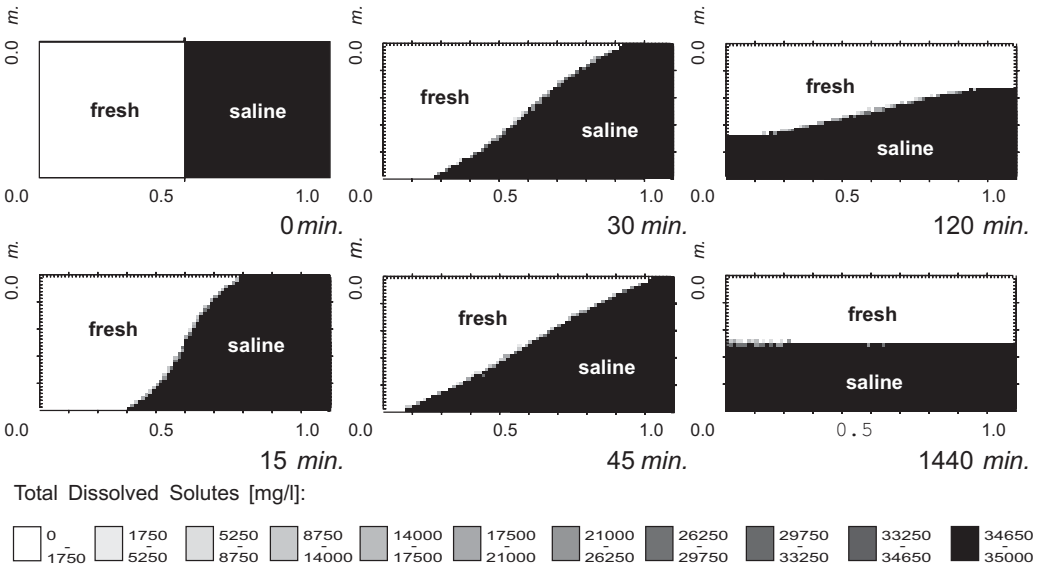

Figure 6.8: Evolution of the interface between fresh and saline groundwater, computed with MOCDENS3D with a grid of 80 × 40 elements.

Table 6.1: Physical parameters for the vertical interface problem and saltwater pocket problem.

Parameter	Vertical interface	Salwater pocket
Hydraulic conductivity k	$10^{-3}\ m\,s^{-1}$	$10^{-3}\ m\,s^{-1}$
Porosity n_e	0.1	0.1
Freshwater density ρ_f at C=0	$1000\ kg\,m^{-3}$	$1000\ kg\,m^{-3}$
Saline water density ρ_s at C=35000	$1025\ kg\,m^{-3}$	$1025\ kg\,m^{-3}$
Longitidinal dispersivity α_L	$0\ m$	$1\ mm$
Transverse dispersivity α_T	$0\ m$	$0.1\ mm$
Effective molecular diffusion D_m	$0\ m^2\,s^{-1}$	$10^{-9}\ m^2\,s^{-1}$

interface between fresh and saline groundwater is (Josselin de Jong, 1977):

$$\Delta v_z = \frac{k}{n_e}\left(\frac{\rho_s - \rho_f}{\rho_f}\right) \tag{6.28}$$

where k=hydraulic conductivity ($L\ \ T^{-1}$), Δv_z=the so-called shear flow along the interface ($L\ \ T^{-1}$). The analytical solution of the initial horizontal velocity v_x for a vertical interface between fresh and saline groundwater is equal to Verruijt (1980):

$$v_x = \frac{k}{n_e}\left(\frac{\rho_s - \rho_f}{\rho_f}\right)\frac{1}{\pi}\ln\tan\left(\frac{\pi z}{2D}\right) \tag{6.29}$$

Fig. 6.10 shows the comparison between the analytical and numerical results. Note that the analytical solutions in the eqn (6.28) and (6.29) are applicable for a geometry which is not limited by no-flow boundaries. As the geometry is bounded in the numerical case, the shear flow velocities Δv_z near the no-flow boundaries obviously differ from the analytical ones, especially for the coarse grid.

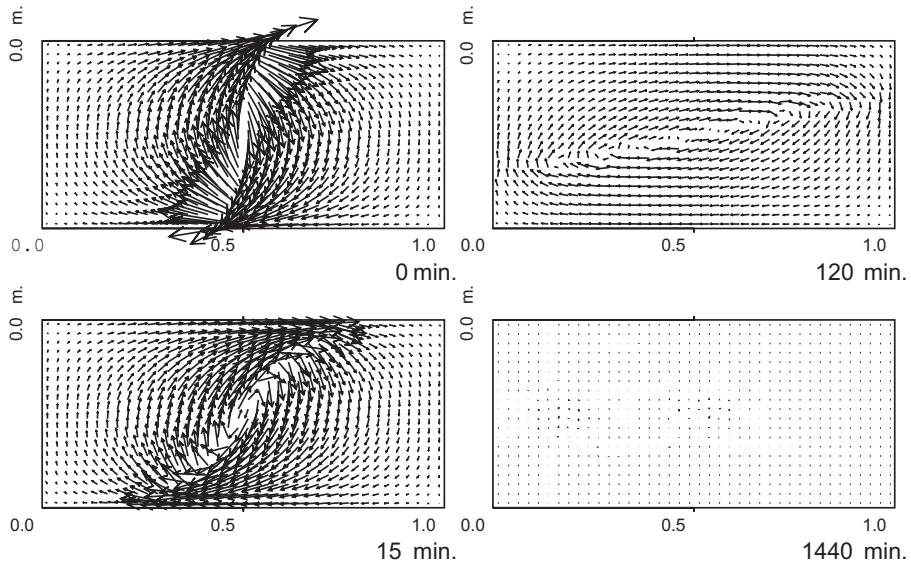

Figure 6.9: Development of the velocity field of an evolving interface between fresh and saline groundwater, computed with MOCDENS3D with a grid of 40 × 20 elements. The lengths of the arrows correspond with the displacement of groundwater during a time step of 864 *sec* (0.01 *day*).

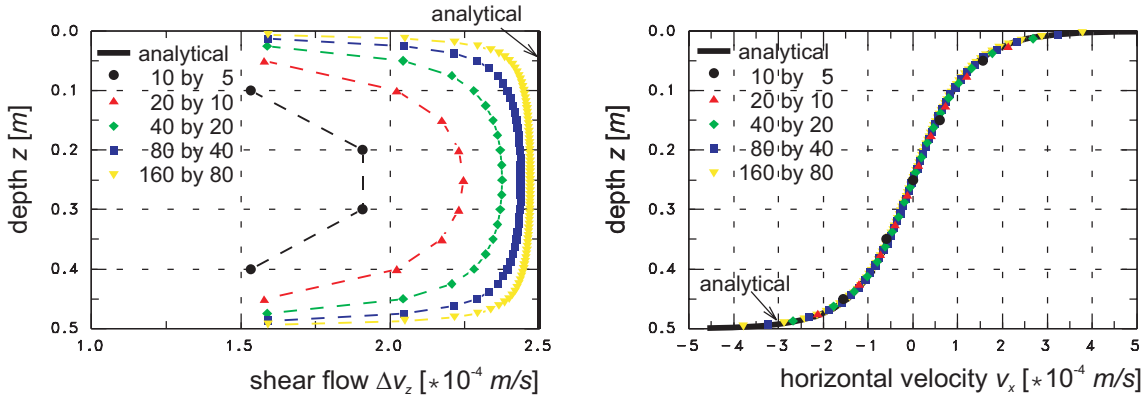

Figure 6.10: Analytical and numerical solutions (for five different number of elements) of: a. Shear flow Δv_z at the interface and b. Horizontal velocity v_x at the interface. As the shear flow Δv_z is based on vertical velocities at a distance of half an element from the vertical interface, the numerical Δv_z differs somewhat from the analytical solution.

6.5.3 Saltwater pocket in a fresh groundwater environment

In this example, a saltwater pocket is present in a fresh groundwater environment (fig. 6.7b). Under influence of gravity, the pocket will subside and mixing will occur due to hydrodynamic dispersion. The initial velocity field in fig. 6.11 shows that a strong rotating groundwater flow (vortex) is present at the left side of the pocket. This phenomenon is already described in the previous subsection. After a short moment in time, saltwater fingers occur at the bottom of the pocket (fig. 6.12). Salt groundwater will subside here faster then at

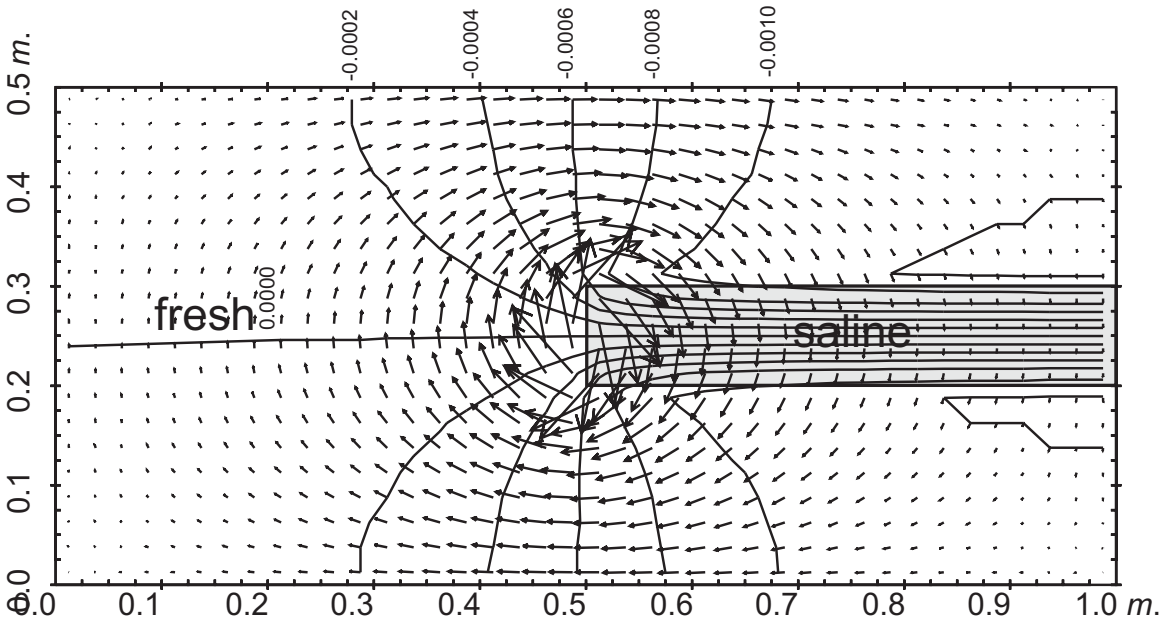

Figure 6.11: Saltwater pocket in a fresh groundwater environment. Initial velocity field, freshwater head and salinity distribution, computed with MOCDENS3D with a grid of 40 × 20 elements. The lengths of the arrows correspond with the displacement of groundwater during a time step of 864 *sec* (0.01 *day*).

the right side of the pocket. At about t=60 *min.*, the left side of the pocket will touch the bottom of the aquifer and fresh water underneath it is enclosed. Due to differences in density, the salt groundwater will sink to the bottom of the aquifer while hydrodynamic dispersion is taking place. Meanwhile, freshwater fingers will wring themselves through the saltwater pocket. Note that the effect of discretisation is large in this example (fig. 6.13): the smaller the elements, the more accurate the fingering will be modelled. Note that the number of fingers is still not constant, even with grids of 640 × 320 elements and 1280 × 640 elements.

6.5.4 Evolution of a freshwater lens

The evolution of the freshwater lens as described in section 4.8 has been modelled as an example for both the two- and the three-dimensional situation by means of a density dependent groundwater flow code, MOCDENS3D (Oude Essink, 1998b, 1999a). Fig. 6.14 gives the evolution of the freshwater lens at six moments in time for the three-dimensional situation. At the initial situation, the aquifer only contains saline groundwater. The lens develops by a constant natural recharge. The boundaries of the model are as follows: bottom impervious, at the four sides hydrostatic conditions. The results of the numerical models are in good agreement with the analytical solutions given in section 4.8.

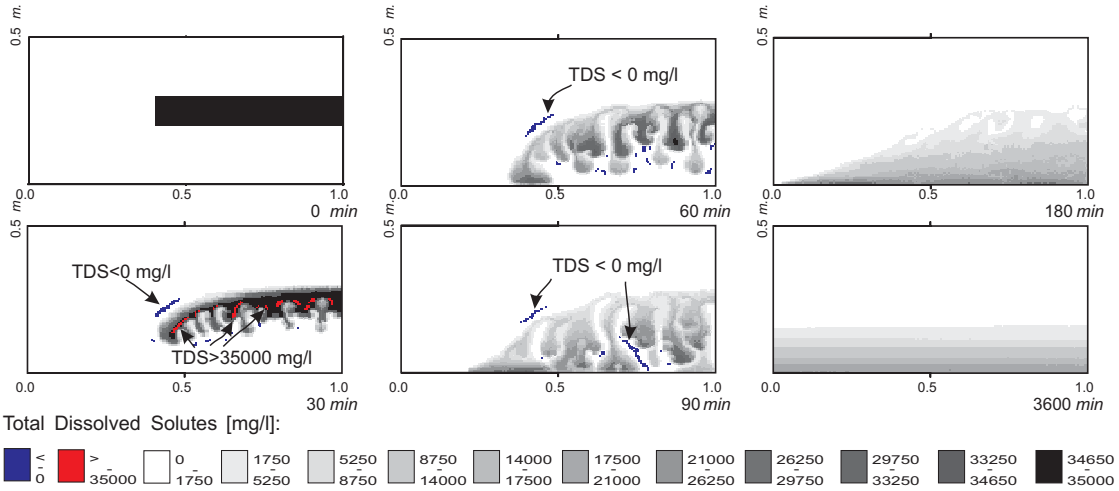

Figure 6.12: Evolution of a saltwater pocket in a fresh groundwater environment, caused by a difference in density. Due to hydrodynamic dispersion, mixing of fresh and saline groundwater is taking place. Grid is 160 by 80 elements (16 particle per elements). Time step Δt equals 180 *sec*.

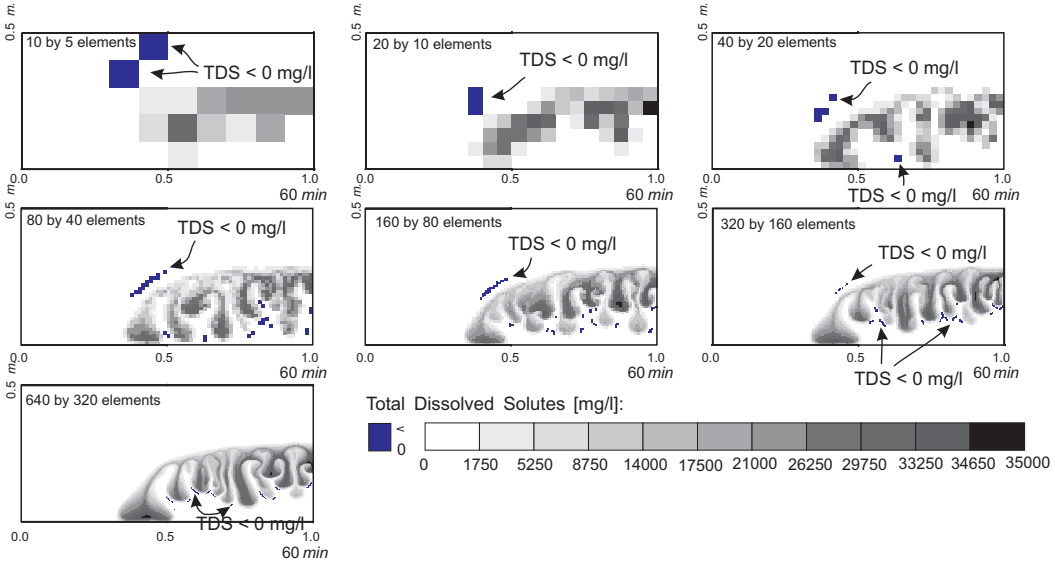

Figure 6.13: Effect of element size on the development of the saltwater pocket in the fresh groundwater environment. The number of saline fingers is not constant and still depends on the grid discretisation.

6.5.5 Henry's problem

In Henry's problem, saline water intrudes a hypothetical rectangular coastal aquifer in the Biscayne aquifer of southeastern Florida and merges by a constant dispersion coefficient. It is common practice to apply Henry's problem (1964) as a benchmark for new computer codes that can simulate density-driven groundwater flow (Segol, 1994). New numerical techniques are often compared with the solution of Henry himself. Various researchers use

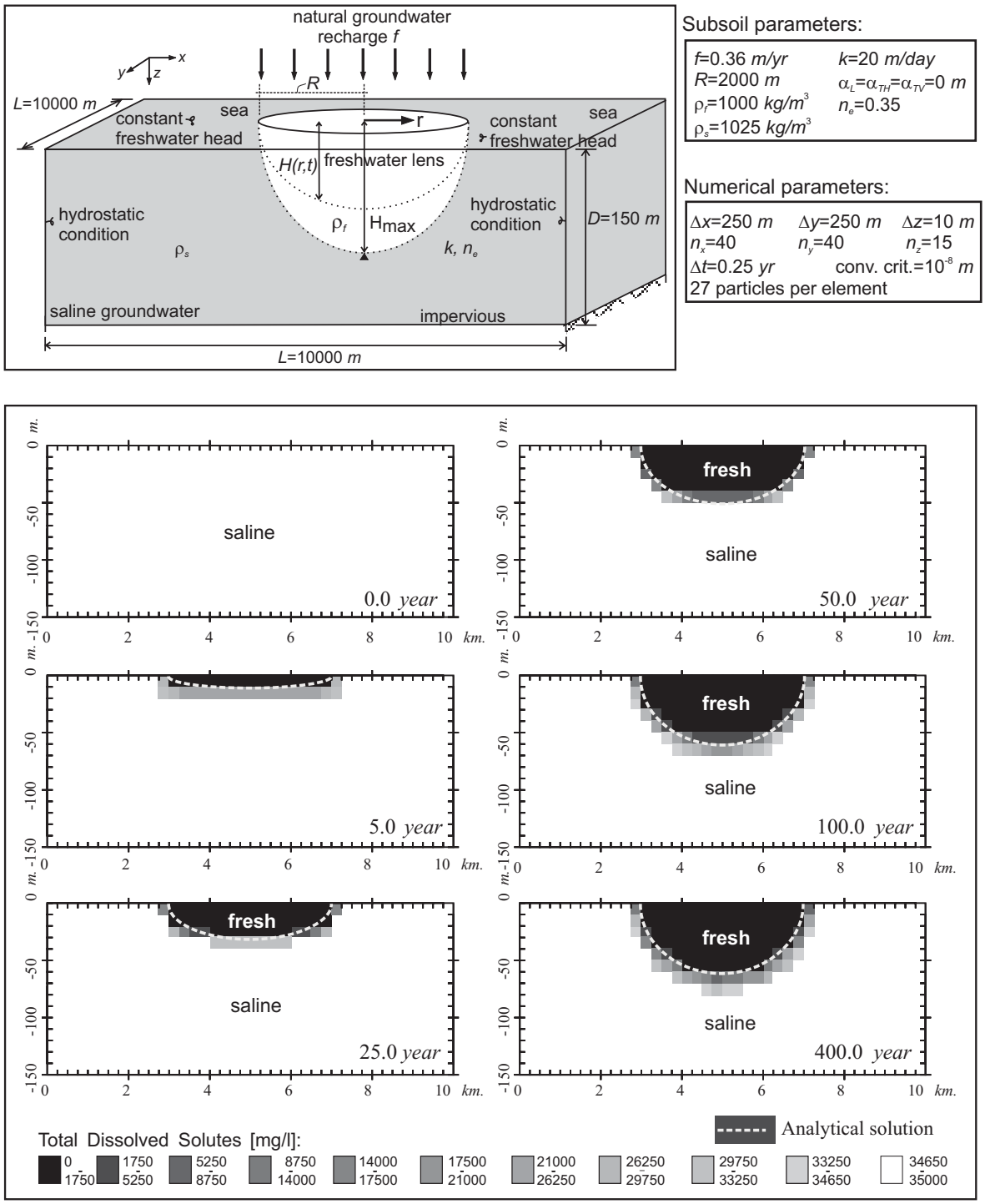

Figure 6.14: Evolution of the freshwater lens: transient interface between fresh and saline groundwater.

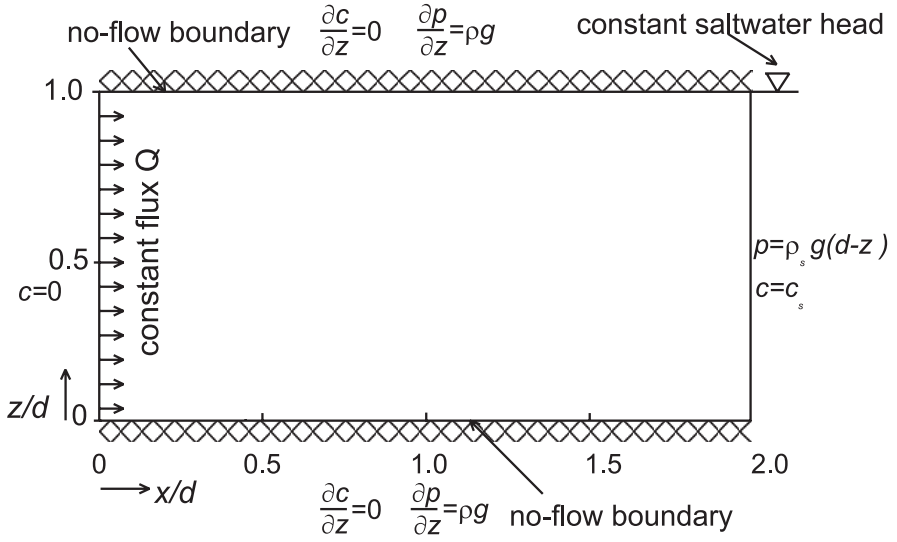

Figure 6.15: Henry's problem (1964): saline water intrudes in a hypothetical rectangular aquifer and merges by a constant dispersion coefficient.

Henry's problem to verify their own model. A few of these scientists, such as Lee & Cheng (1974), compared their numerical solutions with Henry's final steady state solution; other scientists, such as Pinder & Cooper (1970), Segol *et al.* (1975), Frind (1982), Voss (SUTRA, 1984), Sanford & Konikow (1985) and Galeati *et al.* (1992), compared their solutions with the unsteady state solutions of Henry's problem. These unsteady state situations are stages in the evolution of the salt water intrusion.

Geometry

Henry formulated in 1964 the sea water intrusion in a homogeneous, isotropic, confined, rectangular aquifer including dispersion. The effect of dispersion on salt encroachment in coastal aquifers was investigated. He solved the equations with the Galerkin method by using Fourier series.

The boundary conditions of Henry's problem are shown in fig. 6.15. The top and bottom boundaries are impermeable and thus no-flow boundaries. A constant fresh water flux Q enters the aquifer along the vertical at x=0. The seaside boundary at x=l is a constant *saltwater head*. In the solution of Henry, no mass transport over the seaside boundary occurs. Relevant dimensionless variables of this problem are defined as follows:

$$\xi = l/d, \qquad a = Q/k_1 d \qquad \text{and} \qquad b = D_h/Q \tag{6.30}$$

where

- $\xi = l/d$ = aspect ratio $(-)$,
- l = length of the aquifer (L),
- d = height of the aquifer (L),

- D_h = coefficient of hydrodynamic dispersion ($L^2\,T^{-1}$),
- Q = net fresh water discharge per unit length of beach ($L^2\,T^{-1}$),
- $k_1 = k\frac{\rho_s-\rho_f}{\rho_f}$ = hydraulic conductivity k times the relative density difference ($L\,T^{-1}$),
- ρ_f, ρ_s = density of respectively fresh and saline water ($M\,L^{-3}$),
- $b = D_h/Q$ = inverse of the (seepage) Peclet-number Pe ($-$).

The parameters in Henry's problem are set to ξ=2, a=0.263 and b=0.1. Effects of tides and recharge, that make the salt water intrusion problem unsteady, are averaged and all included in the value of the hydrodynamic dispersion coefficient D_h.

In order to satisfy the parameters ξ=2, a=0.263 and b=0.1, the following characteristics are applied in the reference case: a hypothetical aquifer of d=1.0 m by l=2.0 m; a hydraulic conductivity of k=1 cm/s; a fresh water discharge per unit length of beach of Q=6.6 $\times$ 10^{-5} m^2/s, which is uniformly distributed over the number of vertical elements; and an effective porosity of 0.35. No anisotropy occurs in Henry's problem (k_z/k_x=1.0) and the specific storativity S_s is set to zero.

Numerical modelling with MOCDENS3D

The reference case has 800 elements: $40 \cdot 20$, thus the (square) element has a length Δx and a height Δz of 0.05 m. The convergence criterion TOL for the (iterative) calculation of the freshwater head in the groundwater flow equation is 10^{-6} m, and the relative distance in a element, in which a particle is allowed to move during one solute time step, is set to 1.0. Each element has 9 particles. The flow time step is set to 5 min. The constant molecular diffusion coefficient D_d is set to 0.066 cm^2/s.

In the initial condition of the reference case, the entire aquifer only contains fresh groundwater, which has a density equal to 1000 kg/m^3. Saline groundwater has a density equal to 1025 kg/m^3, thus the relative density difference $\frac{\rho_s-\rho_f}{\rho_f}$ is 0.025. During the evolution of the brackish zone, a brackish outflow at the seaside appears in the upper part of the aquifer. It is assumed in this hypothetical case that brackish groundwater, which flows out of the aquifer at the seaside, immediately mixes with salt seawater outside the aquifer and is discharged immediately. Hence, this boundary is kept constantly saline, and thus, a constant saltwater head rather than a brackishwater head is simulated at the upper part of the seaside boundary. Fig. 6.16 shows the freshwater head distribution, several isolines of saltwater fraction and the velocity field after a simulation time of 400 min. Near the seaside, a landward flow of saline water occurs in the lower part of the aquifer and a seaward flow of fresh water occurs in the upper part of the aquifer. Obviously, sea water mixes with fresh water and circulates. Especially in the outgoing fresh water at the seaside the velocities are great. Mixing, which is caused by hydrodynamic dispersion, restricts the landward extent of salt water intrusion. This phenomenon was predicted and observed in the field by Cooper *et al.* (1964).

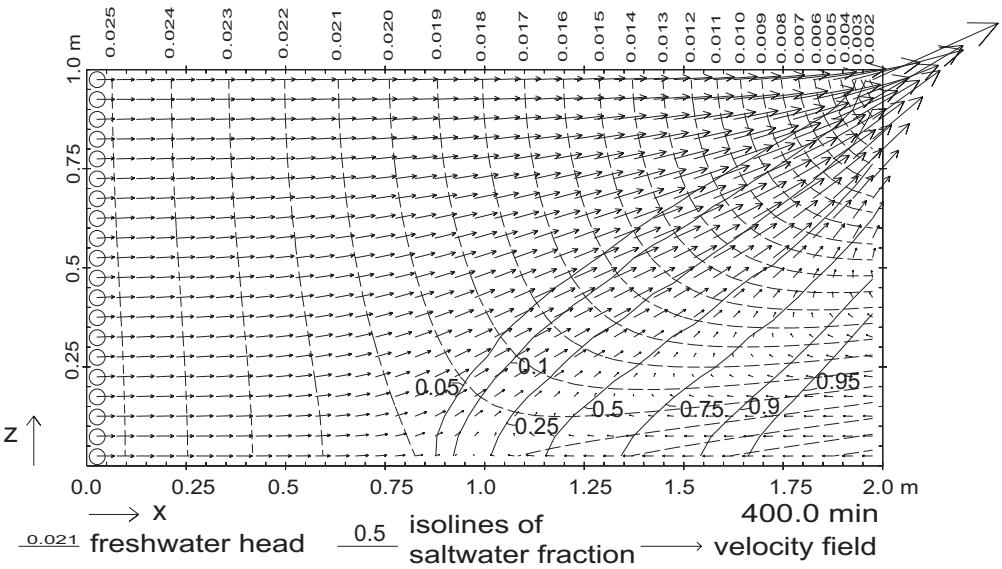

Figure 6.16: Freshwater head distribution (in m), several isolines of saltwater fraction and the velocity field of the reference case, computed with MOCDENS3D. The constant dispersion coefficient equals 0.066 cm^2/s. The simulation time is 400 min. The lengths of the arrows correspond with the displacement of groundwater during a time step of 4.0 min, beginning at the indicated moment in time.

Six other solution techniques

Henry's solution is compared with solutions by six other numerical techniques:

1. Pinder & Cooper (1970) were one of the first to use Henry's problem for testing their numerical model. In a way, their model is a precursor of MOC (Konikow & Bredehoeft, 1978). They used the method of characteristics to solve the transport equation and the iterative alternating-direction implicit procedure (ADI) to solve the groundwater flow equation. They considered an unsteady flow development under conditions similar to Henry's problem, thus with the same seaside boundary. Pinder and Cooper assumed two initial conditions for the salinity distribution in the aquifer: (1) fresh groundwater, and (2) a steady state interface between fresh and saline groundwater.

   Fig. 6.17 shows the position of the isolines of 0.5 saltwater fraction, 30 and 100 min after the beginning of the salt water intrusion for the initially fresh condition. Although they deduced that their numerical solution approaches Henry's steady state solution after a long time, they only showed in their article the unsteady state solutions of the isolines of 0.5 saltwater fraction till 100 min for the initially fresh condition and till 70 min for the initially interface condition. Their results for both conditions cannot clearly demonstrate that the computations are eventually in good agreement with Henry's steady state solution.

2. Segol *et al.* (1975) used a Galerkin Finite Element technique to solve the set of nonlinear partial differential equations. The positions of the isolines of 0.5 saltwater fraction after 30 and 100 min are shown in fig. 6.17. Note that Segol *et al.* had to use

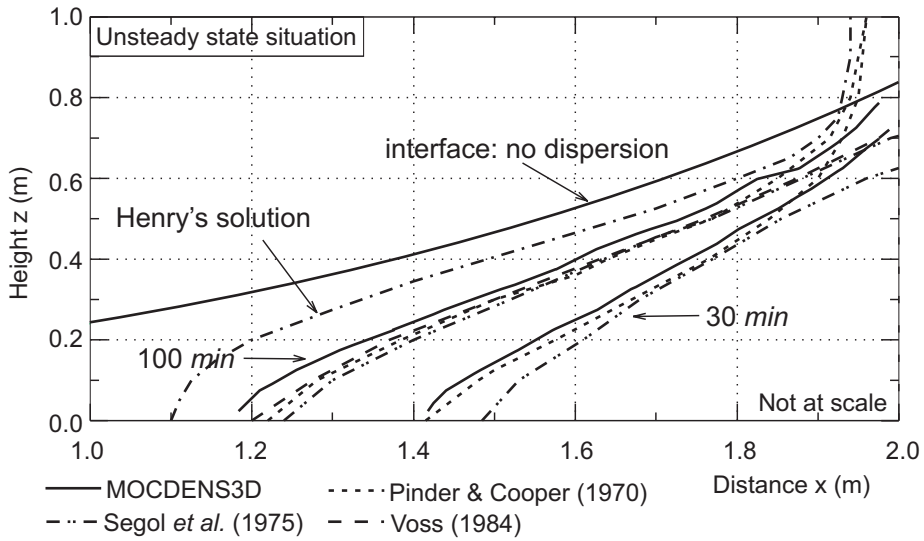

Figure 6.17: Unsteady state situation of the isoline of 0.5 saltwater fraction of Henry's problem, computed by the adapted MOC model (the reference case), Pinder & Cooper (1970), Segol *et al.* (1975) and SUTRA (Voss, 1984). Also the solution of Henry (1964) and the steady state interface with no dispersion are given.

another seaside boundary condition for the transport of solute than Henry because of the application of the finite-element method: the condition is modified to allow mass transport over the top portion of the seaward boundary. Therefore, the top parts of the isolines cannot be compared.

3. Frind (1982) applied the classical Galerkin Finite Element approach to simulate density-dependent transport problems, with emphasis on computing cost-saving measures. The positions of the isolines of 0.5 saltwater fraction of Frind appear to be in very good agreement with Segol *et al.*'s solutions that are shown in fig. 6.17.

4. Galeati *et al.* (1992) compared computations of their technique (a 'modified' method of characteristics, implicit with backward tracking of particles) with Frind's solution (1982). They found that the comparison with Frind was good except near the seaside boundary, which was treated in a different way.

5. Voss (1984) developed the finite-element simulation model SUTRA that employs a two-dimensional hybrid finite-element and integrated finite-difference method to approximate the governing equations (see also subsection 6.3.1). In fig. 6.17, the position of the isoline of 0.5 saltwater fraction is given of the unsteady state situation after 100 *min*, which agrees with the results of the other solution techniques.

6. Lee & Cheng (1974) formulated and solved the coupled nonlinear conservation equation of mass and salt in terms of stream functions by the finite-element method with the aid of iteration and underrelaxation. They used Henry's original seaside boundary condition. Nonetheless, the steady state position of the isoline of 0.5 saltwater

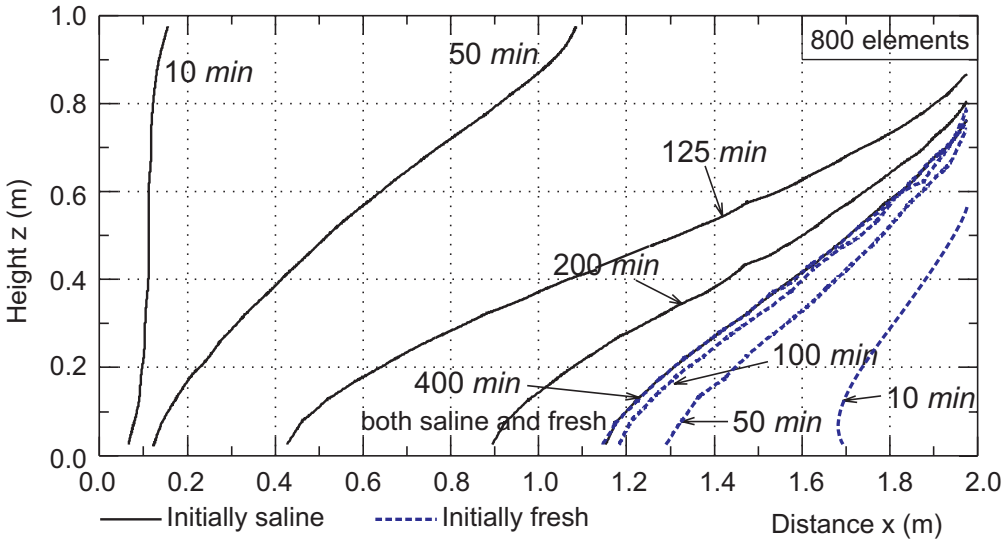

Figure 6.18: The isolines of 0.5 saltwater fraction of several unsteady situations. The cases have 800 elements and the dispersion coefficient is equal to 0.066 cm^2/s.

fraction is not really in good agreement with the position of Henry's solution in the vicinity of the toe of the isoline.

In conclusion, the unsteady state solutions (namely 30 and 100 *min* after the beginning of the salt water intrusion for the initially fresh condition) of the various techniques are in good mutual agreement. By contrast, it appears that currently no method has succeeded in duplicating Henry's steady state solution. Especially near the bottom of the aquifer, Henry's solution substantially differs from all numerical solution techniques. It appeared that the inaccuracies of Henry's results are a consequence of the limited computer facilities[19] at the time (Segol, 1994).

Evolution of the brackish zone

In fig. 6.18, the isolines of 0.5 saltwater fraction are shown during the development to the steady state situation. Calculations are made with two different initial conditions for the density distribution: (1) the aquifer is initially filled with saline groundwater and (2) the aquifer is initially filled with fresh groundwater. As can be seen, the salt water front is rapidly moving in the beginning of the simulation. However, when the steady state situation is approached, the salt water front is moving slowly. These results are in good agreement with computations of Pinder & Cooper (1970) and Segol *et al.* (1975). The final steady state situation of the whole simulation in Henry's aquifer is reached, when the toe of the isoline of 0.5 saltwater fraction near the bottom of the aquifer has approached about x=1.15 m.

[19]Fourier components, as applied by Henry, are very sensitive to the components of the system matrices and intolerant of any mistake. Henry probably started with a poor guess (e.g. isolines too far inland) and he did not reach a full-equilibrium solution. He may also have used a limited number of coefficients (Segol, 1994).

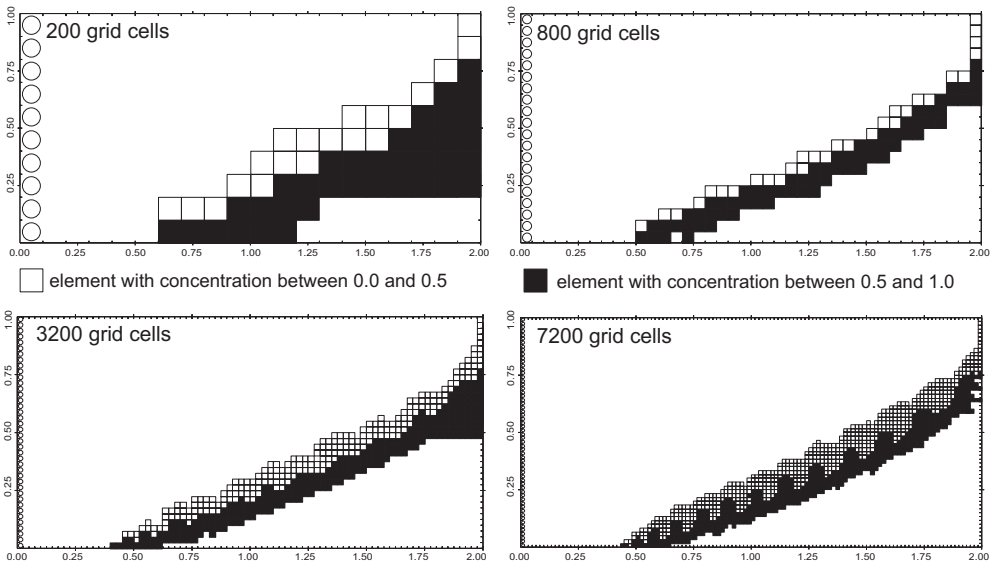

Figure 6.19: Elements with solute concentrations greater than 0.0 and smaller than 1.0 for Henry's problem. A interface is simulated, thus the dispersion coefficient D_h is 0.0 cm^2/s. Four cases with different numbers of elements. The flow time step equals 5 min. The simulation time is 600 min.

Effect of the size of the time step Δt

In order to determine the position of a interface between fresh and saline groundwater, the dispersion coefficient is set equal to 0.0 cm^2/s. In fig. 6.19, the 0.5 saltwater fraction is shown for four cases with different numbers of elements. The results are in reasonable agreement with the solution for the interface by Henry (1964), though the toe of the 0.5 saltwater fraction does not reach x=0.0 m as a result of numerical dispersion.

The figure shows that the cases with more elements, viz. 3200 and 7200, create unstable solutions of the 0.5 saltwater fraction. The explanation of this behaviour is as follows. Applying many elements for Henry's problem means small dimensions of the elements. The case with small elements must have small solute time steps in order to meet the stability criteria (eqns 6.24 and 6.27). Consequently, when the flow time step remains 5 min, more solute time steps and thus more particle movements are necessary. As the velocity field is not adapted during the flow time step, particles in the brackish zone may pass several elements with a completely different density. In addition, if the dispersion coefficient equals zero, only a small brackish zone stretches over only a few elements due to numerical dispersion. Anyway, after the new density distribution is determined, abrupt changes in solute concentration and thus in density may occur in several elements. The densities of elements in the brackish zone may fluctuate during several flow time steps. This process creates unstable isolines (see fig. 6.19).

Fig. 6.20 shows that shortening the length of the flow time step creates more stable isolines.

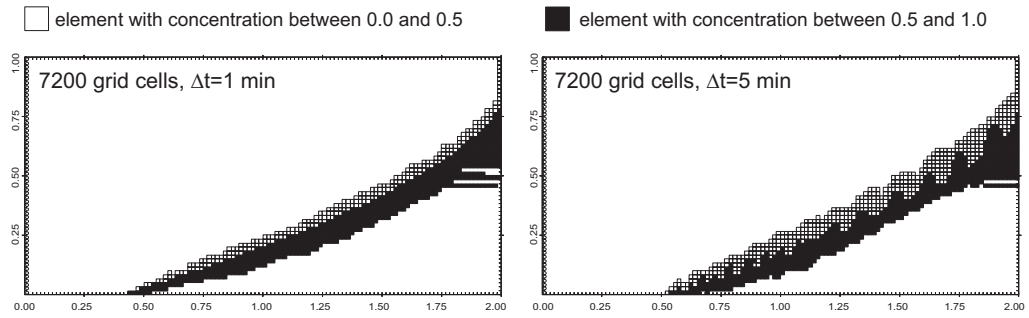

Figure 6.20: Elements with solute concentrations greater than 0.0 and smaller than 1.0. A interface is simulated, thus D_h=0.0 cm^2/s. Both cases have 7200 elements. The flow time step is 1 and 5 min respectively. The simulation time is 200 min.

6.5.6 Hydrocoin, level 1, case 5

The problem is developed to represent a rough approximation at the Gorleben salt dome in Germany, a site (which used to be) under consideration for disposal of high-level nuclear waste. It is a steady state flow and transport problem. As density variations are large (ρ_s=1200 kg/m^3), it is a strongly coupled problem. Geometry and boundary conditions are given in fig. 6.21 and table 6.2 (see also Voss & Souza, 1987; Herbert *et al.*, 1988; Oldenburg & Pruess, 1995; Konikow *et al.*, 1997).

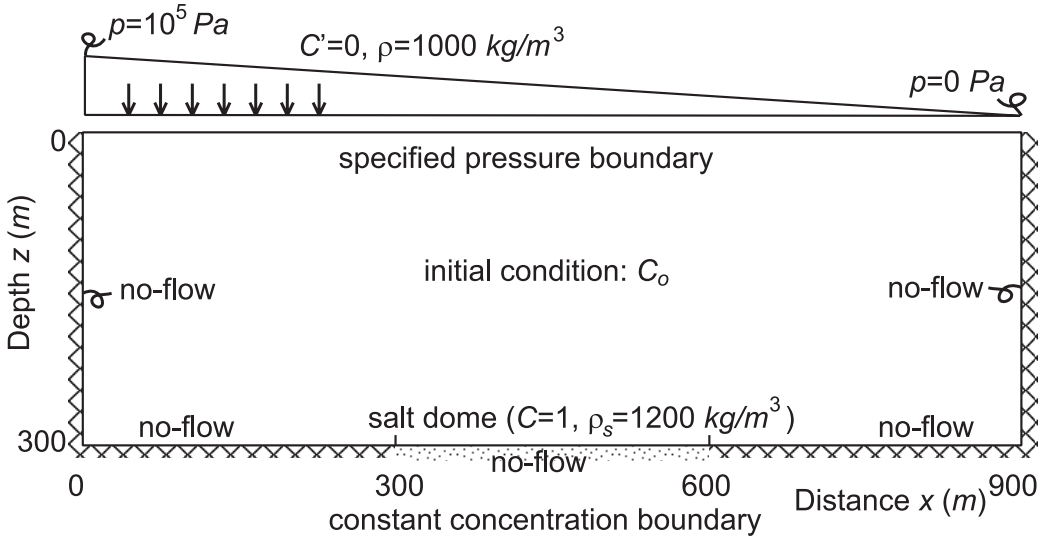

Figure 6.21: Hydrocoin, level 1, case 5: geometry and boundary conditions of the Hydrocoin salt dome problem.

In this problem, fresh groundwater enters the system at the left upper boundary. It flows through the system, passing the brine region at the bottom, and flows out at the right upper boundary. Transport of brine is defined to be by advection and mechanical dispersion (initially molecular diffusion was neglected). In addition, density differences influences the flow field. During the 1980's and early 1990's, there was consensus that the steady flow

Table 6.2: Summary of physical parameters for the original definition of the Hydrocoin problem, level 1, case 5.

Parameter	Value
Permeability κ	$10^{-12}\ m^2$
Porosity n_e	0.2
Viscosity μ	$10^{-3}\ Pa\,s$
Gravitational acceleration g	$9.81\ m\,s^{-2}$
Reference freshwater density ρ_f at C=0.0	$1000\ kg\,m^{-3}$
Saturated brine density ρ_s at C=1.0	$1200\ kg\,m^{-3}$
Longitidinal dispersivity α_L	$20\ m$
Transverse dispersivity α_T	$2\ m$
Effective molecular diffusion D_m	$0\ m^2\,s^{-1}$
Initial fluid pressure at (0,0)	$10^5\ Pa$

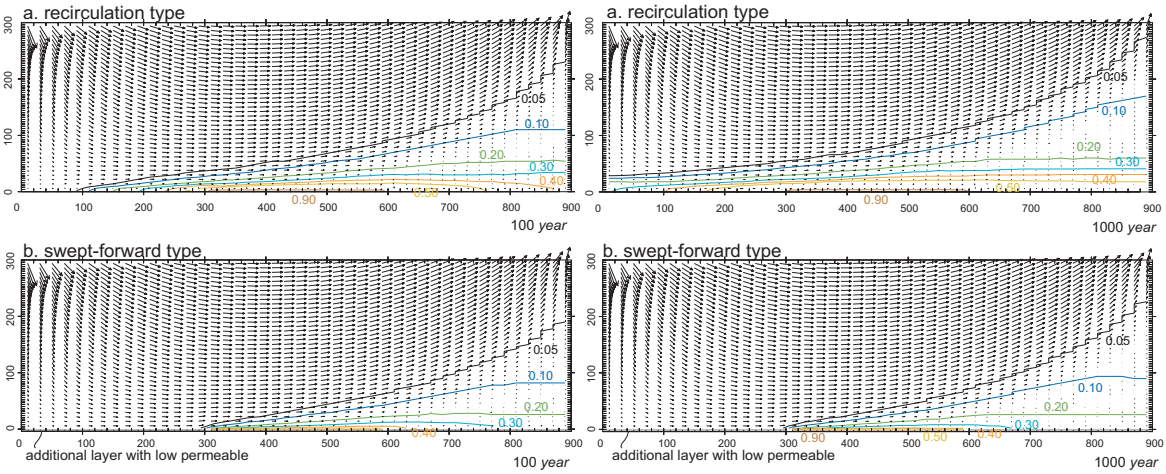

Figure 6.22: Hydrocoin, level 1, case 5: flow field and salt concentrations (as brine mass fraction) of the Hydrocoin problem at t=100 *year* and t=1000 *year*: α_L=20 m, α_L=2 m, D_m=0 $m^2\,s^{-1}$: a. The recirculation type (grid is 45 by 75); b. The swept-forward type (grid is 45 by 76): an additional row of elements is inserted at the bottom of the geometry in order to assure that brine release is only by hydrodynamic dispersion and not also by advection, which is the case in the recirculation type. The lengths of the arrows correspond with the displacement of groundwater during a time step of 1.0 *year*. In z-direction, the velocity is displayed every second element. Sizes of the elements are Δx=20 m and Δz=4 m. The flow time step to recalculate the groundwater flow equation is 1/45 *year*, whereas 16 particles are initially inserted in each element.

field causes a large recirculation of brine in the bottom region (e.g. see fig. 6.22a).

Konikow *et al.* (1997) found out that a constant concentration condition in the active flow field, as applied in the early numerical calculations, causes a solute flux by both advective as well as dispersive processes. However, as the original Hydrocoin benchmark imposes a no-flow boundary at the salt dome boundary, solute transport should only be dispersive and not advective. As such, the condition at that boundary was not correct.

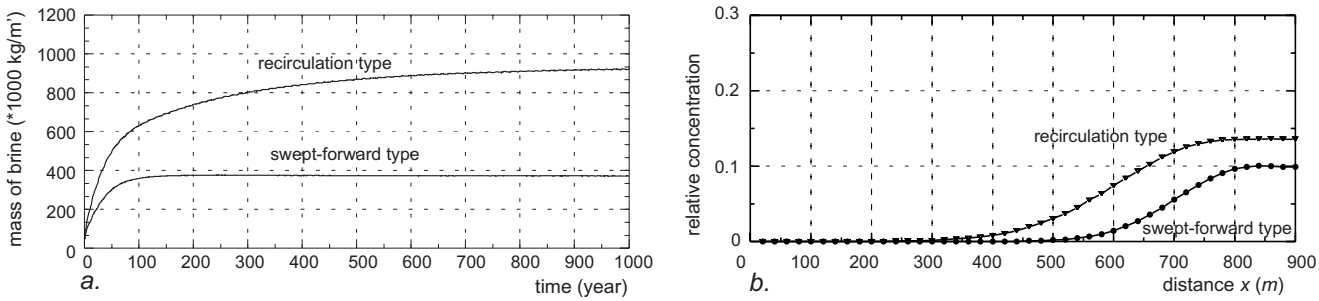

Figure 6.23: Hydrocoin, level 1, case 5: comparison between the recirculation type (45 by 75 elements: fig. 6.22a) and the swept-forward type (45 by 76 elements: fig. 6.22b): a. Total mass of brine as a function of time in the system; b. Brine concentrations (as mass fraction) at depth of 200 m at t=1000 *year*: α_L=20 m and α_L=0.2 m. Both cases are in accordance with the results of Konikow et al. (1997).

Konikow *et al.* (1997) suggested a remedy to leave out advective transport at the constant concentration boundary. They inserted an additional row of elements and reduced the hydraulic conductivity of that additional row of elements three orders of magnitude relative to the other elements. The result can be seen in fig. 6.22b. In this case, the advective term of salt transport is negligible. By comparing part a. and b. of fig. 6.22 with each other, it can be seen that due to advective transport at the constant concentration boundary a substantial larger amount of brine is released in the system. Fig. 6.22a represents the so-called recirculation type as brine even occurs in the upward part of system between x=0 and x=300 m, whereas fig. 6.22b represents the swept-forward type. The swept-forward type implies that no salt is present in the upstream part of the system, viz. between x=0 and x=300 m.

Fig. 6.23a shows the mass of brine as a function of time, whereas fig. 6.23b displays the brine concentration (as mass fraction) at a depth of 200 m. The results are, obviously, in comparison with the results of Konikow *et al.* (1997) as the same numerical technique is applied (viz. method of characteristics and particle tracking).

Effect of molecular diffusion

After revision of the salt dome flow problem at the end of the 1980's, molecular diffusion was introduced in the problem. Fig. 6.24 shows the effect of molecular diffusion on the brine distribution in the system. With this quantity of molecular diffusion, viz. D_m=5 $\times$ 10^{-7} $m^2\,s^{-1}$, the system is in a recirculation state. By decreasing the molecular diffusion, the release of brine to the system is reducing. It appears that with a molecular diffusion smaller than D_m=2 $\times$ 10^{-8} $m^2\,s^{-1}$ the system is in a recirculation state instead of in a swept-forward state (see fig. 6.25). Note that for the case with D_m=5 $\times$ 10^{-8} $m^2\,s^{-1}$ and D_m=2 $\times$ 10^{-8} $m^2\,s^{-1}$ it takes quite some years before the swept-forward type starts to become a recirculating type (respectively 195 and 455 *years*). In case of no additional row of elements, advection of solute will cause that a substantial amount of brine will be present in the aquifer system. This is demonstrated in fig. 6.26, where the hydrodynamic dispersion is neglected: α_L=0 m, α_L=0 m and D_m=0 $m^2\,s^{-1}$, but where advective transport causes

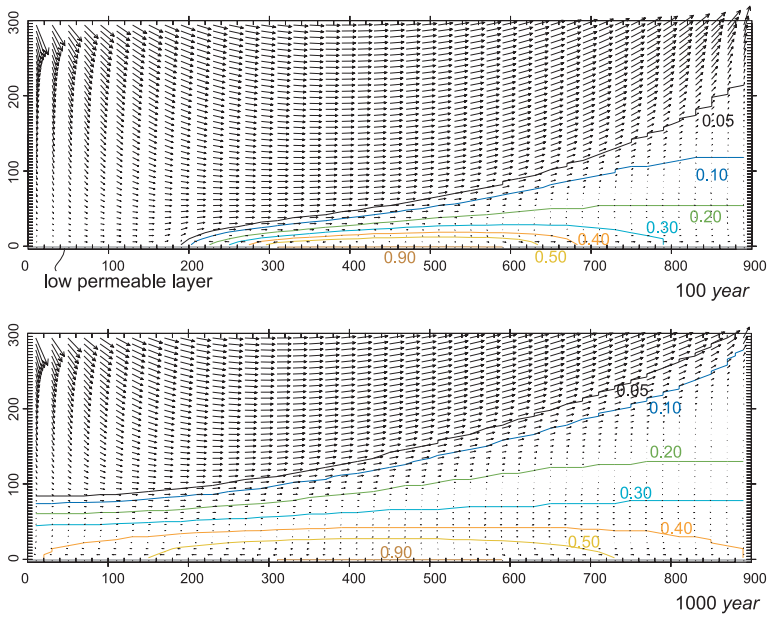

Figure 6.24: Flow field and salt concentrations (as brine mass fraction) of the Hydrocoin problem at t=100 *year* and t=1000 *year*: α_L=0 m, α_L=0 m, D_m=5 $\times$ 10^{-7} $m^2\,s^{-1}$. The lengths of the arrows correspond with the displacement of groundwater during a time step of 1.0 *year*. The grid is 45 by 76: sizes of the elements are Δx=20 m and Δz=4 m. An additional row of elements is inserted at the bottom of the Hydrocoin geometry.

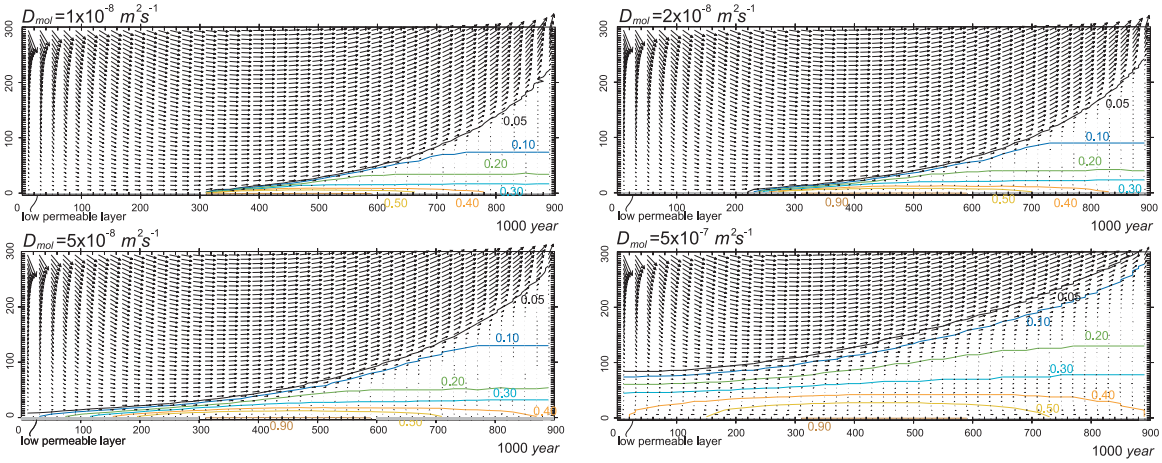

Figure 6.25: Flow field and salt concentrations (as brine mass fraction) of the Hydrocoin problem at t=1000 *year*: α_L=0 m, α_L=0 m and the molecular diffusion D_m varies: 5 $\times$ 10^{-7} $m^2\,s^{-1}$; 5 $\times$ 10^{-8} $m^2\,s^{-1}$; 2 $\times$ 10^{-8} $m^2\,s^{-1}$; and 1 $\times$ 10^{-8} $m^2\,s^{-1}$. The grid is 45 by 76: sizes of the elements are Δx=20 m and Δz=4 m. An additional row of elements is inserted at the bottom of the Hydrocoin geometry.

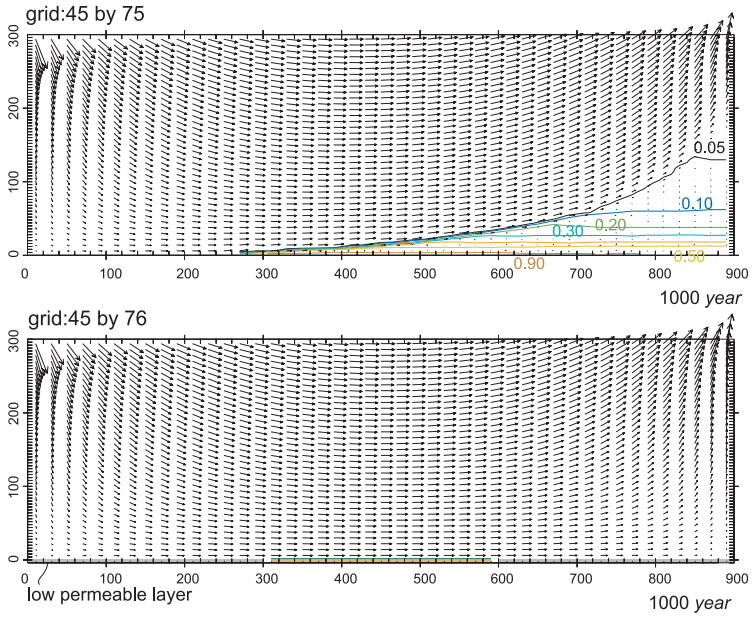

Figure 6.26: Flow field and salt concentrations (as brine mass fraction) of the Hydrocoin problem at t=1000 *year* in case there is no hydrodymanic dispersion: α_L=0 m, α_L=0 m, D_m=0 $m^2\,s^{-1}$. The lengths of the arrows correspond with the displacement of groundwater during a time step of 1.0 *year*. The two cases with a different number of rows are compared: a grid of 45 by 75 and a grid of 45 by 76: sizes of the elements are Δx=20 m and Δz=4 m. The time step to recalculate the groundwater flow equation is 1/45 *year*. In z-direction, the velocity is displayed every second element.

the displacement of brine.

Effect of model parameters: the number of particles, the time step Δt and the number of vertical layers

Fig. 6.27a shows the effect of the number of particles on the brine distribution. As can be seen, inserting initially only 1 particle per element (instead of 16) strongly effects the solution of the advection-dispersion equation. Though brine distribution looks acceptable, the result is very inaccurate (for comparison with the case with 16 particles, see fig. 6.22b, t=1000 *year*). The effect of the size of the flow time step to recalculate the groundwater flow equation is less prominent in this case (fig. 6.27b). In case of a large flow time step, the velocities are not recalculated often enough, and the system becomes even a recirculation type. In addition, the number of vertical layers also affects the salinization process in the groundwater flow domain (fig. 6.28). The smaller the vertical size of the element, the more the recirculation type resembles the swept-forward type. As such, grid convergence is definitely not achieved with 45 by 75 elements.

In conclusion, model parameters should be chosen carefully as they highly effect the salinization process. Especially grid convergence is necessary to model the Hydrocoin domain properly.

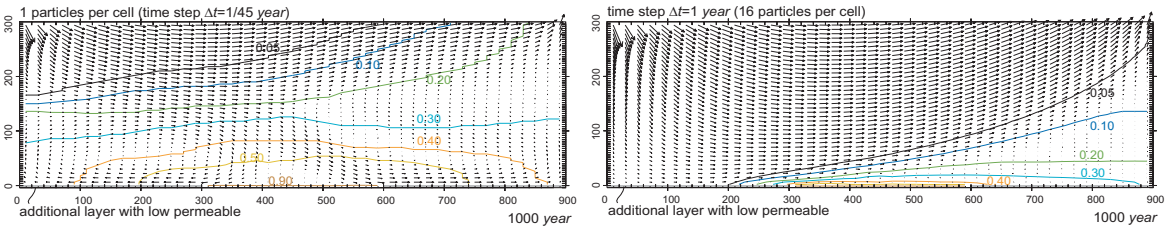

Figure 6.27: Flow field and salt concentrations (as brine mass fraction) of the Hydrocoin problem at t=1000 *year*: α_L=20 m, α_L=2 m, D_m=0 $m^2\,s^{-1}$: a. One particle is initially inserted in each element instead of sixteen; b. The flow time step to recalculate the groundwater flow equation is 1 *year*. The lengths of the arrows correspond with the displacement of groundwater during a time step of 1.0 *year*. In z-direction, the velocity is displayed in every second element. The grid is 45 by 76 (an additional row of elements is inserted at the bottom of the geometry): element sizes are Δx=20 m and Δz=4 m.

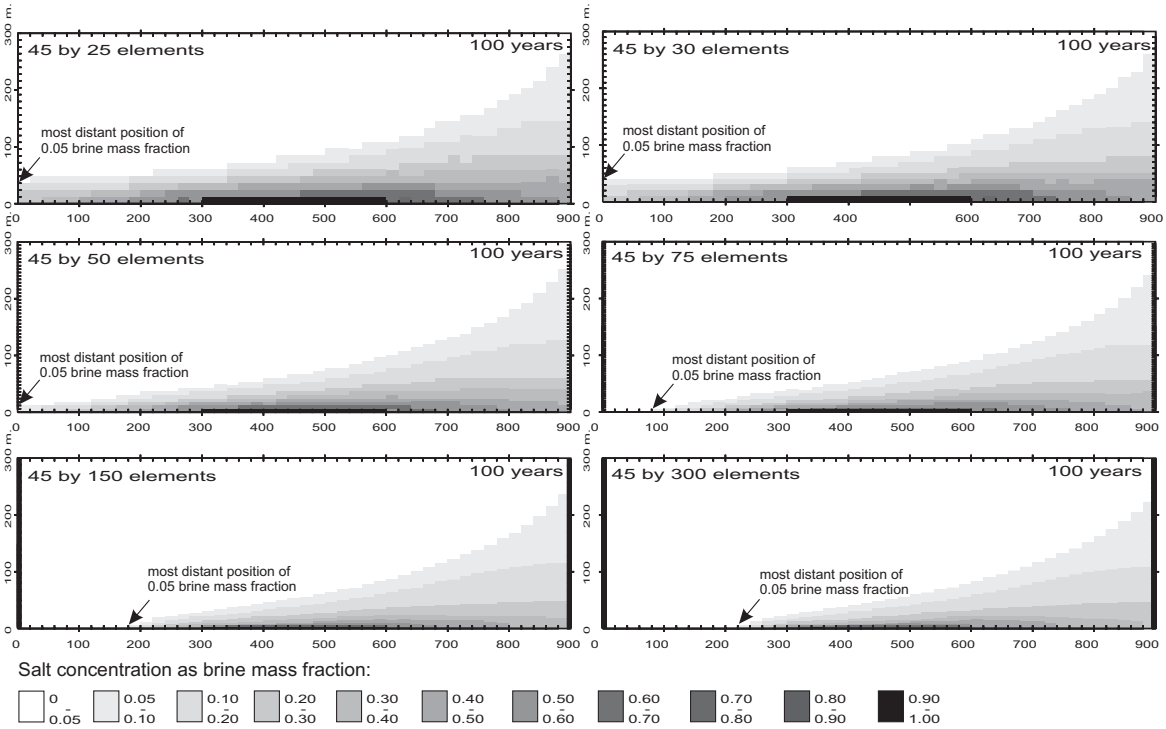

Figure 6.28: Hydrocoin, level 1, case 5: effect of the vertical grid size on the recirculation type. The smaller the vertical size of the element, the more the recirculation type resembles the swept-forward type.

6.5.7 Elder problem

The Elder problem (Elder, 1967) is a free convection problem in a rectangular homogeneous porous medium. The system is partially heated from below. It is originally a heat flow problem, but here it has been adapted as a (density-dependent) solute transport problem

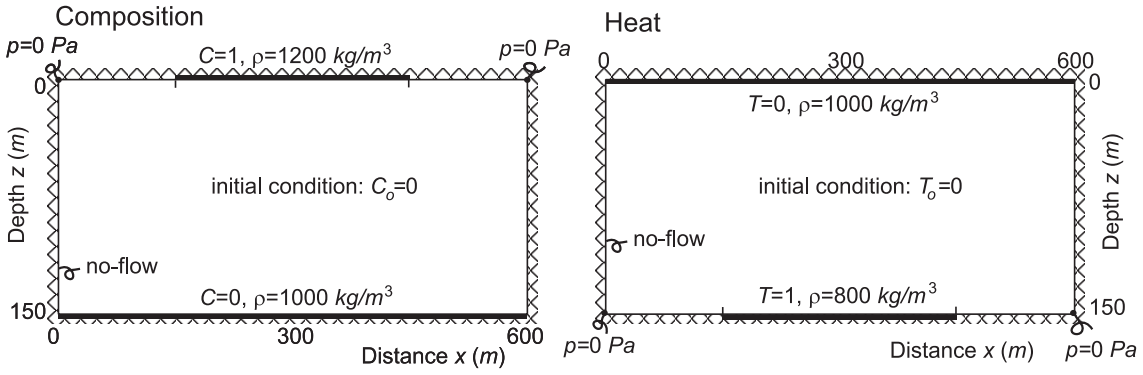

Figure 6.29: Elder problem (1967a, 1967b): geometry (not at scale) and boundary conditions of the free convection problem, converted from heat transport to mass transport.

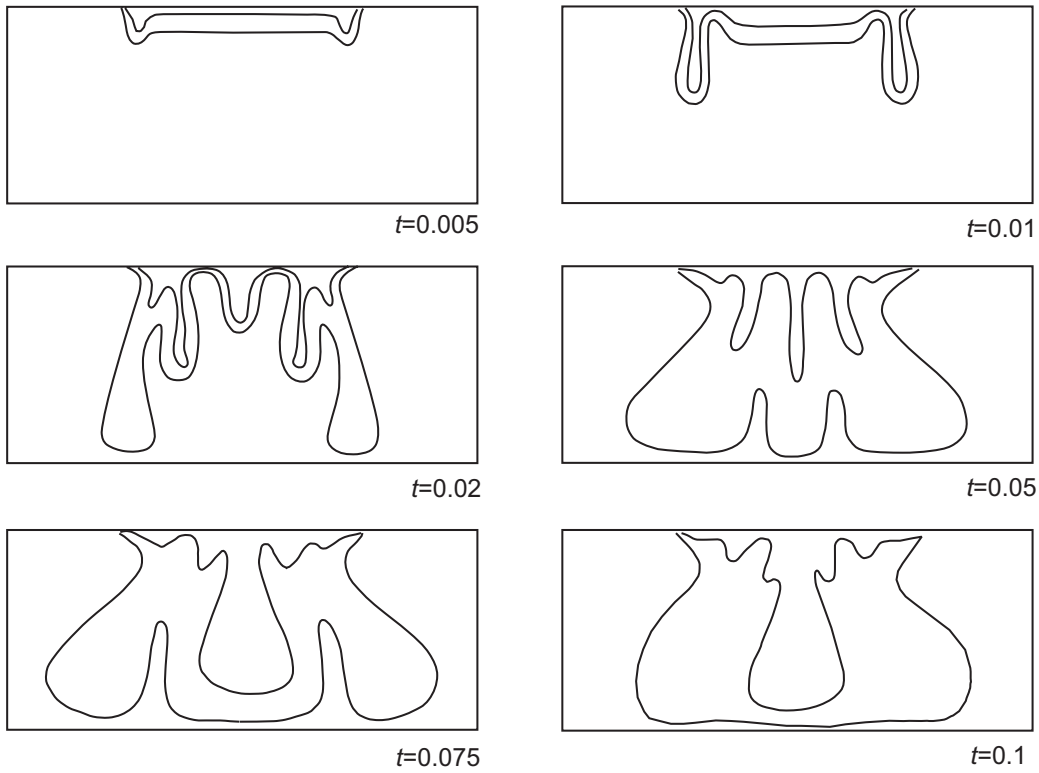

Figure 6.30: Original temperature distribution (0.2 and 0.6 of maximum) of the Elder problem at t=1.0 *year*, t=2.0 *year*, t=4.0 *year*, t=10.0 *year*, t=15.0 *year* and t=20.0 *year* (Elder, 1967).

(fig. 6.29 and 6.30, and table 6.3). The Elder problem has often been used as a benchmark for code-verification, e.g. for the codes SUTRA (Voss & Souza, 1987), TOUGH2 (Oldenburg & Pruess, 1995), FEFLOW (Diersch, 1996) and FAST-C(2D/3D) (Holzbecher, 1998). Here, characteristic results with MOCDENS3D are presented.

Fig. 6.31 shows the velocity field and salt concentrations (0.2 and 0.6 salt fraction) of the Elder problem for six moments in time, calculated with MOCDENS3D. For this fine grid

Table 6.3: Summary of physical parameters for the definition of the Elder problem, converted to mass transport (Voss & Souza, 1987; Oldenburg & Pruess, 1995).

Parameter	Value
Permeability κ	$4.845 \times 10^{-13}\ m^2$
Porosity n_e	0.1
Viscosity μ	$10^{-3}\ Pa\,s$
Gravitational acceleration g	$9.81\ m\,s^{-2}$
Density of pure water ρ_f at C=0.0	$1000\ kg\,m^{-3}$
Density of pure brine ρ_s at C=1.0	$1200\ kg\,m^{-3}$
Longitidinal dispersivity α_L	$0\ m$
Transverse dispersivity α_T	$0\ m$
Effective molecular diffusion D_m	$3.565 \times 10^{-6}\ m^2\,s^{-1}$
Initial fluid pressure at (0,0) and (600,0)	$0\ Pa$

of 160 by 80 elements (Δx=3.75 m and Δz=1.875 m), the salt concentration distribution and velocity field correspond with the results of Oldenburg and Pruess (1995) for their two refined grids.

Effect of the initial distribution of salt

Now, the effect of the initial distribution of salt is demonstrated on the flow process in the domain. Fig. 6.32 surprisingly shows that an small perturbation in initial salt concentration, as indicated in the figure, sets flow in the system in another mode. Now, flow at x=300 m is downwards instead of upwards.

æ

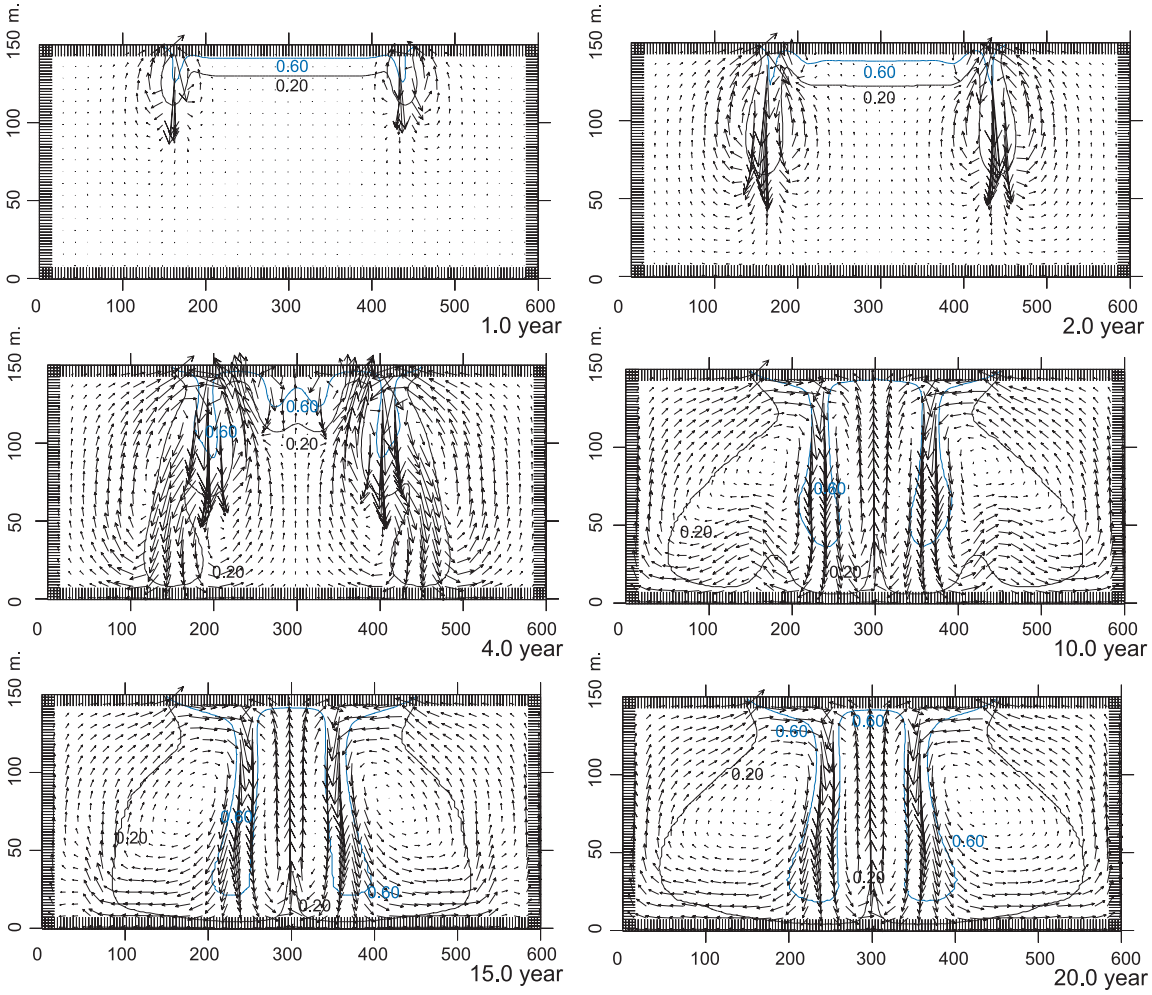

Figure 6.31: Flow field and salt concentrations of the Elder problem during t= 20.0 *year*. The lengths of the arrows correspond with the displacement of groundwater during a time step of 0.5 *year*. The velocity is displayed in every fourth element. The grid is 160 by 80: sizes of the elements are Δx=3.75 m and Δz=1.875 m. The flow time step to recalculate the flow field is 1 *month*.

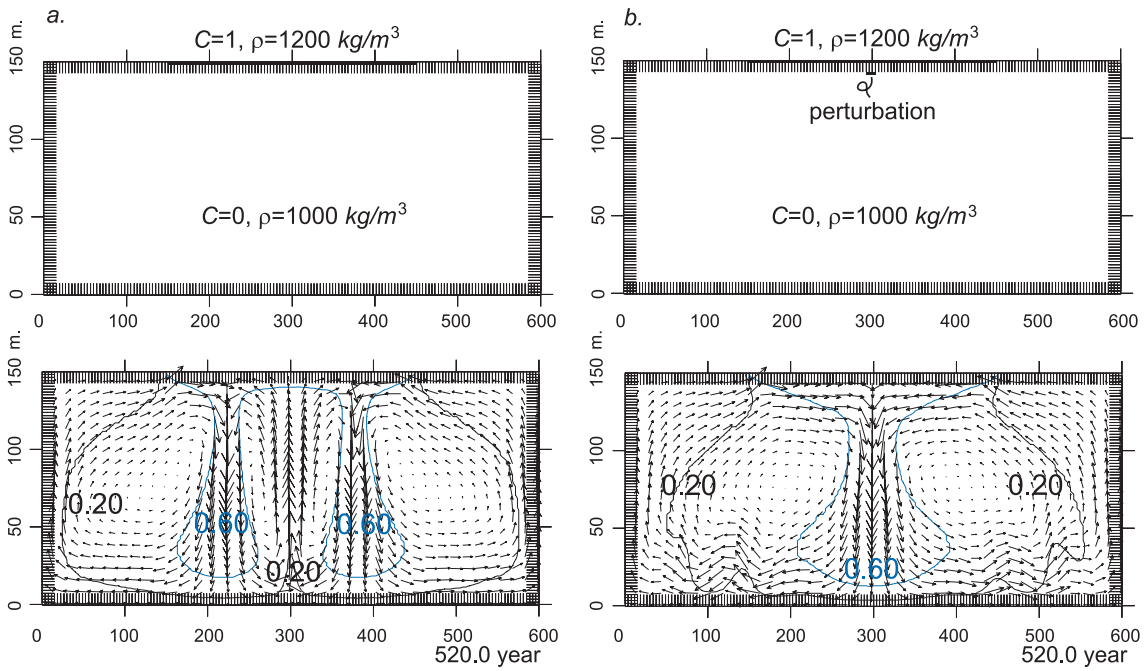

Figure 6.32: Effect of initial salt concentration distribution on the final flow field and salt concentration. Flow field and salt concentrations of the Elder problem are shown on t= 520.0 *year*, viz. after a long time of simulation. The lengths of the arrows correspond with the displacement of groundwater during a time step of 0.5 *year*. The velocity is displayed in every fourth element. The grid is 160 by 80: sizes of the elements are Δx=3.75 m and Δz=1.875 m. The time step to recalculate the flow field is 1 *month*. As can be seen, the convective flow fields differ from each other. The initial perturbation in case b. sets the system in a different mode.

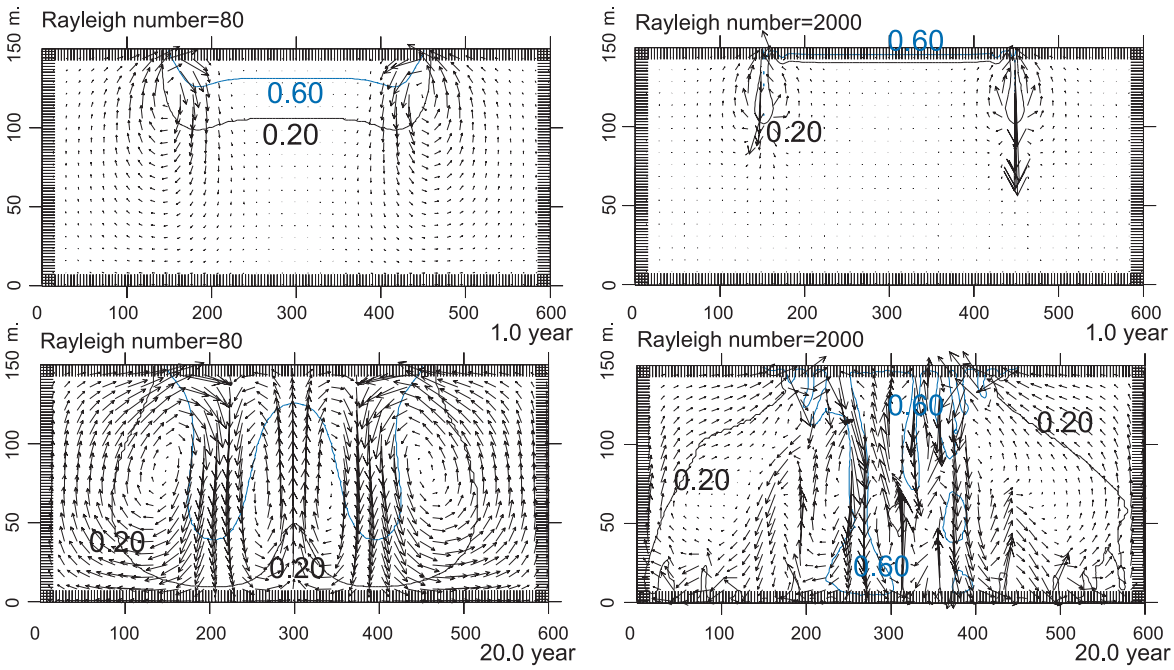

Figure 6.33: Effect of the value of the Rayleigh number. Flow field and salt concentrations of the Elder problem at t= 20.0 *year*. The lengths of the arrows correspond with the displacement of groundwater during a time step of 0.5 *year*. The velocity is displayed in every fourth element. The grid is 160 by 80: sizes of the elements are Δx=3.75 m and Δz=1.875 m. The time step to recalculate the flow field is 1 *month*. The Rayleigh-numbers are 80 and 2000 instead of 400.

Chapter 7

Salt water intrusion in the Netherlands

7.1 Introduction

At present, 2,5 billion people, half of the world's population, lives within 60 kilometres of the shoreline. It is expected that within the next 30 years, the coastal population will be doubled. With the rapid urbanization, the concentration of the urban population in large cities will increase. Coastal zones are experiencing problems such as coastal erosion; loss of habitat for birds, fish and other wild life; the depletion of fischery resources and seafood; land subsidence due to construction and water extraction; the deterioration of marine and coastal environment as areas of amenity; natural disasters including extreme weathers, tsunami, harmful algal blooms; and the potential impact of salt water intrusion on freshwater supplies.

In this chapter, the interest is focussed on the problem of salt water intrusion. At this moment, many coastal groundwater systems in the world are affected by natural processes as well as human interferences. They are vulnerable as they often comprise groundwater with non-uniform density differences. The distribution of fresh, brackish and saline groundwater is investigated in one particular coastal groundwater system: the one of the Netherlands.

The Netherlands is a high-density country with some 8 million people living in the coastal zone. Due to several natural and antropogenic causes, the Dutch coastal groundwater system is threatened by a severe intrusion of saline water, also called salinisation. Salinisation of the groundwater systems may effect water management sectors such as domestic and industrial water supply, flushing of watercourses of low-lying polders and agriculture in terms of salt damage. In addition, a rise in sea level rise will directly affect the Dutch society from an environmental, social and economic point of view. The possible consequences of different scenarios of sea level rise as well as human activities on vulnerable coastal groundwater systems are shortly considered.

7.2 Genesis of the Netherlands: a man-made environment

The major part of the Netherlands consists of lagoon and deltaic areas of the rivers Rhine, Scheldt and Meuse, created by natural processes (e.g. sea level rise, forming of sand-ridges, sea invasions and forming of lakes in invaded land). Before the occupation by man, the area behind the dunes was drained by a system of broad slowly moving streams (fig. 7.1). Flood water from the high river stages and from the sea could easily enter the area. Starting from approximately the third century BC, the inhabitants built dwelling mounds and drained flood plains, *to keep their feet dry*. From about 1100 AD, embankments along the main

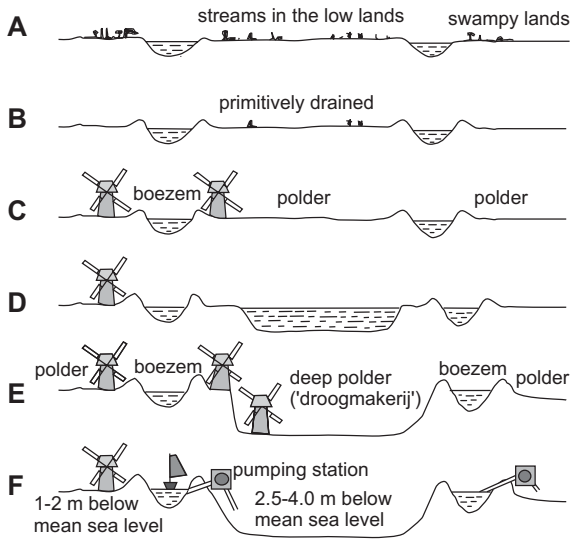

Figure 7.1: Development of the Dutch polder region (Wesseling, 1980, after Hellinga, 1952). A. Before occupation of man; B. After damming of the streams at their mouths and their embankment, separation of 'boezem' and 'polder' by small dikes; C. Subsidence of the peaty polder soils and pumping of windmills; D. Digging out of some polders for peat making; E. After draining of the lake originating from peat making; F. Present situation.

rivers were thrown up and sluices were built at the outlets of smaller streams to protect themselves and their livestock against drowning and their agricultural land against flooding. Gradually, smaller inlets were embanked resulting into a pattern of small impoldered areas (the so-called polders) surrounded by dikes. These dikes asked for a high level of cooperation between villages, eventually resulting in administrative organisations such as *waterschappen* (water boards) and *hoogheemraadschappen* (e.g. the Hoogheemraadschap Rijnland was founded around 1200 AD).

Later on, land subsided because it was drained more efficiently, (fig. 7.2). This especially occurred in Holocene peat areas in the western and northern part of the country. Peat was dug in these areas because it was needed as fuel, and lakes were created. Subsequently, with the improvement of windmills and the paddle wheel from the sixteenth century, water from the polders could be removed easier. In addition, it became also possible to reclaim larger and deeper lakes. Table 7.1 summarises the dates of reclamation of some polders. Especially during the seventeenth century ('the Golden Age'), numerous lakes have been reclaimed in Noord-Holland. These so-called *droogmakerijen* partly originate from digging and drying peat for heating purposes. Later on, the use of steam followed by electrical and diesel engines finally lead to the reclamation of the deepest lakes, viz. low-lying polders (e.g. Haarlemmermeer) and the new IJsselmeer Flevopolders. What has been left from a swampy flat area with some streams and lakes is now a pattern of small and larger polders, each having its own embankment and a controlled phreatic water level (the so-called polder level) with a different elevation. Fig. 7.3 shows the ground surface of the Netherlands. As can be deduced, large parts of especially Noord- and Zuid-Holland are lying below mean sea level. About 25 % of this low-lying land is situated below mean sea level, whereas about

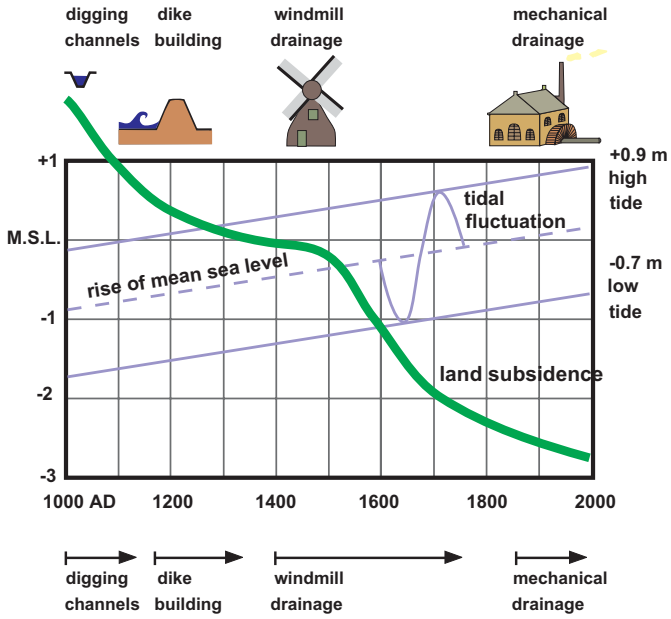

Figure 7.2: Lowering of the grond surface in the Netherlands (schematic). Modified from: Atlas van Nederland: deel 15 Water, 1986.

Table 7.1: Reclamation of some polder areas (after Schultz, 1992).

Name polder	**Reclamation date**	**Surface in *ha***	**Original state**
Beemster	1608-1612	7,100	lake
Purmer	1618-1622	2,756	lake
Wormer	1625-1626	1,620	lake
Schermer	1633-1635	4,770	lake
Haarlemmermeer	1840-1852	18,100	lake
Groot-Mijdrecht	1872-1877	2,020	peat cutting area
Wieringermeer	1927-1930	20,000	estuary
Noordoostpolder	1936-1942	48,000	estuary
Oostelijk Flevoland	1950-1957	54,000	estuary
Zuidelijk Flevoland	1959-1968	43,000	estuary

65 % would be flooded regularly by the sea or the rivers in the absence of dunes and dikes. Accordingly, 8 million people would be endangered.

The reclamation of the lakes initiated changes in groundwater systems. In order to drain the polders, the phreatic water levels in these polders had to be lowered compared to the original water level. Since phreatic water levels in adjacent areas differed, differences in head were created, and consequently, groundwater was set in motion. Seepage in the polders was introduced, because of a difference in phreatic water level and piezometric head in the aquifer. A schematisation of the hydrogeological situation of the western part of the Netherlands is given in fig. 7.4. The intensity of the seepage is highly dependent on the geometry, the phreatic water level and hydrogeological parameters of the polders, such as

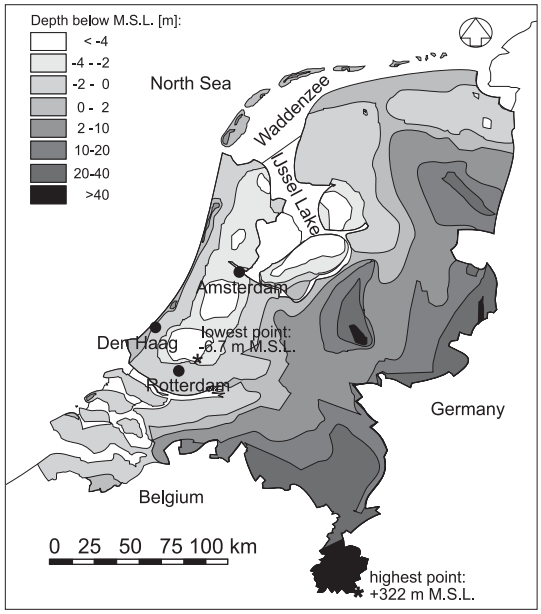

Figure 7.3: Ground surface in the Netherlands (Wesseling, 1980).

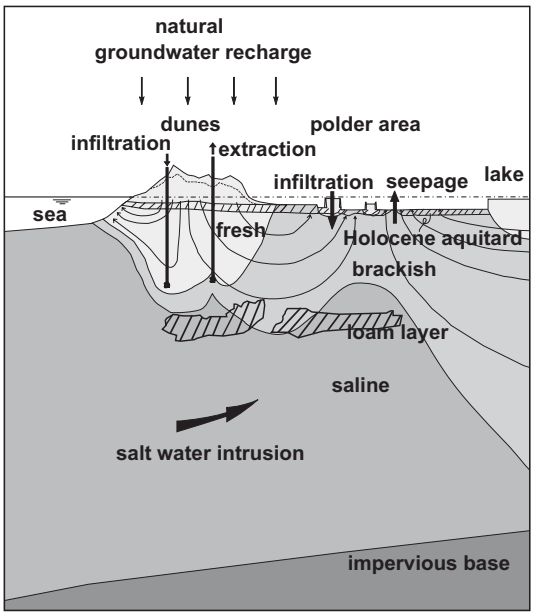

Figure 7.4: A schematisation of the groundwater system in the coastal part of the Netherlands.

thickness and (vertical) hydraulic conductivity of the aquitard (viz. confining layer). The seepage is accompanied by a load of salt, as among others regressions and transgressions of the sea in the western and northern part of the Netherlands created large zones of fresh, brackish and saline groundwater in the upper parts of the groundwater systems (see fig. 7.5). At some polders which are surrounded by lakes, the brackish or saline seepage can later on

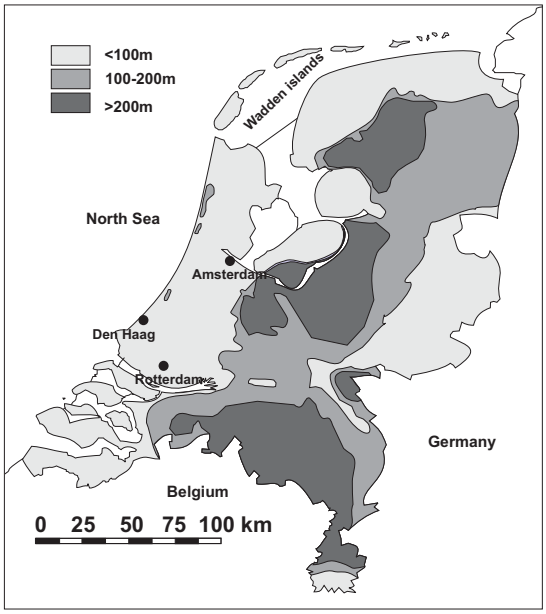

Figure 7.5: Depth of boundary between fresh and brackish groundwater in the Netherlands.

turn into fresh water seepage (van Dam, 1976).

7.3 Land subsidence

Polder areas subside because of compaction, shrinkage and oxidation of peat as well as man-induced processes such as local mining activities (e.g. oil and gas) and groundwater recovery. Actually, land subsidence is analogous to a relative sea level rise, on condition that the subsidence is the same everywhere. In the Netherlands, the average rate of land subsidence in peat areas is in the order of 15 *cm per century*. In large parts of the province Groningen, the ground surface will probably have been subsided at maximum 40 *cm* in 2035 due to local mining activities.

In addition, long response-time scale processes are the melting of continental ice sheets and resultant adjustment of the Earth's crust to changing ice loading. For instance, since the end of the last Ice Age Scandinavia is rising, whereas, at this moment, some parts near the Dutch coast (Noord-Holland and the area near Rotterdam) are falling more than 8 *cm per century* (Noomen, 1989). Note that the northwestern part of the Netherlands subsides with respect to the southeastern with some *cm per century*.

7.4 Sea level rise

Until the beginning of the Industrial Revolution, a complex self-regulating geosphere-biosphere system had determined the concentration of greenhouse gases. However, from about 1850 on, human activities have increased the concentration of greenhouse gases in the atmosphere due to deforestation, changes in land use, and burning of biomass and fossil

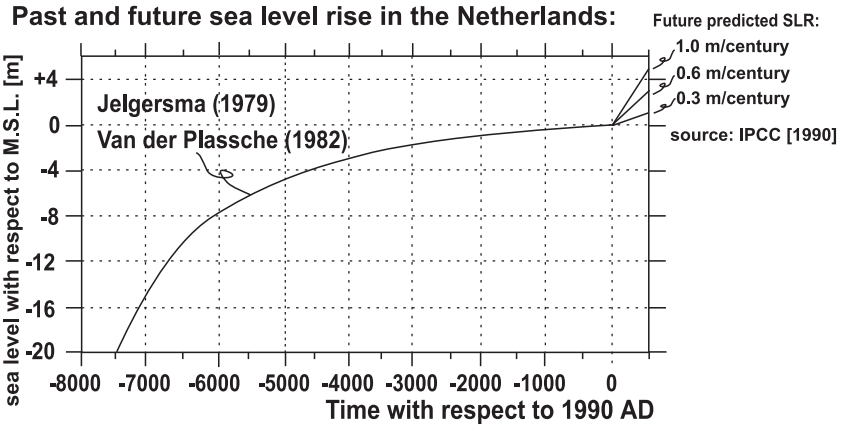

Figure 7.6: Past and future sea level rise in the Netherlands.

fuels. Scientists predict that as a result of human activities, between 2050 and 2100 the concentration of greenhouse gases in the atmosphere will probably have increased compared to that at the beginning of the Industrial Revolution. As a result of the established enhanced greenhouse effect, the temperature will probably have risen some degrees Celsius.

An important consequence of global mean temperature rise is sea level rise. The following physical processes contribute to sea level rise: thermal expansion of ocean water; melting of mountain glaciers and small icecaps; and ablation of polar ice sheets. Note that accumulation on polar ice sheets contributes to sea level fall, whereas the present consensus is that the West Antarctic Ice Sheets do not disintegrate during the next century.

At the beginning of the Holocene, which started about 10,000 year ago, the sea level has risen a few tens of metres within a geologically short period of some millennia, see fig. 7.6. By contrast, during the last three millennia, the sea level has not risen more than a few decimetres. In the period 1880-1980, the sea level has risen only about 10 à 20 *cm per century*.

As the present era is an interglacial, the level of the sea is already high and relatively small amounts of ice masses are stored. Therefore, a sea level rise of only several decimetres for the next century is to be expected. The present range of predictions of the future sea level rise for the next century is rather consistent: in the range of 30 to 100 *cm*. The main contributors to this sea level rise will be thermal expansion of ocean water as well as melting of mountain glaciers and small icecaps, whereas accumulation on and ablation of polar ice sheets are supposed to be in balance.

7.5 Countermeasures

The salinisation rate of the groundwater flow systems will probably increase due to increasing extraction rates and sea level rise. Fortunately, it will probably take a considerable time before the impact on the groundwater flow systems is actually observed, since in the salinisation process enormous volumes of fresh groundwater have to be replaced by saline groundwater. As countermeasures to control the salt water intrusion probably also need a long time to become effective, they should be taken in due time.

Whether or not some countermeasures are feasible from an economic, environmental or political point of view is not really the question here. These countermeasures should only be considered as interesting cases in order to gain a better insight into the range of conceivable human interventions. Examples of possible human activities to compensate the salinisation are:

a. reclaiming land in front of the coast, thus evolving new freshwater lenses;

b. extracting (saline) groundwater, thus decreasing the seepage quantity and chloride load in the polders. This could regrettable result in undesirably low phreatic water levels, especially in shallow coastal groundwater flow regimes. Furthermore, the disposal of the extracted saline or brackish groundwater could meet with problems;

c. infiltrating or injecting fresh surface water (called deep-well infiltration), thus replacing the inflow of saline groundwater. This is already applied in Israel, at Long Island and in Los Angeles (U.S. Department of Energy, 1989);

d. inundating low-lying polders, thus removing the driving force of the salinisation process;

e. widening existing sand-dune areas, thus generating thicker freshwater lenses;

f. creating physical barriers, such as sheet piles, clay trenches and injection of chemicals, thus blocking the free entrance of saline groundwater and halting the salinisation process. This solution is applicable only in shallow thin aquifers and at the expense of high costs. A small physical barrier through pumping of cement grout has been implemented at Okinawa-Jima Island in Japan (U.S. Department of Energy, 1989).

g. increase of (artificial) recharge in upland areas to enlarge the outflow of fresh groundwater through the coastal groundwater flow regime, and thus, to reduce the salinisation;

h. modifying pumping practice through reduction of withdrawal rates and/or adequate location of extraction wells. In most situations, groundwater withdrawal for domestic, agricultural and industrial water supply have not been reduced during periods of droughts, so that salt water intrusion tends to occur;

It is obvious that some of these countermeasures are hypothetical. For example, inundation will probably imply abandoning of valuable land. As such, these countermeasures should only be considered as interesting hypothetical cases in order to gain a better insight into the range of conceivable human interventions. Moreover, these unfeasible countermeasures serve the purpose of illustrating what has unconsciously been provoked during the past centuries by the creation of low-lying (polder) areas.

7.6 Numerical modelling of salt water intrusion in the Netherlands (draft version)

In the section, salt water intrusion in three coastal parts of the Netherlands will briefly be illustrated.

Table 7.2: Physical and model parameters for the 2D profile through Amsterdam Waterworks.

Case	Amsterdam Waterworks
Physical parameters	
Size system $L_x \times L_z$	50 $km \times$ 150 m
Hydraulic conductivity k	10 to 30 m/day
Anisotropy k_z/k_x	0.1
Porosity n_e	0.35
Long. dispersivity α_L (m)	0.2
Trans. dispersivity α_T (m)	0.02
Effective mol. diffusion D_m	0 m^2/s
Model parameters	
Size cell $\Delta x \times \Delta z$ (m)	250 $\times$ 10
Number of cells: $n_x \times n_z$	200 $\times$ 15
Total number of active cells	3000
Flow time step Δt	1.0 $year$
Convergence criterion ϕ_f (m)	3×10^{-6}
Number of particles per cell	5
Total simulated time	250 $year$

7.6.1 The profile Amsterdam Waterworks: the effect of sea level rise and land-reclamation in front of the Dutch coast

The hydrogeologic system, as given in fig. 7.7, shows different processes in the subsoil of the western part of The Netherlands (fig. 7.8). A broad sand-dune area is present between x=11.5 and 15 km. The freshwater lens under the dune area reaches to a depth of at least 80 m below Mean Sea Level ($M.S.L.$). The drinking water company Amsterdam Waterworks has pumped water from this area since the middle of the nineteenth century. Behind the dune area, various low-lying polders are located at a considerable distance from the coast. A polder is an area which is protected from water outside the area and which has a controlled water level. For instance, the Haarlemmermeer polder in the reach 10 to 20 km, which accommodates Schiphol airport, has a phreatic water level of approximately -5.5 m $M.S.L.$ Below the freshwater lens, saline groundwater flows in the direction of the Haarlemmermeer polder. In order to stop the salinisation of the subsoil, several compensating measures can be considered, such as infiltration of fresh surface water, extraction of saline groundwater, widening the existing sand-dune area, inundation of existing polders or creating a physical barrier (Oude Essink, 1996). Here, the feasible compensating measure land-reclamation in front of the coast is considered, whereas a sea level rise of 0.6 m per century is also taken into account. The land-reclamation consists of a strip of land of 3000 m width and with a fixed phreatic groundwater of +1.0 m $M.S.L.$ See table 7.2 for physical and model parameters of this case. In addition, the coefficient of compositional expansion β is 1.34 $\times 10^{-6}$ l/mg Cl^-. Fig. 7.7 shows the effect of sea level rise and the compensating measure land-reclamation in front of the Dutch coast. A new freshwater lens has been developed under the new land. Nevertheless, salt water intrusion is still causes taking place, causing upconing of brackish groundwater in the Haarlemmermeer polder. Based on numerical simulations of compensating measures with MOCDENS3D, it appears that the salinisation process cannot easily be stopped in this area.

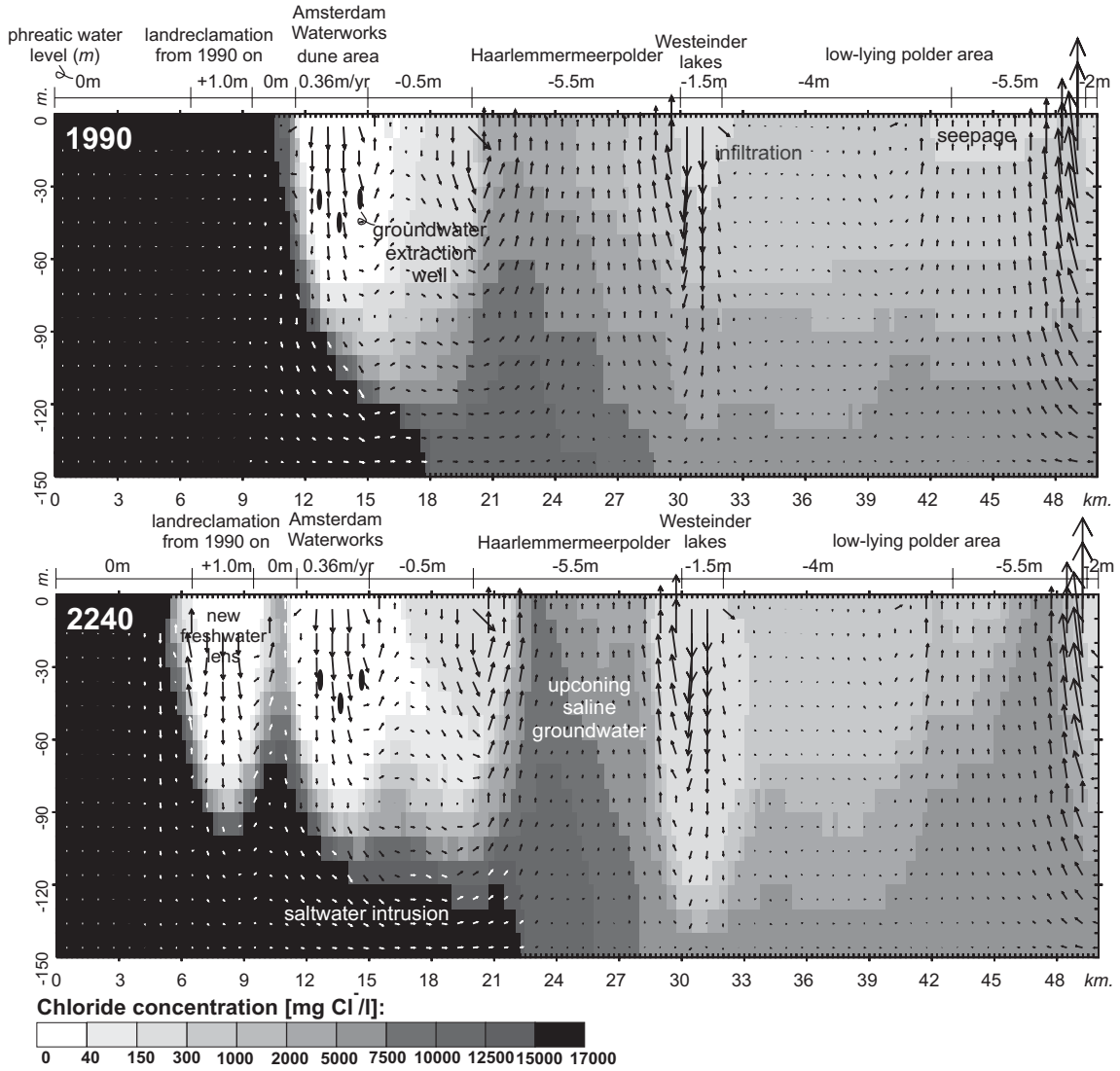

Figure 7.7: The 2D profile Amsterdam Waterworks: effect of sea level rise and the compensating measure land-reclamation in front of the Dutch coast: a. The situation before the implementation of the measure; b. 250 years after the measure became effective: a new freshwaterlens has been evolved in front of the old coast. The lengths of the arrows correspond with the displacement of groundwater during a time step of 10 *years*.

7.6.2 The Head of North-Holland

This coastal groundwater system of approximately 65.00 × 51.25 km^2 in the northern part of the province North-Holland, The Netherlands (fig. 7.8), consists of good permeable aquifers of Quaternary deposits. The aquifers are intersected by a loamy aquitard and overlain by a Holocene aquitard of clayey and peat composite (fig. 7.9).

The hydrogeologic system contains saline, brackish as well as fresh groundwater (fig. 7.10). Seepage is the system is severe (fig. 7.11). A large number of low-lying polders is present

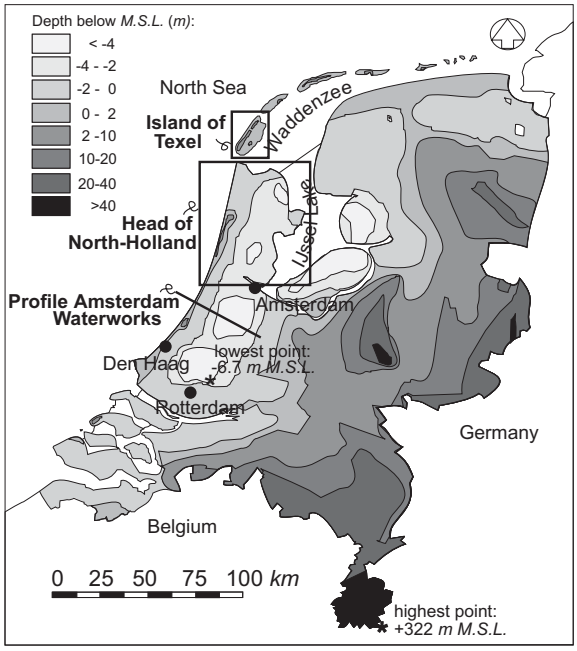

Figure 7.8: The present ground level in The Netherlands and the position of the three cases in the Netherlands: 1. the 2D profile through the Amsterdam Waterworks, 2. the 3D case the Head of North-Holland and 3. the 3D case of the island of Texel.

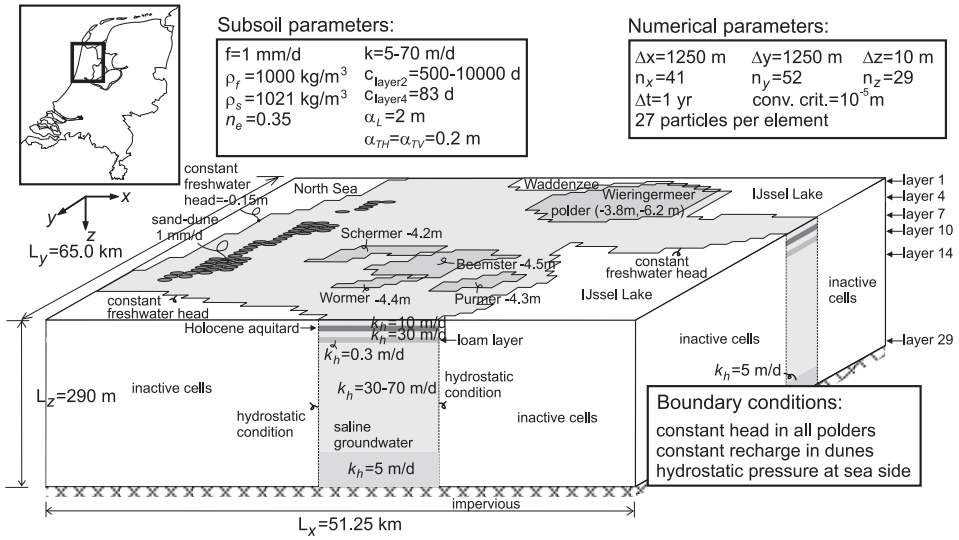

Figure 7.9: The geometry of the groundwater system in *De Kop van Noord-Holland*.

in this system. The phreatic water level differs for each polder, varying from -0.1 m to -6.2 m $M.S.L.$, and is kept constant in time (fig. 7.12). Groundwater is extracted from the sand-dune areas with a total amount of 5.2 million m^3/yr, whereas large industrial withdrawals (22.5 million m^3/yr) are pumped from the southwestern corner of the model. See

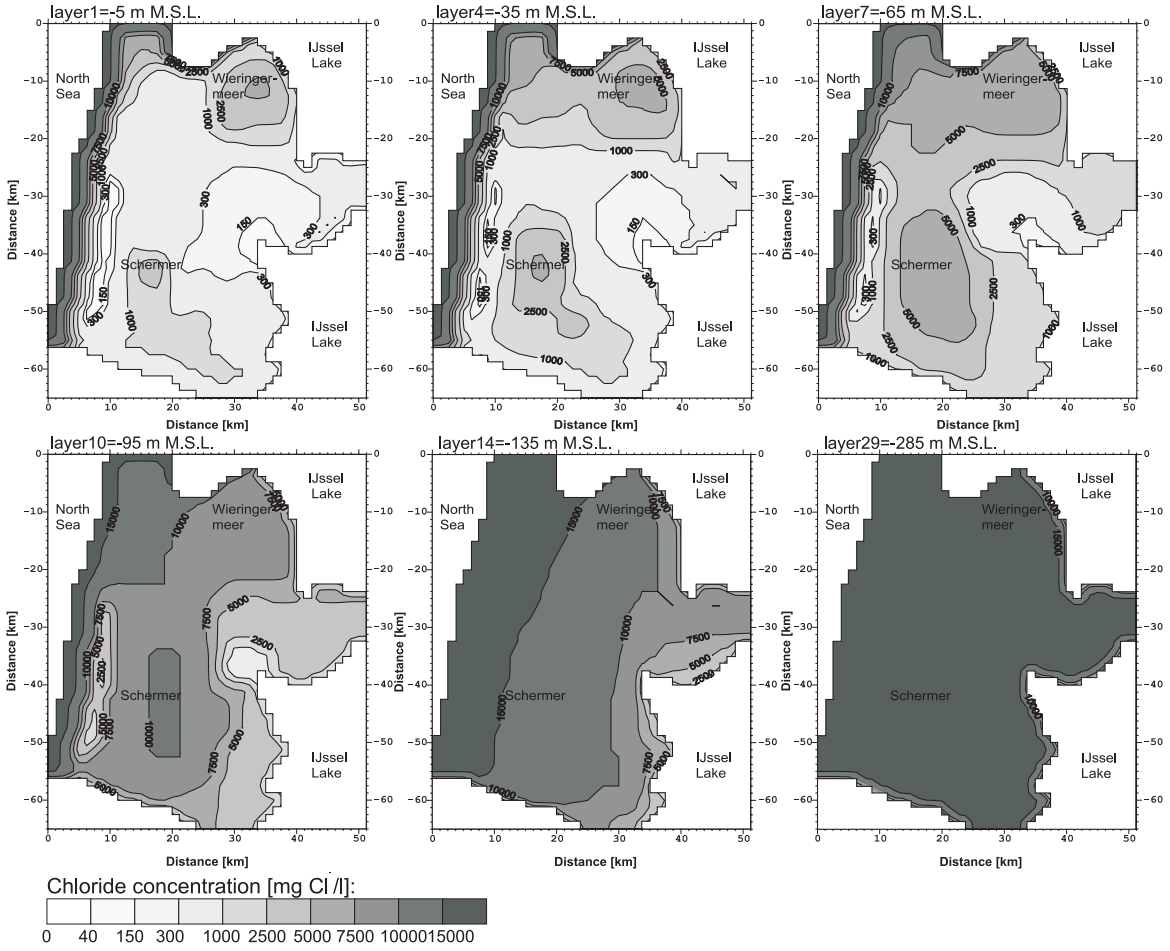

Figure 7.10: Initial chloride concentration in the hydrogeologic system at the beginning of the simulation (1990 AD) at six layers: -5 m, -35 m, -65 m, -95 m, -135 m and -285 m N.A.P.

table 7.3 for other physical and model parameters of this case. Numerical modeling results with MOCDENS3D (Oude Essink, 2001a) suggests that a severe and irreversible salinisation is already occurring. It is estimated that within a few tens to hundreds of years, the salinity of the shallow aquifer increases substantially (fig. 7.13 and 7.14). This salinisation process is a result of human activities such as the reclamation of the low-lying areas during the past centuries. Without changing the present boundary conditions, seepage into the low-lying areas will decrease slightly because of predicted increases in groundwater salinity. However, the rate in salt load through the Holocene aquitard into the low-lying areas will increase significantly due to an increase in salinity in the shallow aquifer. In addition, a relative sea level rise of 0.5 meter per century will intensify the salinisation process, causing an enormous increase in salt load in all low-lying areas in this part of The Netherlands (fig. 7.15).

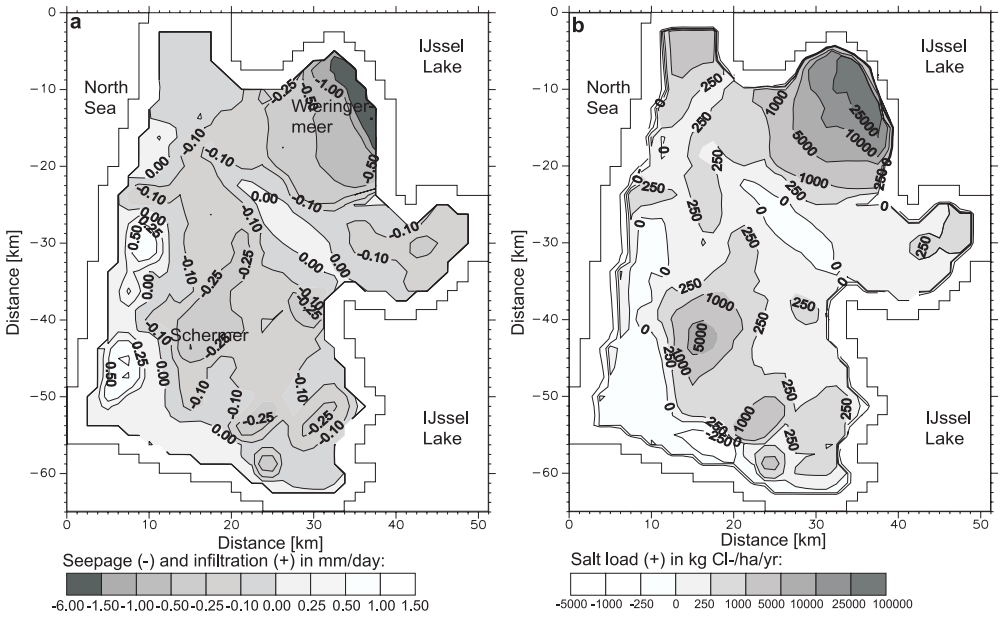

Figure 7.11: Seepage in mm/day (a) and salt load in kg Cl^-/ha/yr (b) at 1990 AD through the top layer at -20 m N.A.P. in the hydrogeologic system.

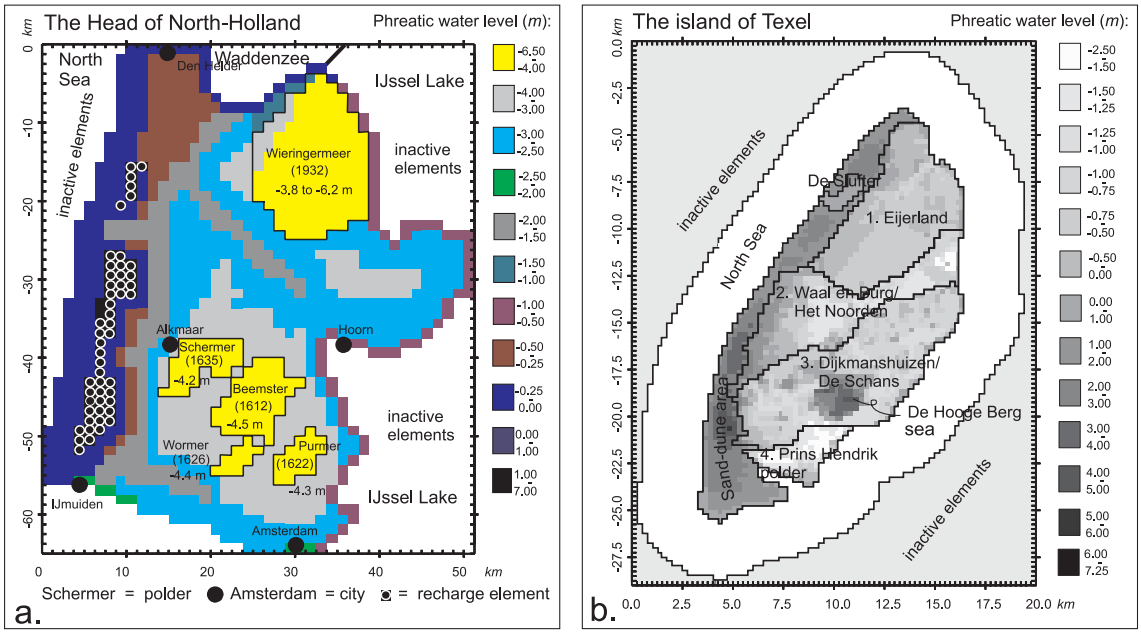

Figure 7.12: Present phreatic water level for the two 3D cases. The recharge in the sand-dune area is equal to 1 mm/day: a. The Head of North-Holland at 1990 AD in the top layer at -5 m $M.S.L.$ Between brackets the date of reclamation of five polders with a very low phreatic water level: Wieringermeer, Schermer, Beemster, Wormer, and Purmer; b. The island of Texel at 2000 AD in the top layer at -0.75 m $M.S.L.$ The position of the four polder areas and sand-dune area is also given.

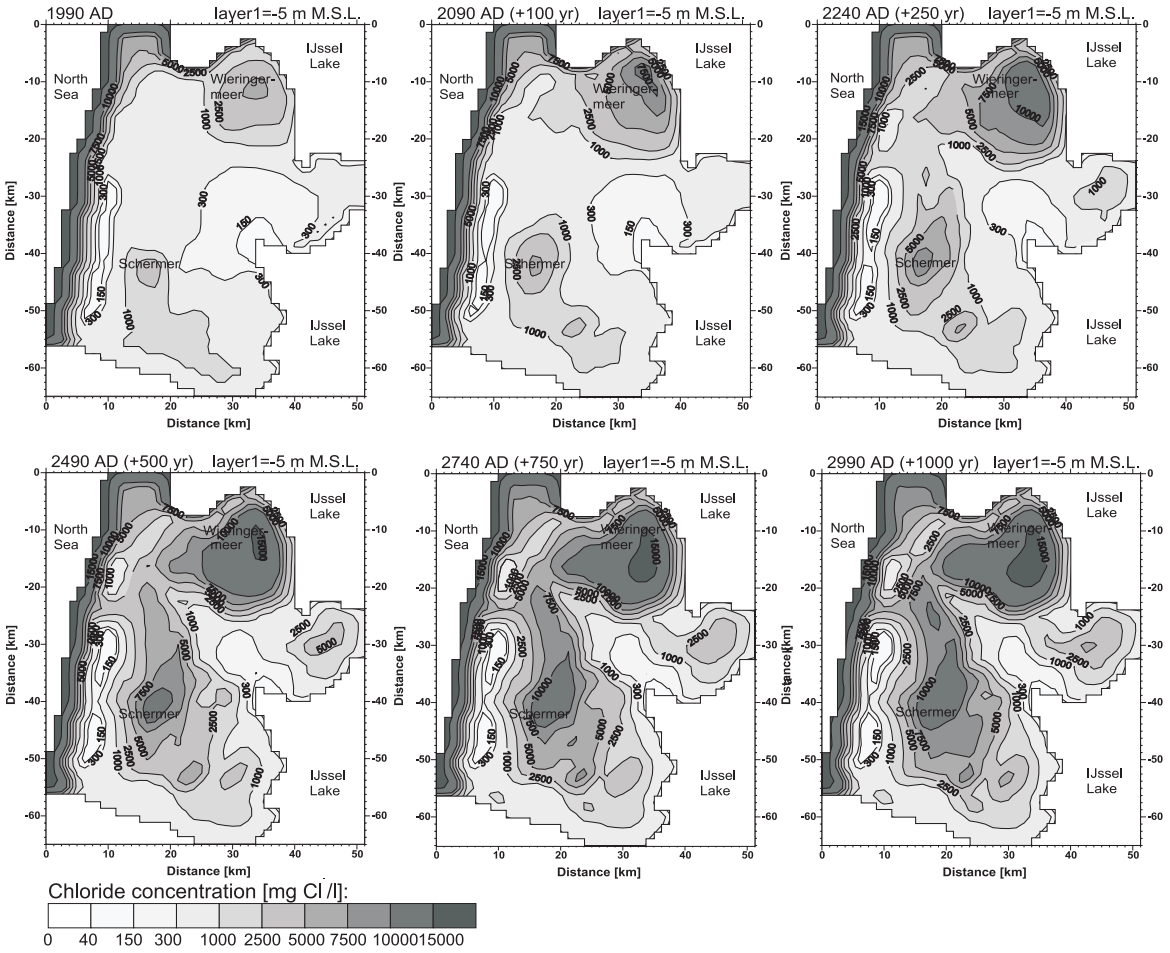

Figure 7.13: Chloride concentration in the top layer at -5 m N.A.P. in the hydrogeologic system at six moments in time: 1990, 2090, 2240, 2490, 2740 and 2990 AD.

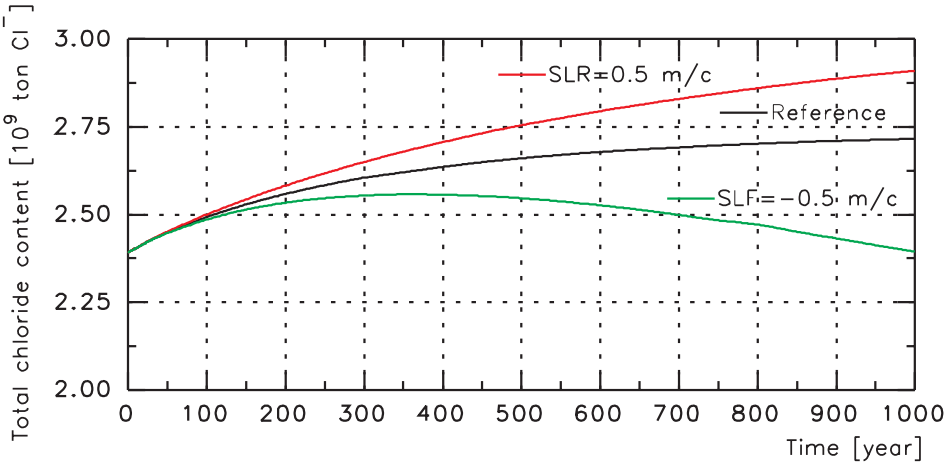

Figure 7.14: Total chloride (in 10^9 ton Cl^-) in the whole hydrogeologic system as a function of time.

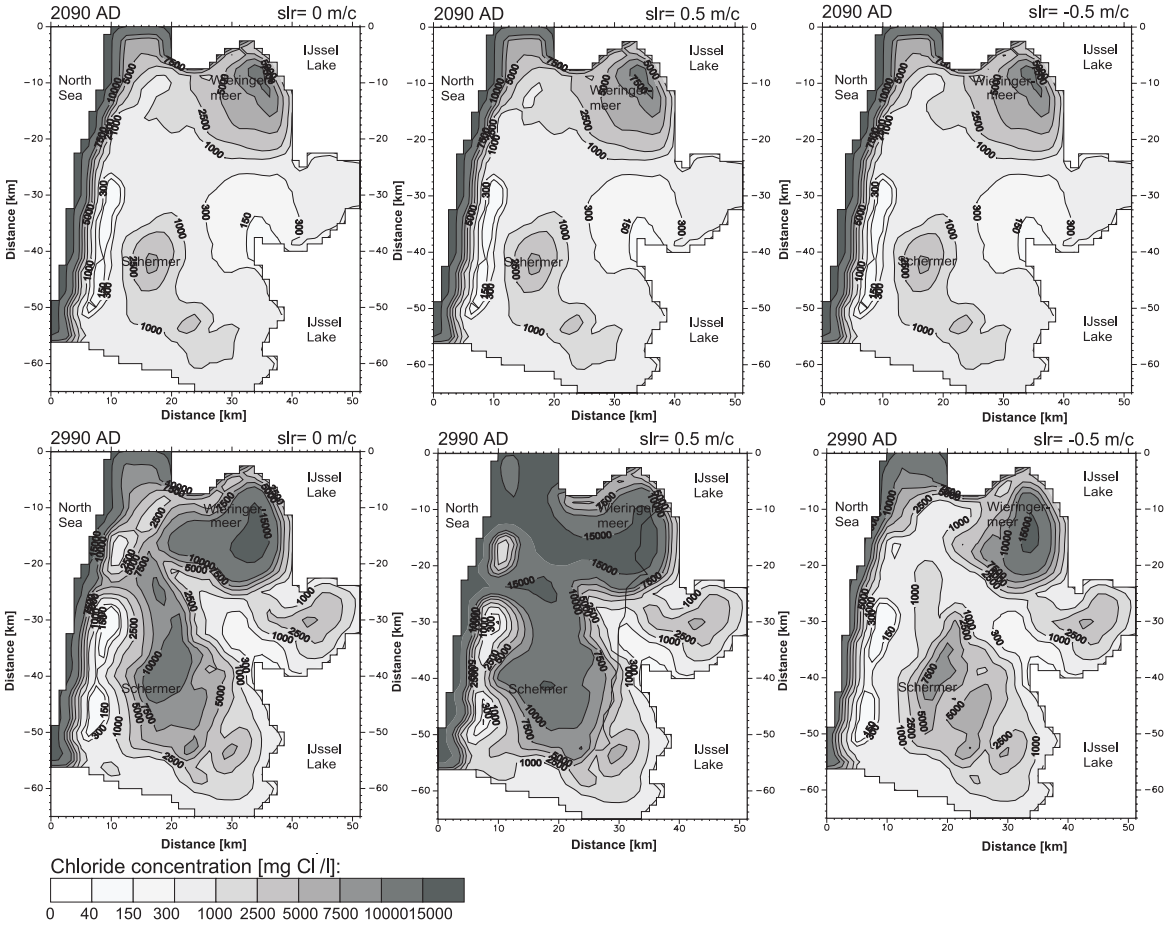

Figure 7.15: Chloride concentration in the top layer at -5 m N.A.P. in the hydrogeologic system for three sea level rise scenarios (0 m/c, 0.5 m/c and -0.5 m/c) at two moments in time: 2090 and 2990 AD.

7.6.3 The island of Texel

Salt water intrusion is investigated at Texel, which is a Wadden island in the northern part of The Netherlands with a surface area of approximately 130 km^2 (fig. 7.8). Four different low-lying areas can be distinguished at the island (fig. 7.12). The phreatic water level in these areas varies from -2.05 m to +4.75 m $M.S.L.$ In this coastal groundwater system of Quaternary deposits, salinisation of the upper layers is taking place. Brackish water already occurs close to the surface of the low-lying polder areas at the eastern part of the island. Freshwater occurs up to 50 m $M.S.L.$ in the sand-dune area at the western part. The numerical model is dimensioned 20 km by 29 km by 302 m depth, whereas about 125,000 active elements and one million particles simulate groundwater flow and salt transport during 500 years (Oude Essink, 2001b). See table 7.3 for physical and model parameters of the Texel case. A relative sea level rise of 0.75 m per century definitely intensifies the salinisation process during the next centuries (fig. 7.16). This process causes a further increase in salinity in the top layer as well as the salt load at the surface of the

Table 7.3: Physical and model parameters for two 3D cases: the Head of North-Holland and the island of Texel. The natural groundwater recharge is 360 mm/day. The density of freshwater ρ_f is 1000 kg/m^3. The concentration of saline groundwater is 35000 mg TDS/l or 18630 $mg\ Cl^-/l$.

Case	Head North-Holland	Island of Texel
Physical parameters		
Size system $L_x \times L_y \times L_z$ (km)	$65 \times 51.25 \times 0.29$	$20 \times 29 \times 0.302$
Hydraulic conductivity k (m/day)	5 to 70	5 to 30
Anisotropy k_z/k_x	0.4	0.4
Porosity n_e	0.35	0.3
Comp. expansion β $(\times 10^{-7})$	7.14 l/mg TDS	13.4 $l/mg\ Cl^-$
Long. dispersivity α_L (m)	2	2
Trans. dispersivity α_{TH}, α_{TV} (m)	0.2	0.2
Molecular diffusion D_m (m^2/s)	10^{-9}	10^{-9}
Model parameters		
Size cell $\Delta x \times \Delta y \times \Delta z$ (m)	$1250 \times 1250 \times 10$	$250 \times 250 \times$ 1.5-20
Number of cells $n_x \times n_y \times n_z$	$41 \times 52 \times 29$	$80 \times 116 \times 23$
Total number of active cells	39,933	125,554
Flow time step Δt $(year)$	1.0	1.0
Convergence criterion ϕ_f (m)	10^{-5}	10^{-5}
Number of particles per cell	27	8
Total simulated time $(year)$	1000	500

polders. As such, the increased salinisation of the top layer will affect the surface water system from an ecological as well as a socio-economical point of view.

æ

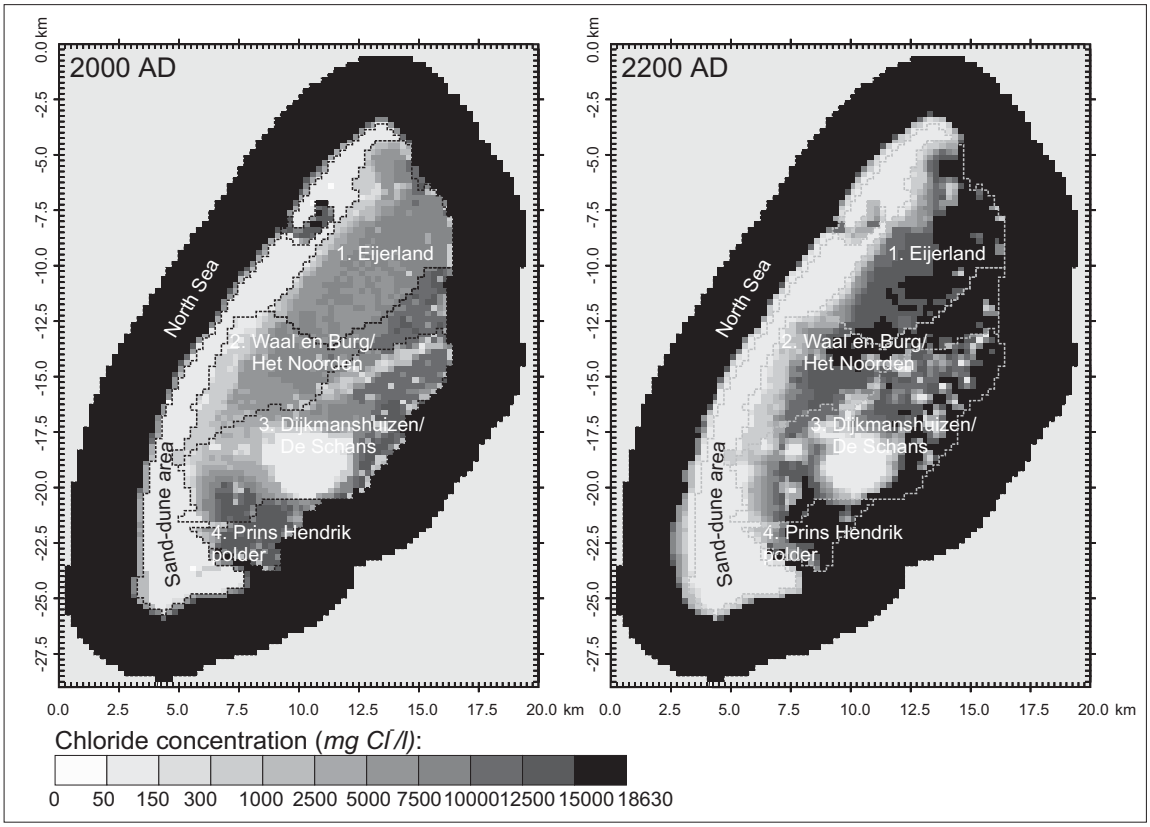

Figure 7.16: Chloride concentration in the top layer at -0.75 m $M.S.L.$ for the years 2000 and 2200 AD. Sea level rise is 0.75 m per century.

Part II

Heat transport in porous media: concept

Chapter 8

Introduction

8.1 Heat transport: conduction-convection equation

The mathematical description of heat transport in the x-direction 1D is as follows (Fourier and convection):

$$h = -\lambda_e \frac{\partial T}{\partial x} + n_e \rho c_f V T \quad \text{with} \quad \lambda_e = n_e \lambda_f + (1 - n_e)\lambda_s \tag{8.1}$$

where

- h=heat flux ($Joule\ m^{-2}\ s^{-1}$) or ($Watt\ m^{-2}$),
- λ_e=thermal conductivity ($Joule\ m^{-1}\ s^{-1}\ {}^oCelcius^{-1}$). λ_f and λ_s are the thermal conductivities of fluid and solid material, respectively,
- T=temperature (${}^oCelcius$),
- c_f, c_s=specific heat capacity of fluid and solid material, respectively ($Joule\ kg^{-1}\ {}^oCelcius^{-1}$),
- ρ, ρ_s= density of fluid and solid material, respectively ($kg\ m^{-3}$),
- V = effective velocity of the fluid ($L\,T^{-1}$),
- n_e = effective porosity ($-$).

Equation of continuity:
$$-\frac{\partial h}{\partial x} = \rho' c' \frac{\partial T}{\partial t} \quad \text{with} \quad \rho' c' = n_e \rho c_f + (1 - n_e)\rho_s c_s \tag{8.2}$$

$$\lambda_e \frac{\partial^2 T}{\partial x^2} - n_e \rho c_f \frac{\partial VT}{\partial x} = \rho' c' \frac{\partial T}{\partial t} \tag{8.3}$$

Steady state:
$$\frac{\partial V}{\partial x} = 0 \Longrightarrow \lambda_e \frac{\partial^2 T}{\partial x^2} - n_e \rho c_f V \frac{\partial T}{\partial x} = \rho' c' \frac{\partial T}{\partial t} \tag{8.4}$$

Heat transport:
$$\frac{\lambda_e}{\rho' c'} \frac{\partial^2 T}{\partial x^2} - \frac{n_e \rho c_f}{\rho' c'} V \frac{\partial T}{\partial x} = \frac{\partial T}{\partial t} \tag{8.5}$$

Analogy with solute transport:
$$\frac{D_x}{R_d} \frac{\partial^2 C}{\partial x^2} - \frac{1}{R_d} V \frac{\partial C}{\partial x} = \frac{\partial C}{\partial t} \tag{8.6}$$

Table 8.1: Some thermal conductivities of rocks, water and air. To convert Calorie to Joule, multiply by 4.187.

Material	**Thermal conductivity**
	λ $(cal\ m^{-1}\ s^{-1}\ ^oCelcius^{-1})$
Quartz	2
Sandstone	0.9
Limestone	0.5
Dolomite	0.4-1
Clay	0.2-0.3
Water	0.11
Air	0.006

8.1.1 Temperature gradient

In general, the range in temperature in the deep aquifers of Dutch groundwater flow systems is small. For instance, data from Stuyfzand (1986, 1988) in sand-dune areas along the Dutch coast show that the temperature of groundwater in the aquifers directly under the Holocene aquitard (at roughly -20 m $N.A.P.$[1]) is normally between 10.0 and 11.0 ^oC, while the annual mean air temperature near the coast is roughly 9.5 ^oC. At deeper layers, the temperature increases. For instance, the mean temperature of the groundwater varies at -250 m $N.A.P.$ between 12.0 and 18.0 ^oC, see fig. 8.1. The infiltration of relatively cold surface water in the Veluwe area can easily be seen. In the United States, most measured geothermal gradients for groundwater temperatures fall within the range from +1.8 to +3.6^oC *per* 100 m below the zone of surface influence (Todd, 1980). In case groundwater flows, smoother gradients can occur (Domenico & Schwartz, 1998). This phenomenon was pointed out by analysing temperature logs in a large number of boreholes. For instance, several boreholes in the Murgia aquifer show a increase in temperature of less than 1.5 ^oC over the top 200 m. On the other hand, changes in temperature near the ground surface due to geothermal flow can sometimes be significant.

8.2 Analogy of heat and solute transport

In this section, the analogy between solute transport and heat transport in porous media is demonstrated. Consider the solute transport equation or advection-dispersion equation:

$$R_d \frac{\partial C}{\partial t} = \frac{\partial}{\partial x_i}(D_{ij}\frac{\partial C}{\partial x_j}) - \frac{\partial}{\partial x_i}(C\,V_i) + \frac{(C - C')\,W}{n_e b} - R_d\,\lambda\,C \tag{8.7}$$

where

- $R_d = 1 + (\rho_b/n_e)K_d$ = retardation factor governing adsorption $(-)$. K_d is the distribution coefficient $(M^{-1}\,L^3)$ and ρ_b is the bulk density of the porous material $(M\,L^{-3})$,

[1] $N.A.P.$ stands for Normaal Amsterdams Peil and is the reference level in the Netherlands. $N.A.P.$ roughly equals Mean Sea Level.

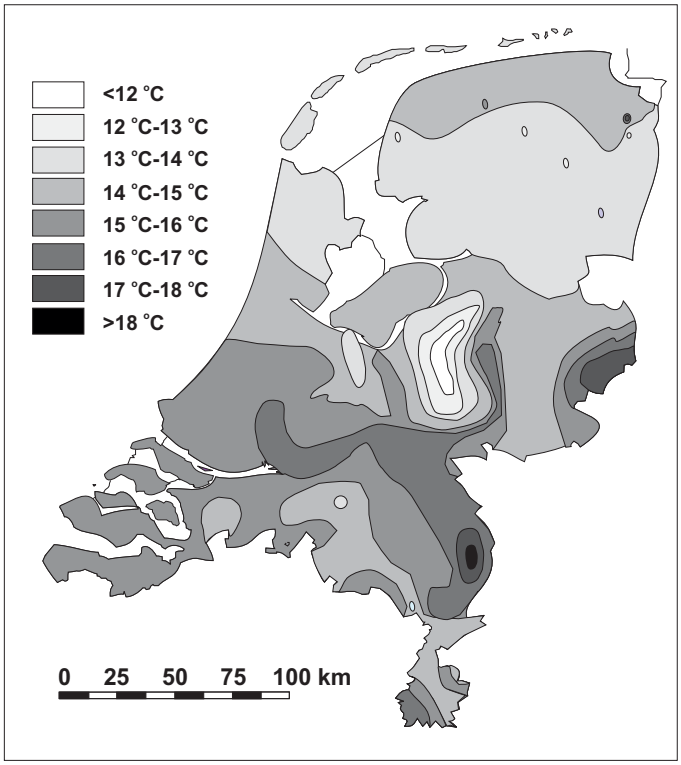

Figure 8.1: Isotherm map of the Netherlands at a depth of 250 m below ground surface.

- λ = first-order rate constant, governing hydrolysis and decay (T^{-1}). Radioactive decay rates are often expressed as half-lives ($t_{1/2}$), where the half-life is the time required for the concentration to decrease to one-half of the original value: $t_{1/2} = (\ln 2)/\lambda$.

The mechanical dispersion coefficient is as follows (Scheidegger, 1961):

$$D_{ij} = \alpha_{ijmn} \frac{V_m V_n}{|V|} \tag{8.8}$$

or

$$D_{ij} = \alpha_T |V| \delta_{ij} + (\alpha_{L-} \alpha_T) \frac{V_i V_j}{|V|} \tag{8.9}$$

where

- D_{ij} = coefficient of mechanical dispersion ($L^2 T^{-1}$),
- α_{ijmn} = geometrical dispersivity tensor of the aquifer (L),
- V_m, V_n = components of the real velocity in m and n direction ($L T^{-1}$),
- $|V|$ = magnitude of the real velocity ($L T^{-1}$),
- $\delta_{ij} = 1$ if $i = j$ and $\delta_{ij} = 0$ if $i \neq j$.

Scheidegger defines the dispersivity tensor for an isotropic aquifer in terms of two constants:

$$\begin{aligned} D_L &= \alpha_L \, |V| \\ D_T &= \alpha_T \, |V| \end{aligned} \tag{8.10}$$

where

- α_L = longitudinal dispersivity of the aquifer (L),
- α_T = transversal dispersivity of the aquifer (L).

For two dimensions, and introducing molecular diffusion:

$$\begin{aligned} D_{xx} &= \alpha_L \frac{(V_x)^2}{|V|} + \alpha_T \frac{(V_z)^2}{|V|} + D_m \\ D_{zz} &= \alpha_T \frac{(V_x)^2}{|V|} + \alpha_L \frac{(V_z)^2}{|V|} + D_m \\ D_{xz} &= D_{zx} \; = \; (\alpha_L - \alpha_T) \frac{V_x \, V_z}{|V|} \end{aligned} \tag{8.11}$$

Writing eqn. 8.7 in another form gives:

$$\begin{aligned} & R_d \tfrac{\partial C}{\partial t} = \\ & \left[\left(\alpha_L \tfrac{(V_x)^2}{|V|} + \alpha_T \tfrac{(V_z)^2}{|V|} \right) + D_m \right] \tfrac{\partial^2 C}{\partial x^2} + \left[\left(\alpha_T \tfrac{(V_x)^2}{|V|} + \alpha_L \tfrac{(V_z)^2}{|V|} \right) + D_m \right] \tfrac{\partial^2 C}{\partial z^2} \\ & + \left[2(\alpha_L - \alpha_T) \tfrac{V_x \, V_z}{|V|} \right] \tfrac{\partial}{\partial x} \tfrac{\partial T}{\partial z} - \left(V_x \tfrac{\partial T}{\partial x} + V_z \tfrac{\partial T}{\partial z} \right) + \tfrac{(C - C') \, W}{n_e b} - R_d \, \lambda \, C \end{aligned} \tag{8.12}$$

Now, the analogy with heat transport will be demonstrated (see also Gielen, 1999). The heat transport eqn. 8.5 in one dimension, describing the steady state temperature distribution in a saturated porous medium, will be transformed into two dimensions (e.g. Smith & Chapman, 1983; Garven, 1995; Person *et al.*, 1996; Domenico & Schwartz, 1998):

$$\rho' c' \frac{\partial T}{\partial t} = \frac{\partial}{\partial x_i} (\Lambda_{ij} \frac{\partial T}{\partial x_j}) - \rho c_f \frac{\partial}{\partial x_i} (T \, q_i) + \Gamma \tag{8.13}$$

where:

$$\rho' c' = n_e \rho c_f + (1 - n_e) \rho_s c_s \tag{8.14}$$

- n_e = effective porosity ($-$),
- ρ, ρ_s= density of fluid and solid material, respectively ($kg \; m^{-3}$),
- c_f, c_s=specific heat capacity of fluid and solid material, respectively ($Joule \; kg^{-1} \; {}^{o}Celcius^{-1}$),
- T=temperature (${}^{o}Celcius$),
- Λ_{ij}=the effective thermal conductivity tensor ($Joule \; m^{-1} \; s^{-1} \; {}^{o}Celcius^{-1}$),
- q_i = Darcian specific discharge of the fluid ($L \, T^{-1}$),

- Γ = the rate of heat addition and removal by chemical reactions ($Joule\ s^{-1}\ m^{-3}$).

Rewriting eqn. 8.13 gives:

$$\rho' c' \frac{\partial T}{\partial t} = \frac{\partial}{\partial x}\left(\Lambda_{xx}\frac{\partial T}{\partial x} + \Lambda_{xz}\frac{\partial T}{\partial z}\right) + \frac{\partial}{\partial z}\left(\Lambda_{zz}\frac{\partial T}{\partial z} + \Lambda_{zx}\frac{\partial T}{\partial x}\right) - \rho c_f\left(q_x\frac{\partial T}{\partial x} + q_z\frac{\partial T}{\partial z}\right) + \Gamma \tag{8.15}$$

The effective thermal conductivity tensor Λ_{ij} can be written explicitly as:

$$\begin{aligned}
\Lambda_{xx} &= n_e\lambda^f_{xx} + \rho c_f\left(\alpha_L\frac{(q_x)^2}{|q|} + \alpha_T\frac{(q_z)^2}{|q|}\right) + (1-n_e)\lambda^s_{xx} \\
\Lambda_{zz} &= n_e\lambda^f_{zz} + \rho c_f\left(\alpha_T\frac{(q_x)^2}{|q|} + \alpha_L\frac{(q_z)^2}{|q|}\right) + (1-n_e)\lambda^s_{zz} \\
\Lambda_{xz} &= \Lambda_{zx} = \rho c_f(\alpha_L - \alpha_T)\frac{q_x\, q_z}{|q|}
\end{aligned} \tag{8.16}$$

where λ^f_{ij} and λ^s_{ij} are terms of the tensor of thermal conductivity of fluid and solid material, respectively. As can be seen, also mechanical mixing (represented by the α's), caused by unspecified heterogeneities within the porous medium, contribute to the transport of heat. If an isotropic medium is assumed, the terms λ^f_{xx}, λ^f_{zz}, λ^s_{xx} and λ^s_{zz} become λ^f and λ^s for fluid and solid material, respectively.

The relation between the Darcian specific discharge q_i and the effective velocity of the groundwater V_i is:

$$V_i = \frac{q_i}{n_e} \qquad \text{or} \qquad q_i = V_i n_e \tag{8.17}$$

Thus:

$$\frac{(q_x)^2}{|q|} = \frac{n_e^2 V_x^2}{n_e\sqrt{V_x^2 + V_z^2}} = \frac{n_e V_x^2}{|V|} \tag{8.18}$$

Rewriting eqn. 8.15 and using the eqn. 8.16, 8.17 and 8.18 gives:

$$\begin{aligned}
&[n_e\rho c_f + (1-n_e)\rho_s c_s]\frac{\partial T}{\partial t} = \\
&\left[n_e\rho c_f\left(\alpha_L\frac{(V_x)^2}{|V|} + \alpha_T\frac{(V_z)^2}{|V|}\right) + n_e\lambda^f_{xx} + (1-n_e)\lambda^s_{xx}\right]\frac{\partial^2 T}{\partial x^2} \\
&+ \left[n_e\rho c_f\left(\alpha_T\frac{(V_x)^2}{|V|} + \alpha_L\frac{(V_z)^2}{|V|}\right) + n_e\lambda^f_{zz} + (1-n_e)\lambda^s_{zz}\right]\frac{\partial^2 T}{\partial z^2} \\
&+ \left[2n_e\rho c_f(\alpha_L - \alpha_T)\frac{V_x V_z}{|V|}\right]\frac{\partial}{\partial x}\frac{\partial T}{\partial z} - n_e\rho c_f\left(V_x\frac{\partial T}{\partial x} + V_z\frac{\partial T}{\partial z}\right) + \Gamma
\end{aligned} \tag{8.19}$$

or, divided by $n_e\rho c_f$:

$$\begin{aligned}
&\left[1 + \frac{(1-n_e)\rho_s c_s}{n_e\rho c_f}\right]\frac{\partial T}{\partial t} = \\
&\left[\left(\alpha_L\frac{(V_x)^2}{|V|} + \alpha_T\frac{(V_z)^2}{|V|}\right) + \frac{n_e\lambda^f_{xx} + (1-n_e)\lambda^s_{xx}}{n_e\rho c_f}\right]\frac{\partial^2 T}{\partial x^2} + \left[\left(\alpha_T\frac{(V_x)^2}{|V|} + \alpha_L\frac{(V_z)^2}{|V|}\right) + \frac{n_e\lambda^f_{zz} + (1-n_e)\lambda^s_{zz}}{n_e\rho c_f}\right]\frac{\partial^2 T}{\partial z^2} \\
&+ \left[2(\alpha_L - \alpha_T)\frac{V_x V_z}{|V|}\right]\frac{\partial}{\partial x}\frac{\partial T}{\partial z} - \left(V_x\frac{\partial T}{\partial x} + V_z\frac{\partial T}{\partial z}\right) + \Gamma`
\end{aligned} \tag{8.20}$$

Now, the analogy between solute transport (eqn. 8.12) and heat transport (eqn. 8.20) becomes clear, see table 8.2. As can be seen:

Table 8.2: *Parameters to accomplish the analogy between solute transport and heat transport.*

Solute transport	Heat transport
C	T
R_d	$1 + \frac{(1-n_e)\rho_s c_s}{n_e \rho c_f}$
D_m	$\frac{n_e \lambda^f + (1-n_e)\lambda^s}{n_e \rho c_f}$
λ	0

- concentration C $(M\,L^{-3})$ is replaced by temperature T $(^oCelcius)$,
- retardation factor R_d $(-)$ is replaced by the heat capacity ratio σ $(\frac{n_e \rho c_f + (1-n_e)\rho_s c_s}{\rho c_f})$ $(-)$ divided by porosity n_e $(-)$,
- molecular diffusion $(L^2\,T^{-1})$ is replaced by the effective thermal heat diffusivity κ_e $(\frac{n_e \lambda^f + (1-n_e)\lambda^s}{\rho c_f})$ $(L^2\,T^{-1})$ divided by porosity n_e $(-)$,
- the solute sources and sinks term $\frac{(C-C')\,W}{n_e b}$ $(M\,L^{-3}\,T^{-1})$ is replaced by the heat sources and sinks term Γ‘ $(^oCelcius\,T^{-1})$.

8.3 Linear stability analysis

In this section, a linear stability analysis is performed to demonstrate under which circumstances the fluid (viz. groundwater) is at rest in a thermal porous medium, where flow of groundwater and transport of heat can take place. It appears that for small so-called Rayleigh numbers Ra heat, supplied from below, will be transported to the cold layers at the top by conduction when the temperature difference (ΔT=$T_1 - T_0$) is small, see fig. 8.2. This means that the vertical groundwater velocity equals zero ($q_z = 0$). However, when the temperature difference ΔT increases, the density ρ decreases, which causes at one specific moment the onset of convection. Once the viscous resistance has been overcome, heat will also be transported by convection. Rayleigh analysed the onset of convection in 1916, though only for fluids. Horton & Rogers (1945) and Lapwood (1948) considered the problem for a porous medium. Note that the Oberbeck(1879)-Boussinesq (1903) assumption is applicable in this stability analysis: difference in density are only not neglected in Darcy's law. Consequently, an incompressible conservation of fluid equation is assumed: $\nabla \cdot q = 0$, or:

$$\frac{\partial q_x}{\partial x} + \frac{\partial q_z}{\partial z} = 0 \tag{8.21}$$

The governing equations are:

$$q_x = -\frac{\kappa}{\mu}\frac{\partial p}{\partial x} \Longleftrightarrow \frac{\partial p}{\partial x} = -\frac{\mu}{\kappa} q_x \tag{8.22}$$

$$q_z = -\frac{\kappa}{\mu}\left(\frac{\partial p}{\partial z} - \rho g\right) \Longleftrightarrow \frac{\partial p}{\partial z} = -\frac{\mu}{\kappa} q_z + \rho g \tag{8.23}$$

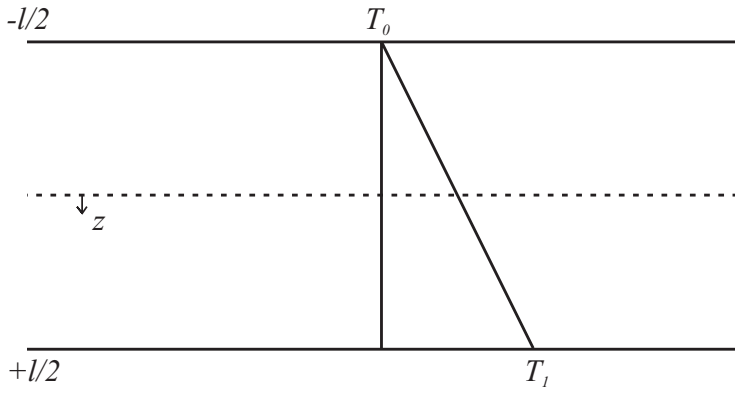

Figure 8.2: Definition of the thermal porous medium heated from below to determine the Rayleigh number.

$$\rho = \rho_0 \left[1 - \alpha_f \left(T - T'\right)\right] \tag{8.24}$$

where ρ_0 = density of fresh water ($kg\ m^{-3}$) and α_f = coefficient of thermal expansion ($^oCelcius^{-1}$). The two-dimensional equation for heat transport in a porous medium is:

$$\rho' c' \frac{\partial T}{\partial t} = \lambda_e \left(\frac{\partial^2 T}{\partial x^2} + \frac{\partial^2 T}{\partial z^2}\right) - \rho c_f \left(q_x \frac{\partial T}{\partial x} + q_z \frac{\partial T}{\partial z}\right) \tag{8.25}$$

In this equation, heat by friction of fluids and compression of moving fluids (pressure force) are neglected.

Equation for conduction

Now, the interest is focussed on conduction only, in order to obtain the conduction equation which will be used in the analysis. This means in terms of equations:

$$q_x = q_z = 0, \quad \frac{\partial}{\partial t} = 0, \quad \frac{\partial}{\partial x} = 0 \tag{8.26}$$

$$\text{steady conduction state:} \qquad \frac{\partial^2 T_{cond}}{\partial z^2} = 0 \Longleftrightarrow T_{cond} = Az + B \tag{8.27}$$

The boundary conditions are:

$$z = -\frac{l}{2}: \quad T_{cond} = T_0 : T_0 = -A\frac{l}{2} + B \tag{8.28}$$

$$z = +\frac{l}{2}: \quad T_{cond} = T_1 : T_1 = A\frac{l}{2} + B \tag{8.29}$$

The constants A and B become:

$$(+): \quad T_0 + T_1 = 2B \Longleftrightarrow B = \frac{T_0 + T_1}{2} \tag{8.30}$$

$$(-): \quad T_0 - T_1 = -Al \Longleftrightarrow A = -\frac{T_0 - T_1}{l} \tag{8.31}$$

This yields the equation for only conduction:

$$T_{cond} = \left(\frac{T_1 - T_0}{l}\right) z + \frac{T_1 + T_0}{2} \tag{8.32}$$

The onset of convection: perturbations

The onset of convection is determined by introducing small perturbations for the temperature, darcian velocities and the density: ΔT, Δq_x, Δq_z and $\Delta \rho$.

$$\Delta T = T - T_{cond} \Longleftrightarrow T = T_{cond} + \Delta T \tag{8.33}$$

$$\rho' c' \frac{\partial \Delta T}{\partial t} = \lambda_e \left[\frac{\partial^2 \Delta T}{\partial x^2} + \frac{\partial^2 \Delta T}{\partial z^2}\right] - \rho c_f \left[\Delta q_x \frac{\partial \Delta T}{\partial x} + \Delta q_z \frac{\partial \Delta T}{\partial z} + \Delta q_z \left(\frac{T_1 - T_0}{l}\right)\right] \tag{8.34}$$

Now, the perturbation equation is analysed. When a small perturbation grows, convection is introduced into the system. So, the interest is focussed on the grow of the perturbation. For that, the perturbations are written in Fourier terms:

$$\Delta T = \varepsilon \mathrm{e}^{t/\tau} \cos\left(\frac{\pi z}{l}\right) \cos\left(\frac{\pi x}{l}\right) \tag{8.35}$$

$$\Delta q_x = -C \mathrm{e}^{t/\tau} \sin\left(\frac{\pi z}{l}\right) \sin\left(\frac{\pi x}{l}\right) \tag{8.36}$$

$$\Delta q_z = -C \mathrm{e}^{t/\tau} \cos\left(\frac{\pi z}{l}\right) \cos\left(\frac{\pi x}{l}\right) \tag{8.37}$$

$$\Delta \rho = -\rho_0 \alpha_f \Delta T \tag{8.38}$$

Now, the constant C is determined:

$$\frac{\partial \Delta p}{\partial x} = -\frac{\mu}{\kappa}\left[-C \mathrm{e}^{t/\tau} \sin\left(\frac{\pi z}{l}\right) \sin\left(\frac{\pi x}{l}\right)\right] \tag{8.39}$$

$$\frac{\partial^2 \Delta p}{\partial x \partial z} = -\frac{\mu}{\kappa}\left[-C \mathrm{e}^{t/\tau} \cos\left(\frac{\pi z}{l}\right) \frac{\pi}{l} \sin\left(\frac{\pi x}{l}\right)\right] \tag{8.40}$$

$$\frac{\partial \Delta p}{\partial z} = -\frac{\mu}{\kappa}\left[-C \mathrm{e}^{t/\tau} \cos\left(\frac{\pi z}{l}\right) \cos\left(\frac{\pi x}{l}\right)\right] - \rho_0 \alpha_f \Delta T g \tag{8.41}$$

$$\frac{\partial^2 \Delta p}{\partial z \partial x} = -\frac{\mu}{\kappa}\left[C \mathrm{e}^{t/\tau} \cos\left(\frac{\pi z}{l}\right) \sin\left(\frac{\pi x}{l}\right) \frac{\pi}{l}\right] + \rho_0 \alpha_f \varepsilon \mathrm{e}^{t/\tau} \cos\left(\frac{\pi z}{l}\right) \sin\left(\frac{\pi x}{l}\right) \frac{\pi}{l} g \tag{8.42}$$

Equate the eqns. 8.40 and 8.42, and dividing by $\mathrm{e}^{\,t/\tau} \cos\left(\frac{\pi z}{l}\right) \sin\left(\frac{\pi x}{l}\right)$ gives:

$$\frac{\mu}{\kappa}\left[C \frac{\pi}{l}\right] = -\frac{\mu}{\kappa}\left[C \frac{\pi}{l}\right] + \rho_0 \alpha_f \varepsilon \frac{\pi}{l} g \tag{8.43}$$

$$\frac{\mu}{\kappa} C = -\frac{\mu}{\kappa} C + \rho_0 \alpha_f \varepsilon g \tag{8.44}$$

$$C = \frac{\rho_0 \alpha_f \varepsilon g \kappa}{2\mu} \tag{8.45}$$

Assuming that the terms $\Delta q_x \frac{\partial \Delta T}{\partial x} + \Delta q_z \frac{\partial \Delta T}{\partial z}$ in eqn. 8.34 can be neglected, this equation becomes:

$$\begin{gathered}\rho' c' \varepsilon \mathrm{e}^{t/\tau} \tfrac{1}{\tau} \cos\left(\tfrac{\pi z}{l}\right) \cos\left(\tfrac{\pi x}{l}\right) = \\ \lambda_e \left[-\varepsilon \mathrm{e}^{t/\tau} \cos\left(\tfrac{\pi z}{l}\right) \cos\left(\tfrac{\pi x}{l}\right) \tfrac{\pi^2}{l^2} - \varepsilon \mathrm{e}^{t/\tau} \cos\left(\tfrac{\pi z}{l}\right) \cos\left(\tfrac{\pi x}{l}\right) \tfrac{\pi^2}{l^2}\right] \\ -\rho c_f \left[-\tfrac{\rho_0 \alpha_f \varepsilon g \kappa}{2\mu} \mathrm{e}^{t/\tau} \cos\left(\tfrac{\pi z}{l}\right) \cos\left(\tfrac{\pi x}{l}\right) \left(\tfrac{T_1 - T_0}{l}\right)\right] \end{gathered} \tag{8.46}$$

Dividing by $\varepsilon\ \mathrm{e}^{t/\tau} \cos\left(\frac{\pi z}{l}\right) \cos\left(\frac{\pi x}{l}\right)$ gives:

$$\rho' c' \frac{1}{\tau} = \lambda_e \left[-\frac{\pi^2}{l^2} - \frac{\pi^2}{l^2}\right] + \rho c_f \left[\frac{\rho_0 \alpha_f g \kappa}{2\mu} \left(\frac{T_1 - T_0}{l}\right)\right] \tag{8.47}$$

Convection currents can arise only when eqn. 8.47 is positive (viz. $\mathrm{e}^{t/\tau}$ increases when $\rho' c' \frac{1}{\tau} > 0$). Thus:

$$\lambda_e \left[-\frac{\pi^2}{l^2} - \frac{\pi^2}{l^2}\right] + \rho c_f \left[\frac{\rho_0 \alpha_f g \kappa}{2\mu} \left(\frac{T_1 - T_0}{l}\right)\right] > 0 \tag{8.48}$$

$$\rho c_f \left[\frac{\rho_0 \alpha_f g \kappa}{2\mu} \left(\frac{T_1 - T_0}{l}\right)\right] > 2\lambda_e \frac{\pi^2}{l^2} \tag{8.49}$$

$$\frac{\rho_0 \alpha_f g \kappa (T_1 - T_0) \rho c_f l}{\mu \lambda_e} > 4\pi^2 \tag{8.50}$$

$$\frac{\rho_0 \alpha_f g \kappa (T_1 - T_0) \rho c_f l}{\mu \lambda_e} > 4\pi^2 \tag{8.51}$$

$$Ra > 4\pi^2 \approx 39.48 \approx 40 \tag{8.52}$$

The critical condition for the temperature gradient is:

$$\left(\frac{T_1 - T_0}{l}\right) > \frac{4\pi^2 \mu \lambda_e}{\rho_0 \alpha_f g \kappa \rho c_f l^2} \tag{8.53}$$

When $\frac{\lambda_e}{\rho c_f} = \kappa_e$ (=thermal diffusivity $M\,L^{-2}$), the so-called Rayleigh number [2] becomes:

$$Ra = \frac{\rho_0 \alpha_f g \kappa (T_1 - T_0) l}{\mu \kappa_e} > 4\pi^2 \tag{8.54}$$

As such, the Rayleigh number characterises the onset of convection. Other derivations of the Rayleigh number can, among others, be found in Scheidegger (1974), Turcotte & Schubert (1982) and Nield & Bejan (1992).

Eqn. 8.54 has been derived for the situation that the upper and lower boundaries are impermeable (no groundwater flux) and conducting (constant temperature). However, other situations with different boundary conditions are also possible (Nield, 1968; Nield & Bejan, 1992), generating other Rayleigh numbers. Only one of these situations can be determined analytically. This case is when both boundaries are impermeable (no groundwater flux) and insulating (constant heat flux). The critical Rayleigh number for this case equals 12.

[2] Note that for viscous fluids, the Rayleigh number is equal to $Ra > \frac{27}{4}\pi^4 \approx 657.48$.

8.4 Double-diffusive convection

The interesting effects of double-diffusive convection[3] arise from the fact that heat diffuses more rapidly than a dissolved substance (Nield & Bejan, 1992). æ

[3]Or thermohaline, if heat and salt are involved.

References

Atlas van Nederland, Deel 15 Water, (in Dutch), Ven, G.P., van de *et al.* (eds), *Staatsuitgeverij, 's-Gravenhage, 1986.*

Anderson, M.P. & Woessner, W.W., Applied groundwater modeling, Simulation of flow and advective transport, *Academy Press, Inc., San Diego, 381 pp., 1992.*

Badon Ghijben W., Drabbe J., Nota in verband met de voorgenomen putboring nabij Amsterdam, (in Dutch), *Tijdschrift van het Koninklijk Instituut voor Ingenieurs 1888-1889: 8-22, 1889.*

Bear, J., Dynamics of fluids in Porous Media, *American Elsevier Publishing Company, Inc., New York, 764 pp., 1972.*

Bear, J. & G. Dagan, Some exact solutions of interface problems by means of the hodograph method, *J. Geophys. Res.,* **69***, 1563-1572, 1964.*

Bear, J. & Verruijt, A., Modeling Groundwater Flow and Pollution, *D. Reidel Publishing Company, Dordrecht, the Netherlands, 414 pp., 1987.*

Bear, J., Cheng, A., Sorek, S., Herrera, I. & Ouazar, D. (eds), *Seawater intrusion in coastal aquifers; concept, methods and practices, 625 pp., Kluwer Academic Publishers, 1999.*

Bethke, C.M., A numerical model of compaction-driven groundwater flow and heat transfer and its application to the paleohydrology of intracratonic sedimentary basins, *J. Geophys. Res.,* **90***, 6817-6828, 1985.*

Boekelman, R.H., Evolution of an interface in phreatic aquifers, (in press), *Communication of the Department of Water Management, Environmental and Sanitary Engineering, 1998.*

Boekelman, R.H. & Grakist, G. Determination of shape and thickness of the freshwater lens of the Haringvreter, (in Dutch), *M.Sc. thesis, Delft University of Technology, 1973.*

Cooper, H.H., jr., Kohout, F.A., Henry, H.R. & Glover, R.E., Sea water in coastal aquifers, *U.S.G.S. Water Supply Paper 1613-C, 84 pp., 1964.*

CRC, Handbook of Chemistry and Physics, 75^{th} Edition. Lide, D.R. (ed), *Chemical Rubber Company Press, Boca Raton, Florida, 1994.*

Custodio, E. & Bruggeman, G.A. (eds), Groundwater Problems in Coastal Areas, *Studies and Reports in Hydrology, UNESCO, International Hydrological Programme, Paris, 1987.*

Dagan, G. & J. Bear, Solving the problem of local interface upconing in a coastal aquifer by the method of small perturbations, *J. Hydraul. Res.,* **6***, 15-44, 1968.*

Dam, J.C., van, Partial depletion of saline groundwater by seepage, *J. of Hydrol.,* **29***, 315-339, 1976.*

Dam, J.C., van, The shape and position of the salt water wedge in coastal aquifers, *Relation of Groundwater Quantity and Quality, Proc. Hamburg Symp. IAHS Publ. no. 146, 59-75, August 1983.*

Dam, J.C., van, Geohydrology, Lecture notes, (in Dutch), *Delft University of Technology, Faculty of Civil Engineering, Section Hydrology, the Netherlands, 1992.*

Dam, J.C., van, Impact of sea-level rise on salt water intrusion in estuaries and aquifers, *Keynote lecture Session III of the International Workshop SEACHANGE'93: Sea Level Changes and their Consequences for Hydrology and Water Management, Noordwijkerhout, the Netherlands, UNESCO, IHP-IV Project H-2-2, 49-60, 1993.*

Dam, J.C., van & Sikkema, P.C., Approximate solution of the problem of the shape of the interface in a semi-confined aquifer, *J. of Hydrol.,* **56***, 221-237, 1982.*

Daus, A.D., Frind, E.O. & Sudicky, E.A., Comparative error analysis in finite element formulations of the advection-dispersion equation, *Adv. Water Resour.,* **8***, 86-95, 1985.*

Diersch, H.J.G., Interactive, graphics-based finite-element simulation system FEFLOW for modeling groundwater flow, contaminant mass and heat transport processes, FEFLOW User's Manual Version 4.5, *Institute for Water Resources Planning and System Research, Ltd., 1996.*

Elder, J.W., Transient convection in a porous medium, *J. Fluid Mech.,* **27***, 609-623, 1967.*

Esch, J.M., van, Personal communications, *Delft Geotechnics, P.O. Box 69, 2600 AB Delft, the Netherlands, 1996.*

Fein, E., *et al.*, D^3F - A simulator for density driven flow modelling, User's Manual, *GRS, Braunscheig, Germany, 1998.*

Frind, E.O., Simulation of long-term transient density-dependent transport in groundwater, *Adv. in Water Resour.,* **5***, 73-88, 1982.*

Frind, E.O. & Pinder, G.F., The principle direction technique for solution of the advection-dispersion equation, *Proc.* 10^{th} *IMACS World Congress on Systems Simulation and Scientific Computation, Concordia University, Montreal, Canada, Aug. 1982, 305-313, 1983.*

Freeze, R.A. & Cherry, J.A., Groundwater, *Prentice-Hall, Inc. New Jersey, 1979.*

Garven, G., Continental-scale groundwater flow and geologic processes, *Annu. Rev. Earth Planet. Sci.,* **23***, 89-117, 1995.*

Galeati, G., Gambolati, G. & Neuman, S.P., Coupled and Partially Coupled Eulerian-Lagrangian Model of Freshwater-Seawater Mixing, *Water Resour. Res.,* **28** *(1), 149-165, 1992.*

Gelhar, L.W., Welty, C. & Rehfeldt, K.R., A Critical Review of Data on Field-Scale Dispersion in Aquifers, *Water Resour. Res.,* **28** *(7), 1955-1974, 1992.*

Gerven, van, M.W. & Schaars, F., The density package, simulation of density driven flow in MODFLOW, In: *Proc. of the 15th Salt Water Intrusion Meeting, Ghent, Belgium, May 1998, 1998a.*

Gerven, van, M.W. & Schaars, F., The density package and MT3DENSE: simulation of density driven flow in MODFLOW, In: *Proc. of the MODFLOW'98 Conf. Golden, Colorado, USA, 283-290, 1998b.*

Gelhar, L.W. & Collins, M.A., General analysis of longitudinal dispersion in nonuniform flow, *Water Resour. Res.,* **7** *(6), 1511-1521, 1971.*

Gielen, T. Numerical modelling of fluid flow and heat transfer in porous media, Adapting a solute transport computer code to calculate heat transfer and two applications, 55 pp., *M.Sc. thesis, Utrecht University, 1999.*

Goldenberg, L.C., Mandel, S. & Magaritz, M. Fluctuating, non-homogeneous changes of hydraulic conductivity in porous media. *Quarterly J. of Eng. Geology, London,* **19***, 183-190, 1986.*

Glover, R.E., The pattern of fresh-water flow in a coastal aquifer, *J. Geophys. Res.,* **64***, 457-459, 1959.*

Guo, W., Bennett, G.D., Simulation of saline/fresh water flows using MODFLOW, In: *Proc. of the MODFLOW'98 Conf. Golden, Colorado, USA, 267-282, 1998b.*

Harbaugh, A.W. & McDonald, M.G., User's documentation for the U.S. Geological Survey modular finite-difference ground-water flow model, *U.S.G.S. Open-File Report 96-485, 56 pp., 1996.*

Hassanizadeh, S.M., Derivation of basic equations of mass transport in porous media, 2, Generalized Darcy's and Fick's laws, *Adv. Water Resour.,* **9***, 207-222, 1986.*

Hassanizadeh, S.M., Mathematical modelling of hydro-geologic processes, lecture notes, *Utrecht University, Institute of Earth Sciences, 1997.*

Hassanizadeh, S.M. & Leijnse, T., On the modeling of brine transport in porous media, *Water Resour. Res.,* **24** *(3), 321-330, 1988.*

Heide, P.K.M., van der & Boswinkel, J.A. 1982. The Fresh-saline Distribution of the Groundwater in the Netherlands. Part 2A. Theoretical Background. (in Dutch). *TNO Institute of Applied Geoscience.*

Henry, H.R., Effects of dispersion on salt encroachment in coastal aquifers, in: *Sea water in coastal aquifers, Cooper, H.H., jr., Kohout, F.A., Henry, H.R. & Glover, R.E., 84 pp., U.S.G.S. Water Supply Paper 1613-C, pp. C70-C84, 1964.*

Herbert, A.W., Jackson, C.P. & Lever, D.A., Coupled groundwater flow and solute transport with fluid density strongly dependent upon concentration, *Water Resour. Res.,* **24** *(10), 1781-1795, 1988.*

Herzberg A., Die Wasserversorgung einiger Nordseebaden, *Zeitung für Gasbeleuchtung und Wasserversorgung; 44: pp. 815-819 & pp. 842-844, 1901.*

Holzbecher, E., Modeling density-driven flow in porous media, Principles, numerics, software, *Springer Verlag, Berlin Heidelberg, 286 p., 1998.*

Huyakorn, P.S., Kretschek, A.G., Broome, R.W., Mercer, J.W. & Lester, B.H., Testing and validation of models for simulating solute transport in ground-water, Development, Evaluation, and Comparison of Benchmark Techniques, *International Ground Water Modeling Center, GWMI 84-13, 1984.*

Huyakorn, P.S., Andersen, P.F., Mercer, J.W. & White, H.O., Jr., Saltwater Intrusion in Aquifers: Development and Testing of a Three-Dimensional Finite Element Model, *Water Resour. Res.,* **23** *(2), 293-312, 1987.*

Huyakorn, P.S. & Pinder, G.F., A pressure-enthalpy finite difference model for simulating hydrothermal reservoirs, *2^{nd} Int. Symp. on Computer Meth. for Part. Diff. Eq. Lehigh Univ. Bethlehem, Pa., June 22-24, 1977.*

ICW, Institute for Land and Water Management Research, Wageningen, Hydrology and water quality of the Central part of the Western Netherlands, (in Dutch), *ICW Regional Studies 9, 101 pp., 1976.*

ILRI, International Institute for Land Reclamation and Improvement, *Veldboek voor Land- en Waterdeskundigen, (in Dutch), Wageningen, The Netherlands, 1972.*

INTERCOMP, A model for calculating effects of liquid waste disposal in deep saline aquifers, *Resource Development and Engineering, Inc. U.S.G.S. Water-Resources Investigations Report 76-96, 263 pp., 1976.*

Jensen, O.K. & Finlayson, B.A., Solution of the convection-diffusion equation using a moving coordinate system, *Second Int. Conf. on Finite Elements in Water Resour., Imperial College, London, July, 4.21-4.32, 1978.*

Josselin de Jong, G., de, Review of vortex theory for multiple fluid flow, *Delft Progress Report,* **2**, *225-236, 1977.*

Kinzelbach, W.K.H., Groundwater Modelling, An introduction with sample programs in BASIC, *Developments in Water Science, 25, Elsevier Science Publishers, Amsterdam, 1986.*

Kinzelbach, W.K.H., Numerische Methoden zur Modellierung des Transport von Schadstoffen im Grundwasser, (In German), *Schriftenreihe GWF Wasser-Abwasser, Band 21, R. Oldenbourg Verlag GmbH, Munchen, 343 pp., 1987a.*

Kinzelbach, W.K.H., Methods for the simulation of pollutant transport in ground water, A model comparison, In: *Proc. Solving Ground Water Problems With Models, Conference and Exposition, Vol. 1, Denver Colorado, USA, 656-675, 1987b.*

Kipp, K.L., Jr., HST3D, A Computer Code for Simulation of Heat and Solute Transport in Three-dimensional Groundwater Flow Systems, *IGWMC, International Ground Water Modeling Center. U.S.G.S. Water-Resources Investigations Report 86-4095, 1986.*

Konikow, L.F. & Bredehoeft, J.D., Computer model of two-dimensional solute transport and dispersion in ground water, *U.S.G.S. Techniques of Water-Resources Investigations, Book 7, Chapter C2, 90 pp., 1978.*

Konikow, L.F., Goode, D.J. & Hornberger, G.Z., A three-dimensional method-of-characteristics solute-transport model (MOC3D), *U.S.G.S. Water-Resources Investigations Report 96-4267, 87 pp., 1996.*

Konikow, L.F., Sanford, W.E. & Campbell, P.J., Constant-concentration boundary codition: Lessons from the HYDROCOIN variable-density groundwater benchmark problem, *Water Resour. Res.,* **33** *(10), 2253-2261, 1997.*

Kooiman, J.W., Peters, J.H. & Eem, J.P., van der., Upconing of brackish and salt water in the dune area of Amsterdam Waterworks and modelling with the Konikow-Bredehoeft program, *Proc. 9^{th} Salt Water Intrusion Meeting, Delft, the Netherlands, May 1986, 343-359, 1986.*

Lantz, R.B., Quantitative Evaluation of Numerical Diffusion (Truncation Error), *Transactions AIME, Soc. of Petroleum Eng. J.* **251***: 315-320, 1971.*

Lee, C.H. & Cheng, R.T., On seawater encroachment in coastal aquifers, *Water Resour. Res.,* **10** *(5), 1039-1043, 1974.*

Lebbe, L.C., Mathematical model of the evolution of the fresh-water lens under the dunes and beach with semi-diurnal tides, *Proc.* 8^{th} *Salt Water Intrusion Meeting, Bari, Italy. Geologia Applicata e Idrogeologia, Vol. XVIII, Parte II, 211-226, 1983.*

Lester, B., SWICHA, A Three-Dimensional Finite-Element Code for Analyzing Seawater Intrusion in Coastal Aquifers, *Version 5.05. GeoTrans, Inc., Sterling, Virginia, U.S.A., IGWMC, International Ground Water Modeling Center, Delft, the Netherlands, 178 pp., 1991.*

Maas, C., The origin of saline groundwater in the Netherlands. (in Dutch). Het vóórkomen van zout grondwater in Nederland. *H_2O (22), no. 7, 214-219, 1989.*

Manning, C.E. & Ingebritsen, S.E., Permeability of the continental crust: implications of geothermal data and metamorphic systems, *Reviews of Geophysics,* **37** *(1), 127-150, 1999.*

McDonald, M.G. & Harbaugh, A.W., A modular three-dimensional finite-difference ground-water flow model, *U.S.G.S. Techniques of Water-Resources Investigations, Book 6, Chapter A1, 586 pp., 1988.*

Mehnert E. & Jennings, A.A. 1985. The effect of salinity-dependent hydraulic conductivity on saltwater intrusion episodes. *J. of Hydrol.,* **80***, 283-298, 1985.*

Meinardi, C.R., The occurrence of brackish groundwater in the lower parts of the Netherlands. (in Dutch). Het zoutwatervoorkomen in de ondergrond van de lage gedeelten van Nederland. *H_2O (6), no. 18, 454-460, 1973.*

Nield, D.A., Onset of thermohaline convection in a porous medium, *Water Resour. Res.,* **11***, 553-560, 1968.*

Nield, D.A. & A. Bejan, Convection in a porous media, *Springer-Verlag, New York, Inc., 408 pp., 1992.*

Noomen, P., Bodembeweging in Nederland, (in Dutch), In: *Zeespiegelrijzing en bodemdaling; welk scenario wordt werkelijkheid ? Symposium 12 april 1989, Delft University of Technology, Delft, 1989.*

Ogata, A. & Banks, R.B., A solution of the differential equation of longitudinal dispersion in porous media, *United States Geological Survey, Professional Paper No. 411-A, 1961.*

Oldenburg, C.M. & Pruess, K., Dispersive transport dynamics in a strongly coupled groundwater-brine flow system, *Water Resour. Res.,* **31** *(2), 289-302, 1995.*

Olsthoorn, T.N., Variable density groundwater modelling with MODFLOW. In: *Proc.* 14^{th} *Salt Water Intrusion Meeting, Malmö, Sweden, June 1996, 51-60, 1996.*

Oude Essink, G.H.P. & Boekelman, R.H., Problems with large-scale modelling of salt water intrusion in 3D, In: *Proc. of the 14th Salt Water Intrusion Meeting, Malmö, Sweden, June 1996, 16-31, 1996.*

Oude Essink, G.H.P., Impact of sea level rise on groundwater flow regimes, A sensitivity analysis for the Netherlands, *Ph.D. thesis. Delft University of Technology, 411 pp., 1996.*

Oude Essink, G.H.P., Simuleren van 3D dichtheidsafhankelijke grondwaterstroming: MOCDENS3D, (in Dutch), In: *Stromingen,* **4***, (1), 5-23, 1998a.*

Oude Essink, G.H.P., MOC3D adapted to simulate 3D density-dependent groundwater flow, In: *Proc. of the MODFLOW'98 Conf. Golden, Colorado, USA, 291-303, 1998b.*

Oude Essink, G.H.P., Simulating density dependent groundwater flow: the adapted MOC3D, In: *Proc. of the 15th Salt Water Intrusion Meeting, Ghent, Belgium, May 1998, 69-79, 1999a.*

Oude Essink, G.H.P., Impact of sea level rise in the Netherlands, in: *Seawater intrusion in coastal aquifers; Concepts, methods and practices, edited by J. Bear, A.H-D. Cheng et al., 507-530, Kluwer Academic Publishers, 1999b.*

Oude Essink, G.H.P., Improving Fresh Groundwater Supply - Problems and Solutions, submitted to Ocean & Coastal Management, 2000a.

Oude Essink, G.H.P., Saltwater intrusion in 3D large-scale aquifers: a Dutch case, accepted in Phys. & Chem. of the Earth, 2000b.

Oude Essink, G.H.P., Groundwater Modelling I, *Utrecht University, Institute of Earth Sciences, The Netherlands, ftp://ftp.geo.uu.nl/pub/people/goe/gwm1/gwm1.pdf, 2000c.*

Oude Essink, G.H.P., Salt Water Intrusion of a Three-dimensional Groundwater System in the Netherlands: a Numerical Study, accepted in Transport in Porous Media, 2001a.

Oude Essink, G.H.P., Density dependent groundwater at the island of Texel, the Netherlands, submitted to Water Resources Research, 2001b.

Peaceman, D.W., Fundaments of numerical reservoir simulation. *Developments in Petroleum Science 6, Elsevier Scientific Publishing Company, Amsterdam, 1977.*

Person, M., Raffensperger, J.P., Ge, S. & Garven, G., Basin-scale hydrogeologic modeling, *Reviews of Geophysics,* **34** *(1), 61-87, 1996.*

Pinder, G.F. & Cooper, H.H, Jr., A numerical technique for calculating the transient position of the saltwater front, *Water Resour. Res.,* **6** *(3), 875-882, 1970.*

Pinder, G.F. & Gray, W.G., Finite element simulation in surface and subsurface hydrology. *Academic Press, 295 pp., 1977.*

Reilly, Th.E. & Goodman, A.S., Quantitative analysis of saltwater-freshwater relationships in groundwater systems – a historical perspective, *J. of Hydrol.,* **80***, 125-160, 1985.*

Sanford, W.E. & Konikow, L.F., A two-constituent solute-transport model for ground water having variable density, *U.S.G.S. Water-Resources Investigations Report 85-4279, 1985.*

Sauter, F.J., Leijnse, A. & Beusen, A.H.W., METROPOL's User's Guide, *Report number 725205.003. National Institute of Public Health and Environmental Protection. Bilthoven, the Netherlands, 1993.*

Schaars, F., Implementation of a method for spatial modelling of simultaneous flow of fresh, brackish and saline groundwater in the sand-dune area of Amsterdam Waterworks, (in Dutch), *M.Sc. thesis, Delft University of Technology, 102 pp., 1996.*

Scheidegger, A.E., General theory of dispersion in porous media, *J. of Geophys. Res.,* **66** *(10), 3273-3278, 1961.*

Scheidegger, A.E., The physics of flow through porous media, *3rd ed., Toronto, Univ. of Toronto Press, 1974.*

Schmorak, S. & Mercado, A., Upconing of fresh-water sea-water interface below pumping wells, field study, *Water Resour. Res.,* **5***, 1290-1311, 1969.*

Schultz, E., Water Management of the Drained Lakes in the Netherlands, (in Dutch), *Ph.D. thesis, Delft University of Technology, Rijkswaterstaat, Directie Flevoland, Lelystad, ISBN 90-369-1087-0, 507 pp., 1992.*

Segol, G., Classic groundwater simulations, Proving and improving numerical models, *Prentice-Hall, Inc. New York, 531 pp., 1994.*

Segol, G., Pinder, G.F. & Gray, W.G., A Galerkin finite-element technique for calculating the transient position of the saltwater front, *Water Resour. Res.,* **11** *(2), 343-347, 1975.*

Shamir, U. & Harleman, D.R.F., Numerical and analytical solutions of dispersion problems in homogeneous and layered aquifers, *M.I.T. Dept. Civil Eng., Hydrodynamics Lab. Rept. 89, May, 1966.*

Shiklomanov I.A., World Fresh Water Resources, Chapter 16, *Proc. of the Unesco International Symposium to commemorate the 25 years of IHD/IHP, Paris, 15-17 March 1990.*

Sikkema, P.C. & Dam, J.C., van, Analytical formulae for the shape of the interface in a semi-confined aquifer, *J. of Hydrol.,* **56***, 201-220, 1982.*

Singh, S.N., Boekelman, R.H., Rientjes, T.H.M. & Dam, J.C., van, Behaviour of groundwater of the polder Groot-Mijdrecht, *Delft University of Technology, 1990.*

Smith, L. & Chapman, D.S., On the thermal effects of groundwater flow: 1. Regional scale systems, *J. Geophy. Res.,* **88** *(B1), 593-608, 1983.*

Sorey, M.L., Numerical modeling of liquid geothermal systems, *U.S. Geological Survey Prof. Pap. 16044-D, 1978.*

Souza, W.R. & Voss, C.I., Analysis of an anisotropic coastal aquifer system using variable-density flow and solute transport simulation, *J. of Hydrol.,* **92***, 17-41, 1987.*

Stuyfzand, P.J., A new hydrochemical classification of watertypes: principles and application to the coastal dunes aquifer system of the Netherlands, *Proc.* 9^{th} *Salt Water Intrusion Meeting, Delft, the Netherlands, 641-655, 1986.*

Stuyfzand, P.J., Composition, genesis and quality variations of shallow groundwater in coastal dunes, (in Dutch), *KIWA SWE-91.008, 175 pp., 1991.*

Stuyfzand, P.J., Hydrochemistry and hydrology of the coastal dune area of the Western Netherlands, *Ph.D. thesis, Vrije Universiteit Amsterdam, The Netherlands, 366 pp., 1993.*

Sudicky, E.A., The Laplace Transform Galerkin Technique: a time-continuous finite element theory and application to mass transport in groundwater, *Water Resour. Res.,* **25** *(8), 1833-1846, 1989.*

SWIM-Delft'86: *Proc.* 9^{th} *Salt Water Intrusion Meeting, Delft, the Netherlands, 688 pp., May 1986.*

SWIM-Barcelona'92: *Proc.* 12^{th} *Salt Water Intrusion Meeting, Barcelona, Spain, 770 pp., Nov. 1992.*

SWIM-Malmö'96: *Proc.* 14^{th} *Salt Water Intrusion Meeting, Malmö, Sweden, 327 pp., June 1996.*

SWIM-Gent'98: *Proc. of the 15th Salt Water Intrusion Meeting, Ghent, Belgium, 307 pp., May 1998.*

Todd, D.K., Groundwater Hydrology, *John Wiley & Sons, New York, 1980.*

Turcotte, D.L. & Schubert, G., Geodynamics, 450 pp., *John Wiley & Sons, New York, 1982.*

Uffink, G.J.M., Analysis of dispersion by the random walk method, *Ph.D. thesis, Delft University of Technology, 150 pp., 1990.*

U.S. Department of Energy, Workshop on Sea Level Rise and Coastal Processes, *9-11 March, 1988, Palm Coast, Florida, 1989.*

Verruijt, A., Theory of Groundwater Flow, *Macmillan, London, 1970.*

Verruijt, A., The rotation of a vertical interface in a porous medium, *Water Resour. Res.,* **16** *(1), 239-240, 1980.*

Verweij, J.M., Application of fluid flow system analysis to reconstruct the post-Carboniferous hydrogeohistory of the onshore and offshore Netherlands, *Marine and Petroleum Geology,* **16***, 561-579, 1999.*

Voss, C.I. SUTRA – A finite element simulation for saturated-unsaturated, fluid-density-dependent ground-water flow with energy transport or chemically reactive single-species solute transport, *U.S.G.S. Water-Resources Investigations Report 84-4369, 409 pp., 1984.*

Voss, C.I. & Souza, W.R., Variable density flow and solute transport simulation of regional aquifers containing a narrow freshwater-saltwater transition zone, *Water Resour. Res.,* **23** *(10), 1851-1866, 1987.*

Walraevens, K., Lebbe, L.C., *et al.*, Salt/fresh-water flow and distribution in a cross-section at Oostduinkerke (Western Coastal Plain of Belgium), *Proc.* 12^{th} *Salt Water Intrusion Meeting, Barcelona, Spain, Nov. 1992, 407-420, 1993.*

Wesseling, J. Saline seepage in the Netherlands, occurrence and magnitude. In: *Research on possible changes in the distribution of saline seepage in the Netherlands, Proc. and Inform. No.* **26***, Committee for Hydrological Research-TNO, 1980.*

Ward, D.S., Data Input for SWIFT/386, version 2.50, *Geotrans Technical Report, Sterling, Va., 1991.*

Ward, D.S. & Benegar, J., Data Input Guide for SWIFT-98, version 2.57, *HSI Geotrans, Inc., Sterling, Va., 1998.*

Weast, R.C., Handbook of Chemistry and Physics, 63 rd ed., pp. D261, *CRC Press, Boca Raton, Fla., 1982.*

Yeung, Y., Personal communications, *Chinese University of Hong Kong, 1999.*

Zheng, C., MT3D: A modular three-dimensional transport model for simulation of advection, dispersion and chemical reaction of contaminants in groundwater systems, *S.S. Papadopolous and Associates, Rockville, Maryland, 20852, 1990.*

Interesting web-sites

http://www.ce.udel.edu/faculty/cheng/saltnet/index.html
Saltwater Intrusion Network

http://water.usgs.gov/software/ground_water.html.
United States Geological Survey (U.S.G.S.). *Watstore Program Office, 437 National Center, Reston VA 22092, USA. Fax: 1-703-648-5295.*

http://www.wmo.ch/web/homs/hwrphome.html
Hydrological Operational Multipurpose System (HOMS). *Office, Hydrology and Water Resources Department, World Meteorological Organization Secretariat (WMO), Case postale No. 2300, CH-1211 Geneva 2, Switzerland.*

http://www.hsigeotrans.com/software.html
http://www.hsigeotrans.com/swift.html
GeoTrans, Inc. *46050 Manekin Plaza, Suite 100, Sterling, Virginia 22170, USA. Fax: 1-703-444-1685.*

http://www.flowpath.com/
Waterloo Hydrogeologic, *180 Columbia Street West Waterloo, Ontario, Canada, N2L 3L3.*

http://www.wlu.ca/~wwwiahs/
International Association of Hydrological Sciences.

http://www.itc.nl/
ITC. 1996. ILWIS. The Integrated Land and Water Information System. *International Institute for Aerospace Survey and Earth Sciences. Hengelosestraat 99, P.O. Box 6, 7500 AA Enschede, the Netherlands. Fax: 31-53-4874484. E-mail: ilwis@itc.nl*

http://www.mines.edu/research/igwmc/
http://magma.mines.edu/igwmc/software/igwmcsoft/saltwatr.htm
International Ground Water Modeling Center (IGWMC). *Colorado School of Mines, Golden, CO 80401-1887, USA. Fax: 1-303-273-3278.*

http://www.scisoftware.com/
http://www.scisoftware.com/products/cat_saltwater/cat_saltwater.html
Scientific Software Group. 1996. Updated Product Guide. *P.O. Box 23041, Washington, D.C. 20026-3041, USA. Fax: 1-703-620-6793.*

http://www.uovs.ac.za/igs/software.htm
Institute for Groundwater Studies, the University of the Orange Free State, *P.O. Box 339, Bloemfontein, 9300, South Africa.*

http://water.usgs.gov/software/ground_water.html.
United States Geological Survey (U.S.G.S.). *Watstore Program Office, 437 National Center, Reston VA 22092, USA. Fax: 1-703-648-5295.*

Interesting textbooks

Bear, J. & Verruijt, A., Modeling Groundwater Flow and Pollution, *D. Reidel Publishing Company, Dordrecht, the Netherlands, 414 pp., 1987.*

Bear, J., Cheng, A., Sorek, S., Herrera, I. & Ouazar, D. (eds), *Seawater intrusion in coastal aquifers; concept, methods and practices, 625 pp., Kluwer Academic Publishers, 1999.*

Custodio, E. & Bruggeman, G.A. (eds), Groundwater Problems in Coastal Areas, *Studies and Reports in Hydrology, UNESCO, International Hydrological Programme, Paris, 1987.*

Holzbecher, E., Modeling density-driven flow in porous media, Principles, numerics, software, *Springer Verlag, Berlin Heidelberg, 286 pp., 1998.*

Ingebritsen, S.E., & Sanford, W.E., Groundwater in geological processes, *Cambridge University Press, 341 pp., 1998.*

Nield, D.A. & A. Bejan, Convection in a porous media, *Springer-Verlag, New York, Inc., 408 pp., 1992.*

Phillips, O.M., F.R.S, Flow and reactions in permeable rocks, *Cambridge University Press, 285 pp., 1991.*

Turcotte, D.L. & Schubert, G., Geodynamics, 450 pp., *John Wiley & Sons, New York, 1982.*

æ

Index

æ